

UNCLASSIFIED

AD NUMBER

AD826458

LIMITATION CHANGES

TO:

Approved for public release; distribution is unlimited.

FROM:

Distribution authorized to U.S. Gov't. agencies and their contractors;  
Administrative/Operational Use; 01 NOV 1967.  
Other requests shall be referred to Air Force Technical Application Center, ATTN: VELA  
Seismological Observatory, Washington, DC 20333.

AUTHORITY

AFTAC ltr dtd 25 Jan 1972

THIS PAGE IS UNCLASSIFIED

AD82458

TECHNICAL REPORT NO. 67-75

EVALUATION OF MULTIPLE ARRAY PROCESSORS AT THE UINTA BASIN SEISMOLOGICAL OBSERVATORY

STATEMENT #2 UNCLASSIFIED

This document is subject to special export controls and each transmittal to foreign governments or foreign nationals ~~may be~~ made only with prior approval of *Air Force Technical Applications Center, Attn: VELA Seismological Observatory* Washington, D.C. 20333

D D C  
RECEIVED  
FEB 12 1968  
RECEIVED  
G



GEOTECH

A TELEDYNE COMPANY

REPRODUCTION OF THIS DOCUMENT IS PROHIBITED. ALL RIGHTS RESERVED. THIS DOCUMENT IS UNCLASSIFIED.

**BEST  
AVAILABLE COPY**

TECHNICAL REPORT NO. 67-75

EVALUATION OF MULTIPLE ARRAY PROCESSORS AT  
THE UINTA BASIN SEISMOLOGICAL OBSERVATORY

Sponsored by

Advanced Research Projects Agency  
Nuclear Test Detection Office  
ARPA Order No. 624

TELEDYNE INDUSTRIES  
GEOTECH DIVISION  
3401 Shiloh Road  
Garland, Texas

1 November 1967

**ORIGINAL CONTAINS COLOR PLATES: ALL DOC  
REPRODUCTIONS WILL BE IN BLACK AND WHITE.  
ORIGINAL MAY BE SEEN IN DOC HEADQUARTERS.**

IDENTIFICATION

AFTAC Project No:	VELA T/6705
Project Title:	Operation of UBSO
ARPA Order No:	624
ARPA Program Code No:	6F10
Name of Contractor:	Teledyne Industries, Geotech Division Garland, Texas
Date of Contract:	1 May 1966
Amount of Contract:	\$624,897
Contract No:	AF 33(657)-16563
Contract Expiration Date:	31 October 1967
Program Manager:	B. B. Leichter, BR1-2561 Garland, Texas

## CONTENTS

	<u>Page</u>
ABSTRACT	
1. INTRODUCTION	1
1.1 Authority	1
1.2 History	1
2. DESCRIPTION OF MAP SYSTEMS	2
2.1 General	2
2.2 MAP band-pass filter	2
2.3 MAP I	3
2.4 MAP II	3
3. MAINTENANCE REQUIREMENTS	3
3.1 Maintenance schedule	3
3.2 Multifrequency relative amplitude	7
4. SYSTEM GAINS AND GAIN NORMALIZING FACTORS	7
4.1 Changes in operational gains	7
4.2 Gain normalizing factors	7
5. NOISE DATA	9
5.1 Visual noise measurements data	9
5.2 Power spectral density estimates	10
5.2.1 Procedure and results	10
5.2.2 Discussion	10
6. CHARACTERISTICS OF SIGNALS AND NOISE RECORDED BY MAP I SYSTEMS	12
7. CHARACTERISTICS OF SIGNALS AND NOISE RECORDED BY MAP II SYSTEMS	14
7.1 General	14
7.2 Deghost filters	14
7.3 Beam-steered summations of vertical array elements	15
8. VISUAL SIGNAL-TO-NOISE RATIO COMPARISON	16
8.1 General	16
8.2 Procedure	16

CONTENTS, Continued

	<u>Page</u>
8.3 Results	16
8.4 Discussion	18
9. DETECTION CAPABILITY COMPARISON	18
9.1 Data sample	18
9.2 Procedure and results	19
9.3 Evaluation of subsystems	19
10. DISCUSSION AND CONCLUSIONS	24
10.1 General	24
10.2 MAP I	24
10.3 MAP II	24
10.4 Possible other uses of the MAP systems	25
11. RECOMMENDATIONS	25
12. REFERENCES	27

## ILLUSTRATIONS

<u>Figure</u>		<u>Page</u>
1	Orientation and configuration of UBSO arrays	28
2	Relative frequency responses of the filtered summation of the shallow-buried array ( $\Sigma$ SSF) and of the MAP band-pass filter operating on elements of a surface array (Z or SZ) and on elements of the vertical array (DH)	29
3	Cumulative frequency distributions of noise amplitudes in the period band 0.4 - 1.4 seconds recorded by MAP I and Primary systems, 1 January through 12 March 1967	30
4	Cumulative frequency distributions of noise amplitudes in the period band 0.4-1.4 seconds recorded by MAP II systems, 1 January through 12 March 1967	31
5	Power spectral density estimate of a sample of low-level microseismic noise, recorded by $\Sigma$ SSF	32
6	Power spectral density estimate of a sample of low-level microseismic noise, recorded by MCF4	33
7	Power spectral density estimate of a sample of low-level microseismic noise, recorded by MCF1	34
8	Power spectral density estimate of a sample of low-level microseismic noise, recorded by MCF3	35
9	Power spectral density estimate of a sample of low-level microseismic noise, recorded by MCF11	36
10	Power spectral density estimate of a sample of low-level microseismic noise recorded by MCF12	37
11	Power spectral density estimate of a sample of low-level microseismic noise recorded by MCF13	38
12	Power spectral density estimate of a sample of low-level microseismic noise, with road noise, recorded by $\Sigma$ SSF	39
13	Power spectral density estimate of a sample of low-level microseismic noise, with road noise, recorded by MCF4	40

ILLUSTRATIONS, Continued

<u>Figure</u>		<u>Page</u>
14	Power spectral density estimate of a sample of low-level microseismic noise, with road noise, recorded by MCF1	41
15	Power spectral density estimate of a sample of low-level microseismic noise, with road noise, recorded by MCF3	42
16	Power spectral density estimate of a sample of low-level microseismic noise, with road noise, recorded by MCF11	43
17	Power spectral density estimate of a sample of low-level microseismic noise, with road noise, recorded by MCF12	44
18	Power spectral density estimate of a sample of low-level microseismic noise, with road noise, recorded by MCF13	45
19	Power spectral density estimate of a sample of intermediate-level microseismic noise, recorded by $\Sigma$ SSF	46
20	Power spectral density estimate of a sample of intermediate-level microseismic noise, recorded by MCF4	47
21	Power spectral density estimate of a sample of intermediate-level microseismic noise, recorded by MCF1	48
22	Power spectral density estimate of a sample of intermediate-level microseismic noise, recorded by MCF3	49
23	Power spectral density estimate of a sample of intermediate-level microseismic noise, recorded by MCF11	50
24	Power spectral density estimate of a sample of intermediate-level microseismic noise, recorded by MCF12	51
25	Power spectral density estimate of a sample of intermediate-level microseismic noise, recorded by MCF13	52

ILLUSTRATIONS, Continued

<u>Figure</u>		<u>Page</u>
26	Power spectral density estimate of a sample of high-level microseismic noise, recorded by $\Sigma$ SSF	53
27	Power spectral density estimate of a sample of high-level microseismic noise, recorded by MCF4	54
28	Power spectral density estimate of a sample of high-level microseismic noise, recorded by MCF1	55
29	Power spectral density estimate of a sample of high-level microseismic noise, recorded by MCF3	56
30	Power spectral density estimate of a sample of high-level microseismic noise, recorded by MCF11	57
31	Power spectral density estimate of a sample of high-level microseismic noise, recorded by MCF12	58
32	Power spectral density estimate of a sample of high-level microseismic noise, recorded by MCF13	59
33	MAP I seismogram illustrating response of MAP I system to strong road noise. (X10 enlargement of 16-millimeter film)	60
34	Primary system seismogram illustrating response of primary systems to strong road noise. (X10 enlargement of 16-millimeter film)	61
35	MAP I seismogram illustrating response of MAP I systems to high frequency cultural noise, not road noise. (X10 enlargement of 16-millimeter film)	62
36	Primary system seismogram illustrating response of primary system to high-frequency cultural noise, not road noise. (X10 enlargement of 16-millimeter film)	63
37	MAP I seismogram illustrating response of MAP I systems to near regional signal. Epicentral data: $O = 05:34:58.5$ , $\Delta = 1.9^\circ$ , azimuth = $285^\circ$ , $h = 5$ km. (X10 enlargement of 16-millimeter film)	64

ILLUSTRATIONS, Continued

<u>Figure</u>		<u>Page</u>
38	Primary system seismogram, illustrating response of primary system to near-regional signal. Epicentral data: $O = 05:34:58.5$ , $\Delta = 1.9^\circ$ , azimuth = $285^\circ$ , $h = 5$ km. (X10 enlargement of 16-millimeter film)	65
39	MAP I seismogram, illustrating response of MAP I systems to close teleseism. Epicentral data: $O = 15:47:32.0$ , $\Delta = 26.1^\circ$ , azimuth = $155^\circ$ , $h = 33$ km, USC&GS magnitude = 3.7. (X10 enlargement of 16-millimeter film)	66
40	Primary system seismogram illustrating response of primary system to near teleseism. Epicentral data: $O = 15:47:32.0$ , $\Delta = 20.1^\circ$ , azimuth = $155^\circ$ , $h = 33$ km, USC&GS magnitude = 3.7. (X10 enlargement of 16-millimeter film)	67
41	MAP I seismogram, illustrating response of MAP I systems to weak teleseism in road noise. Epicenter unknown. (X10 enlargement of 16-millimeter film)	68
42	Primary system seismogram, illustrating response of primary system to weak teleseism in road noise. Epicenter unknown. (X10 enlargement of 16-millimeter film)	69
43	MAP I seismogram, illustrating response of MAP I systems to weak teleseism, background free of road noise. Epicentral data: $O = 10:13:30.2$ , $\Delta = 50.6^\circ$ , azimuth = $137^\circ$ , $h = 214$ km, USC&GS magnitude = 3.7. (X10 enlargement of 16-millimeter film)	70
44	Primary system seismogram, illustrating response of primary system to weak teleseism, background free of road noise. Epicentral data: $O = 10:13:30.2$ , $\Delta = 50.6^\circ$ , azimuth = $137^\circ$ , $h = 214$ km, USC&GS magnitude = 3.7. (X10 enlargement of 16-millimeter film)	71
45	MAP II seismogram illustrating precursor effect on MCF15 epicenter unknown. (X10 enlargement of 16-millimeter film)	72

ILLUSTRATIONS, Continued

<u>Figure</u>		<u>Page</u>
46	Vertical array seismogram of same event as is illustrated in figure 45. Epicenter unknown. (X10 enlargement of 16-millimeter film)	73
47	One-way and two-way travel times for the vertical array	74
48	MAP II seismogram, illustrating response of the MAP II systems to a simple P wave. Epicentral data: O = 01:35:18, $\Delta = 86.4^\circ$ , azimuth = $240^\circ$ , h = 280 km, USC&GS magnitude = 4.1. (X10 enlargement of 16-millimeter film)	75
49	Vertical array seismogram, illustrating response of vertical array to a simple P wave. Epicentral data: O = 01:35:18.0, $\Delta = 86.4^\circ$ , azimuth = $240^\circ$ , h = 280 km, USC&GS magnitude = 4.1. (X10 enlargement of 16-millimeter film)	76
50	MAP II seismogram, illustrating response of MAP II systems to a short-duration Rayleigh wave. (X10 enlargement of 16-millimeter film)	77
51	Vertical array seismogram, illustrating response of vertical array to a short-duration Rayleigh wave. (X10 enlargement of 16-millimeter film)	78
52	MAP II seismogram, illustrating response of MAP II systems to a complex signal (PKP). Epicentral data: O = 01:36:04.7, $\Delta = 121.1^\circ$ , azimuth = $330^\circ$ , h = 27 km, no USC&GS magnitude. (X10 enlargement of 16-millimeter film)	79
53	Vertical array seismogram, illustrating response of vertical array to a complex signal (PKP). Epicentral data: O = 01:36:04.7, $\Delta = 121.1^\circ$ , azimuth = $330^\circ$ , h = 27 km, no USC&GS magnitudes. (X10 enlargement of 16-millimeter film)	80
54	Cumulative frequency distributions of S/N for MAP I and Primary systems	81
55	Cumulative frequency distributions of S/N for MAP II systems	82

## TABLES

<u>Table</u>		<u>Page</u>
1	Locations of vertical array seismometers in the deep hole	1
2	Description of MAP I systems	4
3	Description of MAP II systems	5
4	Maintenance schedule for the UBSO MAP systems	8
5	Gain correction factors for MAP systems utilizing time delays	9
6	Average noise trace amplitude in the period band 0.4 second to 1.4 seconds, normalized to a magnification of 1000K at 1 cps, for MAP I, MAP II, and primary systems; from visual noise measurements	11
7	Average S/N for each system ( $\overline{S/N}_{\text{Sys}}$ ) relative to average S/N for $\Sigma$ SBS ( $\overline{S/N}_{\Sigma\text{SBS}}$ ), for MAP I, MAP II, and primary systems	17
8	Percent of events with S/N greater than, equal to, and less than the S/N for $\Sigma$ SBS, for MAP I, MAP II, and primary systems	17
9	Number of C&GS-located hypocenters as a function of epicentral distance from ULSO and C&GS magnitude	20
10	Percent of C&GS-located events detected by each system, as a function of epicentral distance from UBSO	21
11	Percent of C&GS-located events detected by each system, as a function of C&GS magnitude	22
12	Average detection grades for subsystems, MAP I	23
13	Average detection grades for subsystems, MAP II	23

EVALUATION OF MULTIPLE ARRAY PROCESSORS AT  
THE UINTA BASIN SEISMOLOGICAL OBSERVATORY

1. INTRODUCTION

1.1 AUTHORITY

The work described in this report was supported by the Advanced Research Projects Agency, Nuclear Test Detection Office, and was monitored by the Air Force Technical Applications Center under Contract AF 33(657)-16563.

1.2 HISTORY

Two Multiple Array Processors were designed and constructed by Texas Instruments, Incorporated (TI), and installed at UBSO in September 1965. One of the Multiple Array Processors (MAP I) is a 10-channel unit operating on the 10 elements of the UBSO surface array. The other Multiple Array Processor (MAP II) is a 19-channel unit operating on the 10 elements of the shallow-buried array and the 6 elements of the vertical array. The UBSO array configuration is presented in figure 1. The depths of the elements of the vertical array are listed in table 1.

Table 1. Locations of vertical array seismometers  
in the deep hole

<u>Seismometer</u>	<u>Depth (feet)</u>
DH6	3907
DH5	4901
DH4	5894
DH3	6910
DH2	7903
DH1	8895

Results of the TI analysis of the UBSO noise field, which formed the basis for design of the MAP systems were reported by TI in a UBSO noise report (Edwards, 1965a). Descriptions of the MAP systems were reported by TI in their MAP final report (Edwards, 1965b). Additional data on UBSO noise and the MAP systems were reported in Ti's Special Report No. 22 (Burrell and Lintz, 1967)

MAP I became operational on 8 September 1965. MAP II operated from 20 September until 8 November 1965, at which time operation was temporarily suspended because of unavailability of vertical array data.

A preliminary evaluation of data recorded by MAP I was reported on 28 December 1965 (Alsup, 1965), and an evaluation of operating and maintenance requirements of the two MAP systems was reported on 26 May 1966 (Alsup, 1966). The preliminary evaluation of MAP I data indicated that the MAP systems did not appreciably attenuate a noise type associated with traffic on U. S. Highway 40 located north and west of the observatory. This road noise, whose energy is concentrated in the frequency band from 2 to 3 cps, is common during the daylight hours and occurs intermittently through the night. TI designed a multichannel filter from a noise sample containing road noise. Resistor boards for this road noise filter were fabricated by the Geotech Division of Teledyne Industries (Geotech). The road noise filter was installed in MAP I in late summer of 1966, replacing one of the multichannel filters.

Operation of MAP II was begun in October 1966, following final installation of the vertical array.

On 31 May 1967, operation of MAP II was suspended, pending overhaul of the vertical array. Operation of MAP I was terminated on 1 July 1967 when the operation of the surface array was discontinued.

## 2. DESCRIPTION OF MAP SYSTEMS

### 2.1 GENERAL

Each of the MAP units is an analog processor using a combination of passive delay lines and resistive networks to achieve the desired processing. In addition, band-pass frequency filtering is applied to each input channel before processing. MAP I has the capacity to process 10 channels of input data, and MAP II has a 19-channel capacity. Each delay line has a maximum time delay of 2.000 seconds, with taps at 50-millisecond intervals. Each tap is provided with an equalizer amplifier to isolate the delay line and to compensate for attenuation in the delay line. Each equalizer amplifier is provided with controls so that the signal level and dc balance of the output from the delay line tap can be adjusted. There are a total of 410 test points in MAP I and 819 test points in MAP II.

### 2.2 MAP BAND-PASS FILTER

All seismograph inputs to each of the MAP units are routed directly from the phototube amplifiers and are subjected to band-pass filtering immediately

following a gain trim section and before other processing. The MAP band-pass filter is operated with a high-cut corner frequency of 3 cps at 6 dB per octave cutoff rate and a low-cut corner frequency of 1 cps at 12 dB per octave cutoff rate. The relative frequency responses of the MAP band-pass filter applied to an element of the surface array and to an element of the vertical array are shown in figure 2. These curves show the frequency filtering to which input data are subjected prior to being operated on by the multichannel filters. Figure 2 also shows the relative frequency response of the filtered summation of the 10 elements of the shallow-buried array ( $\Sigma$ SSF).  $\Sigma$ SSF operates with a high-cut corner frequency of 3 cps and a low-cut corner frequency of 0.8 cps, both at a cutoff rate of 12 dB per octave.

### 2.3 MAP I

MAP I operates on the outputs of the 10 elements of the surface array and provides 10 processed output channels. Three of the MAP I processors are multichannel filters (MCF), six are beam-steered summations (BSS), and one is a simple summation ( $\Sigma$ SBS). Specifications of the MAP I processors are given in table 2. A complete description of the MAP I systems is given in the Texas Instruments MAP Final Report (Edwards, 1965b).

### 2.4 MAP II

MAP II operates on the outputs of the 10 elements of the shallow-buried array and the outputs of the 6 elements of the vertical array and provides 14 channels of processed data. Two of the MAP II processors utilize data from both the subsurface array elements and the vertical array elements. One processor operates on the outputs of the elements of the shallow-buried array only. The remaining 11 processors operate on the outputs of the elements of the vertical array only. Seven of the MAP II processors are multichannel filters, including four deghosting filters; six are beam-steered summations of the vertical array elements (BSSV), and one is a simple summation of the 10 elements of the shallow-buried array and the 6 elements of the vertical array ( $\Sigma$ DVS). Specifications of the MAP II processors are given in table 3. A complete description of the MAP II systems is given in the MAP final report (Edwards, 1965b).

## 3. MAINTENANCE REQUIREMENTS

### 3.1 MAINTENANCE SCHEDULE

In the preliminary evaluation of MAP operational and maintenance requirements (Alsop, 1966), modifications to the test procedures, prescribed by TI, were recommended. Further slight modifications were incorporated into the

Table 2. Description of MAP I Systems

<u>System</u>					
MCF4	Multichannel Filter	Surface Array (Z1 - Z10)	Velocity - Infinite	Measured noise, including road noise	
MCF1	Multichannel Filter	Surface Array (Z1 - Z10)	Velocity - Infinite	Measured noise, not including road noise	
MCF3	Multichannel Filter	Surface Array (Z1 - Z10)	Velocity, 8.1 km/sec to infinite	Measured noise, not including road noise	
BSS1	Beam-Steered Summation	Surface Array (Z1 - Z10)	8.1 km/sec velocity 0° azimuth	----	
BSS2	Beam-Steered Summation	Surface Array (Z1 - Z10)	8.1 km/sec velocity 60° azimuth	----	
BSS3	Beam-Steered Summation	Surface Array (Z1 - Z10)	3.1 km/sec velocity 120° azimuth	----	
BSS4	Beam-Steered Summation	Surface Array (Z1 - Z10)	8.1 km/sec velocity 180° azimuth	----	
BSS5	Beam-Steered Summation	Surface Array (Z1 - Z10)	8.1 km/sec velocity 240° azimuth	----	
BSS6	Beam-Steered Summation	Surface Array (Z1 - Z10)	8.1 km/sec velocity 300° azimuth	----	
ΣSBS	Simple Summation	Surface Array (Z1 - Z10)	Velocity - Infinite	----	

Table 3. Description of MAP II Systems

<u>System</u>	<u>System Type</u>	<u>Input Channels</u>	<u>Signal Model</u>	<u>Noise Model</u>
MCF11	Multichannel Filter	Shallow-Buried Array (SZ1 - SZ10)	Velocity - Infinite	Measured noise
MCF12	Multichannel Filter	Shallow-Buried and Vertical Array (SZ1 - 10, DH1 - 6)	Velocity - Infinite	Theoretical isotropic surface - mode noise
MCF13	Multichannel Filter	Vertical Array (DH1 - DH6)	Velocity - Infinite	Theoretical isotropic surface - mode noise
MCF14	Deghost filter	DH1, DH3, DH5 Up-going	Up-going Velocity - Infinite	Down-going infinite velocity, signal and theoretical surface - mode noise
MCF15	Deghost filter	DH1, DH3, DH5 Down-going	Down-going Velocity - Infinite	Up-going, infinite velocity, signal and theoretical surface - mode noise
MCF16	Deghost filter	DH2, DH4, DH6 Up-going	Up-going Velocity - Infinite	Down-going, infinite velocity, signal and theoretical surface - mode noise
MCF17	Deghost filter	DH2, DH4, DH6 Down-going	Down-going Velocity - Infinite	Up-going, infinite velocity, signal and theoretical surface - mode noise

Table 3. Description of MAP II Systems, continued

<u>System</u>	<u>System Type</u>	<u>Input Channels</u>	<u>Signal Model</u>	<u>Noise Model</u>
BSSV1	Beam Steered Summation	Vertical Array (DH1 - DH6)	Velocity - Infinite Up-going P-wave	Not Applicable
BSSV2	Beam Steered Summation	Vertical Array (DH1 - DH6)	8 km/sec velocity Up-going P-wave	Not Applicable
BSSV3	Beam Steered Summation	Vertical Array (DH1 - DH6)	8 km/sec velocity Up-going S-wave	Not Applicable
BSSV4	Beam Steered Summation	Vertical Array (DH1 - DH6)	Velocity - Infinite Down-going P-wave	Not Applicable
BSSV5	Beam Steered Summation	Vertical Array (DH1 - DH6)	8 km/sec velocity Down-going P-wave	Not Applicable
BSSV6	Beam Steered Summation	Vertical Array (DH1 - DH6)	8 km/sec velocity Down-going S-wave	Not Applicable
$\Sigma$ DVS	Simple Summation	Shallow-Buried and Vertical Array (SZ1-10, DH1-6)	---	Not Applicable

maintenance schedule during the MAP evaluation. The maintenance schedule used, together with the man-hours required to perform each test, is presented in table 4. The adjustment of dc balance of the input amplifier and input level trim are considered to be the most important adjustments in the maintenance schedule. If the input dc balance and input level are maintained, other required adjustments of the MAP systems are usually minor. If operation of the MAP systems at UBSO is continued, we recommend that this maintenance schedule be followed.

### 3.2 MULTIFREQUENCY RELATIVE AMPLITUDE RESPONSES

Multifrequency relative amplitude responses were run on MCF's 1, 3, and 4 of MAP I in March 1967. For MCF1, 13 of the amplitude ratios differed from the corresponding theoretical values by more than 20 percent. For MCF3, 16 of the amplitude ratios differed by more than 20 percent from the corresponding theoretical values. Theoretical values of the amplitude ratios were not available for MCF4 (the road noise filter). A total of 60 man-hours was required to perform this test instead of the 24 man-hours that had been estimated. If operation of the MAP systems is continued, a less time-consuming method of checking the operation of the systems should be developed.

## 4. SYSTEM GAINS AND GAIN NORMALIZING FACTORS

### 4.1 CHANGES IN OPERATIONAL GAINS

In order to make the recorded background levels of the MAP II systems more nearly equal, the gains on MCF16 and MCF17 were increased by a factor of 2.0, and the gains of MCF14 and MCF15 and BSSV1 through BSSV6 were increased by a factor of 2.5 on 23 January 1967.

### 4.2 GAIN NORMALIZING FACTORS

Operational gains for the MAP systems were determined from the 1 cps routine calibrations, performed daily. The calibration signal was applied simultaneously to all of the inputs of a given system. Consequently, a gain correction factor must be applied to the gains calculated from simultaneous calibration for those MAP systems which use time delays (the beam-steered summations of MAP I and all MAP II systems which operate on elements of the vertical array). The gain correction factors for the appropriate systems are listed in table 5. All gains specified in this report have been corrected. The gains, therefore, represent for each system, the gain for a 1 cps signal of the type for which the system was designed. However, because the frequency responses of the MAP channels may differ markedly from the frequency responses of the

Table 4. Maintenance schedule for the UBSO MAP systems

<u>Daily</u>	<u>Man-Hours</u>		
	<u>MAP I</u>	<u>MAP II</u>	
Sine-wave calibration	0.5	0.8	
Input dc balance adjustment	0.2	---	
Input level trim	0.6	---	
Subtotal	1.3	0.8	
TOTAL			2.1
<u>Weekly</u>			
Step-function calibration	0.2	0.3	
Input dc balance adjustment	---	0.3	
Input level trim	---	1.1	
Subtotal	0.2	1.7	
TOTAL			1.9
<u>Monthly</u>			
Spot check equalizer amplifier dc balance	1.0	1.5	
Spot check equalizer amplifier gain trim	1.0	1.5	
Subtotal	2.0	3.0	
TOTAL			5.0
<u>Quarterly</u>			
Equalizer amplifier dc balance	10.0	15.0	
Equalizer amplifier gain trim	8.0	12.0	
Subtotal	18.0	27.0	
TOTAL			45.0
<u>Annual</u>			
Multifrequency relative amplitude response	60.0	100.0	
Subtotal	60.0	100.0	
TOTAL			160.0
<u>Yearly Man-Hours Required</u>			
Daily	766.5		
Weekly	98.8		
Monthly	60.0		
Quarterly	180.0		
Annual	160.0		
TOTAL	1265.3		

standard instrumentation, the 1 cps magnifications are not representative of the overall system gain.

Table 5. Gain correction factors for MAP systems utilizing time delays

	<u>System</u>	<u>Gain Correction Factor</u>
MAP I	BSS1	1.177
	BSS2	1.177
	BSS3	1.177
	BSS4	1.177
	BSS5	1.177
	BSS6	1.177
MAP II	MCF12	1.124
	MCF13	1.359
	MCF14	1.245
	MCF15	1.247
	MCF16	1.380
	MCF17	1.380
	BSSV1	1.359
	BSSV2	1.217
	BSSV3	2.740
	BSSV4	1.359
	BSSV5	1.217
	BSSV6	2.880

## 5. NOISE DATA

### 5.1 VISUAL NOISE MEASUREMENTS DATA

Visual noise measurements were made for 10 MAP systems, using the sampling and measuring techniques that are used for the routine noise measurements from the standard UBSO seismograms. The measurements were made from 16-millimeter film seismograms recorded during the period from 1 January 1967 through 12 March 1967. Cumulative frequency distributions of trace amplitude, normalized to a gain of 1000K at 1 cps are presented in figures 3 and 4 for the MAP I and MAP II systems, respectively. Figure 3 includes distributions for SZ10 and  $\Sigma$ SSF covering the same period of time.

Table 6 lists, for each system, the average trace amplitude computed from the visual noise measurements, normalized to a gain of 1000K at 1 cps, over the period band 0.4 second to 1.4 seconds.

## 5.2 POWER SPECTRAL DENSITY ESTIMATES

### 5.2.1 Procedure and Results

Power spectral density estimates were computed for samples of noise recorded by  $\Sigma$ SSF of the primary system, MCF4, MCF1, and MCF3 of MAP I, and MCF11, MCF12, and MCF13 of MAP II. Samples, 149 seconds in duration, were selected from four conditions of noise as follows:

- a. Low microseismic noise without road noise (noise type E);
- b. Low microseismic noise with strong road noise (noise type ER);
- c. Intermediate microseismic noise without road noise (noise type F);
- d. High microseismic noise without road noise (noise type G).

The noise samples for each system, which had been recorded on analog magnetic tape at UBSO, were anti-alias filtered and digitized at a rate of 25 samples per second. Power spectra were computed by means of Program FTBLKY1, using 10 percent lags. Power spectra for the four noise types for systems  $\Sigma$ SSF, MCF4, MCF1, MCF3, MCF11, MCF12, and MCF13 are presented in figures 5 through 32, respectively. The six MAP channels were each recorded at a higher level than the  $\Sigma$ SSF, consequently, the tape noise for the  $\Sigma$ SSF was closer to the seismic noise than was the tape noise on the MAP systems. All the spectra for noise type G show sharp peaks at 3 and 4 cps. These spectral peaks represent system noise and should be disregarded in interpreting these data. The spectra for noise types E, F, and G as recorded by  $\Sigma$ SSF show a sharp peak at 2.7 cps. The MAP systems recorded the same peak for noise types E, F, and G, but less strongly. The road noise power (noise type ER) is centered at the same frequency. However, the fact that this noise peak of noise types E, F, and G was recorded more strongly by MCF4 than by MCF1 indicates that it does not represent road noise present in the samples selected for noise types E, F, and G.

### 5.2.2 Discussion

The level of the noise power recorded by MCF12 was generally 5 to 10 dB less than the level of the noise power recorded by MCF11. This is attributed to the fact that MCF12 operates on the 6 elements of the vertical array in addition to the 10 elements of the shallow-buried array; whereas, MCF11 operates on the 10 elements of the shallow-buried array only. The level of the noise power recorded by MCF13, which operates on the 6 elements of the vertical array only, was 10-20 dB greater than the noise level recorded by MCF11. This high noise power recorded by MCF13 seems unreasonable, but is consistent with the results of the visual noise measurements (section 5.1).

Table 4. Average noise trace amplitude in the period band 0.4 second to 1.4 seconds, normalized to a magnification of 1000K at 1 cps, for MAP I, MAP II, and primary systems; from visual noise measurements

System	Primary		MAP I			MAP II						
	SZ10	ΣSSF	MCF4	MCF1	MCF3	ΣSBS	MCF11	MCF12	MCF13	MCF14	MCF16	BSSVI
Average trace amplitude (mm X10 view at 1000K)	3.68	1.38	2.10	2.07	2.04	1.99	1.96	1.22	6.88	2.18	2.12	0.79

Comparison of the noise spectra for the systems which operate only on elements of the surface array or the shallow-buried array give the following results:

a. In the frequency range 0.33 to 0.80 cps, MCF's 1, 3, and 4, each recorded less noise power than did  $\Sigma$ SSF. Of these three MCF seismographs, the noise power in this frequency band was smallest on MCF3 and greatest on MCF4 for all noise types. MCF11 recorded about the same level of noise as did  $\Sigma$ SSF, except for noise type G.

b. In the frequency range 0.8 to 2.0 cps, which is the frequency band in which most signal power normally occurs for teleseismic P-wave signals, differences in noise power recorded by the five systems were minor for all noise types. The greatest difference in noise power in this frequency band occurred for the road noise sample (noise type ER), for MCF4, which was designed specifically to attenuate this type of noise, recorded the lowest noise level. The difference in noise power recorded by MCF4 and the noise power recorded by  $\Sigma$ SSF in this frequency band was about 2 dB.

c. In the frequency range 2.0 to 3.0 cps, MCF11 recorded the smallest level of noise power, MCF1 or  $\Sigma$ SSF recorded the second smallest noise level, MCF4 recorded the third smallest noise level, and MCF3 recorded the largest noise level for noise types E, F, and G. For noise type ER, the noise power recorded by MCF4 was much less than that recorded by the other systems. The noise power recorded by MCF4 was about 10 dB less than the noise power recorded by MCF1 for noise type ER in this frequency band. The noise sample selected for this noise type is an extreme example of the road noise observed at UBSO.

It is clear from these results that, except perhaps for MCF13, these MAP systems successfully attenuate the noise that they were designed to attenuate. It is also clear that the major improvement in noise attenuation of the MAP systems over the noise attenuation of the simple summation occurs at frequencies outside the frequency band of major interest. Within the frequency band in which the power of most signals of interest is concentrated, none of the MAP systems rejected significantly more noise power than did  $\Sigma$ SSF. Note that within this frequency band (0.8 to 2.0 cps), the frequency responses of  $\Sigma$ SSF and the MAP band-pass filter are identical (figure 2).

## 6. CHARACTERISTICS OF SIGNALS AND NOISE RECORDED BY MAP I SYSTEMS

The characteristics of signals and noise as recorded by MCF's 1, 3, and 4 and  $\Sigma$ SBS of MAP I are in general quite similar. MCF3 typically records a higher level of high frequency noise than the other systems. MCF4 attenuates

the road noise to a greater degree than the other systems, but usually records a higher noise level under other noise conditions. This behavior is to be expected from the design of the systems. An example of strong road noise as recorded by the MAP I systems is presented in figure 33. The same noise sample as recorded by the primary data system is shown in figure 34. This figure shows a part of the noise sample used to compute power spectral density estimates discussed in section 5.2. MCF4 attenuates this particular noise much better than do the other systems. Amplitudes of the noise recorded by individual elements of the shallow-buried array indicate that the energy propagated in a southeasterly or south-southeasterly direction and was attenuated as it traveled across the array (figure 34). Phase relations among SZ10 and the two horizontal seismograms indicate that the noise is a Rayleigh wave. Note that the noise was recorded more strongly on BSS2 than on the other beam-steered summations (figure 33). BSS2 is steered to a velocity of 8.1 kilometers/second and an azimuth of 60 degrees. Using a frequency of 2.7 cps for the road noise, BSS2 is steered to a wave number of 0.334 cycles/kilometer and an azimuth of 60 degrees. It is clear that the beam-steered summations are aliasing this high frequency Rayleigh noise. A velocity of about 1.2 kilometers/second and a south-southeasterly direction of propagation of the noise will account for the road noise being recorded most strongly on BSS2. This velocity is a reasonable value for fundamental mode Rayleigh energy at a frequency of 2.7 cps for the UBSO area, and the direction of propagation is consistent with the direction estimated from the primary data.

An example of high-frequency noise that is not road noise as recorded by the MAP I systems and by the primary data system is presented in figures 35 and 36, respectively. MCF4 recorded a higher level of noise than MCF1 or  $\Sigma$ SBS in this case, as expected.

An example of a near-regional signal from an epicentral distance of 1.9 degrees and an azimuth of 285 degrees from UBSO as recorded by the MAP I systems and by the primary system is presented in figures 37 and 38, respectively. MCF3, which was designed from a conical signal model of 8.1 kilometers/second to infinite velocity, recorded the  $P_n$  phase of this signal much better than did MCF4 or MCF1, both of which were designed from a line signal model of infinite velocity. As expected, the beam-steered summation whose steered azimuth is closest to the azimuth of the signal source (BSS6), recorded  $P_n$  more strongly than did the other beam-steered summations or the simple summation ( $\Sigma$ SBS), and MCF3 recorded  $P_n$  well. The beam-steered summations are effective in determining the approximate azimuth to the source of signals from near-regional distances. However, a steered velocity of 7.9 kilometers/second would be a more reasonable value of  $P_n$  velocity for the UBSO area than is 8.1 kilometers/second, the value used in the design of the MAP I beam-steered summations.

An example of a near teleseismic signal from an epicentral distance of 26.1 degrees and an azimuth of 155 degrees from UBSO as recorded by the MAP I

systems and by the primary system is shown in figures 39 and 40, respectively. The signal character as recorded by MCF3 is not significantly different from the signal character as recorded by MCF1, MCF4, or  $\Sigma$ SBS. The direction indication given by the beam-steered summations is weak, although still useful for signals from events in this distance range. For signals from greater distances, beam-steered summations of an array the size of the present UBSO array will not give a direction or velocity determination.

An example of a weak teleseismic signal occurring in a road noise background is presented in figures 41 and 42 as recorded by the MAP I systems and by the primary system, respectively. MCF4 did not record this signal appreciably better than did the other systems.

An example of a weak teleseismic signal (C&GS magnitude 3.7) occurring in a background free of road noise is shown in figures 43 and 44 as recorded by the MAP I systems and by the primary system, respectively. The performance of the simple summation in recording this signal was slightly superior to the performance of the multichannel filters of MAP I.

## 7. CHARACTERISTICS OF SIGNALS AND NOISE RECORDED BY MAP II SYSTEMS

### 7.1 GENERAL

The response of MCF11, which is a multichannel filter operating on the elements of the shallow-buried array, to signals and noise is very similar to the responses of the MAP I systems, except that signals as recorded on MCF11 usually are slightly more readily detected than they are as recorded on the MAP I systems (see section 8). MCF12, which operates on elements of the shallow-buried array and elements of the vertical array records a lower noise level than does MCF11, but the signal level recorded by MCF12 is also lower than the signal level recorded by MCF11. Overall, MCF12 proved to be slightly inferior to MCF11.

All of the systems which use vertical array data exhibit a high level of high-frequency noise, due to the frequency response of the elements of the vertical array (figure 2). Use of a frequency response with greater attenuation at the high-frequency end of the spectrum should improve the performance of these systems to some degree.

### 7.2 DEGHOST FILTERS

Of the two pairs of deghost filters, the pair MCF16-17, operating on the vertical array elements at 7903 feet, 5894 feet, and 3907 feet, usually records signals slightly better than does the pair MCF14-15, which operates on the

vertical array elements at 8895 feet, 6910 feet, and 4901 feet. For both pairs of deghost filters, the difference in arrival times of upgoing and downgoing deghosted output traces is valuable in identifying the signal wave type. For a vertically incident P-wave, this arrival time difference is 1.1 seconds. For weak signals at the threshold of detectability, the arrival-time difference between incident and reflected waves cannot be determined accurately, and the similarity in signature is obscured by noise. The deghost filters, especially MCF14-15, exhibit a precursor effect which, in some cases, interferes with accurate interpretation of the signal. An example of this precursor effect is presented in figure 45, which shows a teleseismic P-wave signal as recorded by the MAP II systems. The same signal recorded by the vertical array is shown in figure 46. Note the clearer recording of the signal on BSSV1-4 and MCF16-17 (figure 45) than on MCF14-15.

### 7.3 BEAM-STEERED SUMMATIONS OF VERTICAL ARRAY ELEMENTS

The beam-steered summations of vertical array elements designed to enhance 8.1 kilometers/second P-waves (BSSV2 and BSSV5) and 8.1 kilometers/second S-waves (BSSV3 and BSSV6) contribute nothing to the capability of the MAP II system. The difference in moveout across the vertical array between a 7.9 kilometers/second P-wave and a vertically incident P-wave is only about 0.15 second, which is inadequate to serve as a criterion to distinguish these wave types. A velocity of 4.5 kilometers/second would be a reasonable steered velocity for  $S_n$  in the UBSO area.

On the other hand, the two beam-steered summations designed to enhance vertically incident P-waves (BSSV1 for up-going wave and BSSV4 for down-going wave), in conjunction with the individual elements of the vertical array (DH1 - DH6), form a very effective system. The difference in signal arrival time recorded by the up-going (BSSV1) and down-going (BSSV4) beam-steered summations affords valuable evidence of signal type, as is the case with the deghost filters. For signals strong enough to be well recorded by the individual elements of the vertical array, the moveout across the vertical array is valuable in distinguishing P-wave signals from horizontally-traveling energy. One-way and two-way travel times across the vertical array are given in figure 47. The pair of beam-steered summations BSSV1 and BSSV4 show essentially the same signal character as the pair of deghost filters MCF16 and MCF17, except for long-duration signals. The beam-steered summations usually exhibit a greater S/N than do the deghost filters (section 9). This is probably attributable to the fact that the beam-steered summations operate on six elements, whereas, the deghost filters operate on only three elements. An example of a P-wave signal with simple character as recorded by the MAP II systems and as recorded by the vertical array is presented in figures 48 and 49, respectively. Note the similarity in signal character recorded by

BSSV1 and MCF16.) An example of a short-duration pulse of horizontally-traveling energy as recorded by the MAP II systems and as recorded by the vertical array is shown in figures 50 and 51, respectively. Note the lack of step-out recorded by the up-going and down-going deghost filters and beam-steered summations (figure 50) and the simultaneous arrival time recorded by the elements of the vertical array (figure 51). Note also, the weak P-wave signal arriving 5.3 seconds after the start of the Rayleigh pulse (figure 50). An example of a longer duration P-wave signal is presented in figures 52 and 53 as recorded by the MAP II systems and as recorded by the vertical array, respectively. Note that the signal waveform recorded by BSSV is almost identical to the signal waveform recorded by MCF16 for the first 2-1/2 cycles of the signal.

## 8. VISUAL SIGNAL-TO-NOISE RATIO COMPARISON

### 8.1 GENERAL

A comparison of signal-to-noise ratio (S/N), based on visual measurements of signal and noise amplitudes and periods, was made for 10 MAP systems together with an individual seismograph of the shallow-buried array (SZ10) and the filtered shallow-buried array seismograph ( $\Sigma$ SSF) for approximately 100 signals.

### 8.2 PROCEDURE

For each signal, the peak-to-peak amplitude and its associated period were measured from the film seismograms recorded by each system. The peak-to-peak amplitude and its associated half-period of each half cycle of the noise in the 10-second interval immediately preceding the signal onset were also measured for each system. From these noise measurements, the average noise amplitude in the period range within  $\pm 0.3$  second of the signal period was computed for each system. The S/N for each system was then computed as the ratio of signal amplitude to average noise amplitude for the given system.

### 8.3 RESULTS

Cumulative frequency distributions of S/N for MCF4, MCF1, MCF3, and  $\Sigma$ SBS of MAP I and SZ10 and  $\Sigma$ SSF of the primary system are presented in figure 54. Cumulative frequency distributions of S/N for MCF11, MCF12, MCF13, MCF14, MCF16, and BSSV1 of MAP II are presented in figure 55. The average S/N for each system ( $S/N_{Sys}$ ) relative to the average S/N for  $\Sigma$ SBS ( $S/N_{\Sigma SBS}$ ) is given in table 7. For each system, the percent of events with S/N greater than, equal to, and less than the S/N recorded by  $\Sigma$ SBS are listed in table 8. The  $\Sigma$ SBS was used as the reference system because it is a

Table 7. Average S/N for each system  $(\overline{S/N})_{\text{Sys}}$  relative to average S/N for  $\Sigma\text{SBS}$   $(\overline{S/N})_{\Sigma\text{SBS}}$ , for MAP I, MAP II, and primary systems

System	MAP I				MAP II							
	$\Sigma\text{SSF}$	$\overline{\text{MCF4}}$	$\overline{\text{MCF1}}$	$\overline{\text{MCF3}}$	$\Sigma\text{SBS}$	$\overline{\text{MCF11}}$	$\overline{\text{MCF12}}$	$\overline{\text{MCF13}}$	$\overline{\text{MCF14}}$	$\overline{\text{MCF16}}$	$\overline{\text{BSSV1}}$	
$(\overline{S/N})_{\text{Sys}} / (\overline{S/N})_{\Sigma\text{SBS}}$	0.55	1.11	0.94	0.98	0.99	1.00	1.06	1.01	0.87	0.92	0.94	1.06

Table 8. Percent of events with S/N greater than, equal to, and less than the S/N for  $\Sigma\text{SBS}$ , for MAP I, MAP II, and primary systems

System	MAP I				MAP II							
	$\Sigma\text{SSF}$	$\overline{\text{MCF4}}$	$\overline{\text{MCF1}}$	$\overline{\text{MCF3}}$	$\Sigma\text{SBS}$	$\overline{\text{MCF11}}$	$\overline{\text{MCF12}}$	$\overline{\text{MCF13}}$	$\overline{\text{MCF14}}$	$\overline{\text{MCF16}}$	$\overline{\text{BSSV1}}$	
$\%(\overline{S/N})_{\text{Sys}} > (\overline{S/N})_{\Sigma\text{SBS}}$	7.2	58.3	38.2	41.2	36.2	0	49.5	47.9	35.4	39.4	36.4	47.9
$\%(\overline{S/N})_{\text{Sys}} = (\overline{S/N})_{\Sigma\text{SBS}}$	4.1	14.6	14.4	15.5	17.0	100.0	19.6	13.3	8.3	7.4	5.7	9.4
$\%(\overline{S/N})_{\text{Sys}} < (\overline{S/N})_{\Sigma\text{SBS}}$	88.7	27.1	47.4	43.3	46.8	0	30.9	38.8	56.3	53.2	57.9	42.7

simple summation with the frequency filtering used in all the MAP systems. Therefore, any improvement in noise rejection or signal enhancement due to multichannel filtering over that achieved by summation and frequency filtering should appear as an increase in S/N over the S/N observed on  $\Sigma$ SBS.

#### 8.4 DISCUSSION

The only systems which show a significantly greater average S/N than  $\Sigma$ SBS are  $\Sigma$ SSF, MCF11, and BSSV1. The superiority of  $\Sigma$ SSF over  $\Sigma$ SBS is attributed to the narrower pass band of the frequency filter of  $\Sigma$ SSF and to the fact that  $\Sigma$ SSF operates on the elements of the shallow-buried array, whereas,  $\Sigma$ SBS operates on the elements of the surface array. The superior performance of MCF11 over that of  $\Sigma$ SBS is attributed to the fact that MCF11 operates on elements of the shallow-buried array rather than to the fact that MCF11 is a multichannel filter whose design is based on measured noise correlations. The multichannel filters designed from measured noise correlations which operate on elements of the surface array (MCF1, MCF3, and MCF4) all proved to be inferior to the simple summation operating on the same elements ( $\Sigma$ SBS). The only MAP system using elements of the vertical array which proved to be appreciably superior to  $\Sigma$ SBS in the S/N study was BSSV1, which is a simple beam-steered summation using all six elements of the vertical array, with time delays to enhance vertically-incident P-waves. BSSV1 was superior to both MCF14 and MCF16, each of which is a deghosting filter operating on 3 elements of the vertical array, and was much superior to MCF13, which is a multichannel filter operating on all 6 elements of the vertical array, designed from a theoretical noise model.

### 9. DETECTION CAPABILITY COMPARISON

#### 9.1 DATA SAMPLE

Using data recorded at UBSO from 1 February through 12 March 1967, a comparison was made of the detection capabilities of three systems, defined as follows:

System 1 - (Primary data system): SZ1 - SZ10,  $\Sigma$ SS,  $\Sigma$ SSF

System 2 - (MAP I data system): MAP I systems plus Z1, Z2, Z3, Z5, Z6, Z10

System 3 - (MAP II data system): those systems of MAP II which use only elements of the vertical array plus DH1 - DH6,  $\Sigma$ DH,  $\Sigma$ DHF.

Only data intervals during which all systems were fully operational were used. Only first arrivals (P or PKP phase) from earthquakes at teleseismic distance from UBSO were used. During routine analysis of data recorded on system 1, 1080 events were identified as teleseismic by experienced station analysts at UBSO. Experienced analysts independently read seismograms recorded on systems 2 and 3 and graded each subsystem as to how well it detected each event recorded by the given system. A total of 483 events, identified as teleseismic by the analysts, were recorded by system 2, and a total of 519 teleseismic events were recorded by system 3 in the data interval. The difference in the number of detections is not necessarily indicative of the relative detection capabilities of the systems because there is no way to know how many of the analyst selections are valid teleseisms. The C&GS located 273 hypocenters at teleseismic distance from UBSO during the data interval. The number of C&GS hypocenters used in the study are given in table 9 as a function of epicentral distance from UBSO and C&GS magnitude.

## 9.2 PROCEDURE AND RESULTS

The signals called on systems 2 and 3 were tested for association with the C&GS-located earthquakes using the same criteria of association as those used in the Automated Bulletin Program (and also in associating system 1 data); i. e., arrival time residuals from predicted arrival times (computed by Seismic Data Laboratories) of +7 seconds to -6 seconds for P and +15 seconds to -12 seconds for PKP. The percent of C&GS-located events detected by each of the three systems and by combinations of the systems are presented in table 10 as a function of epicentral distance from UBSO and in table 11 as a function of C&GS magnitude. Of the 273 C&GS-located earthquakes that occurred more than 70 degrees from UBSO, the primary data system (system 1) detected 75.5 percent, the MAP I data system (system 2) detected 61.1 percent, and the MAP II data system (system 3) detected 59.0 percent. Of the 273 events, 77.7 percent were detected by at least one of the three systems. Six events were missed by the primary system and detected by MAP I and/or MAP II. Forty-five events were missed by MAP I and detected by the primary system and/or MAP II. Fifty-one events were missed by MAP II and detected by the primary system and/or MAP I. The primary system detected 39 events which were missed by both MAP I and MAP II. MAP I detected only one event which was missed by both the primary system and MAP II. MAP II detected no events which were missed by both the primary system and MAP I. Sixty-one of the 273 events were missed by all three systems. Of these, 51 were in the shadow zone and/or had no C&GS magnitude, indicating they were probably weak.

## 9.3 EVALUATION OF SUBSYSTEMS

While analyzing the MAP I and MAP II seismograms, the analysts graded each subsystem as to how well it detected each event. The grading system is based on a grade value range of 0 to 10 (0 failed to detect the event; 10 detected the event best), with intermediate grade values uniformly distributed

Table 9. Number of C&GS-located hypocenters as a function of epicentral distance from UBSO and C&GS magnitude

Epicentral distance (degrees)	No mag. reported	<u>C&amp;GS MAGNITUDE</u>							<u>Total</u>
		<u>3.5</u>	<u>4.0</u>	<u>4.5</u>	<u>5.0</u>	<u>5.5</u>	<u>6.0</u>	<u>6.5</u>	
20-30	0	4	9	4	1	1	0	0	19
30-40	1	0	8	4	1	1	0	0	15
40-50	0	1	14	18	3	0	1	0	37
50-60	0	1	3	9	3	1	0	0	17
60-70	1	0	3	8	2	0	0	0	14
70-80	0	0	7	9	0	3	0	0	19
80-90	2	1	5	22	12	3	0	1	46
90-100	6	0	2	21	18	6	2	0	55
100-110	1	0	0	7	10	2	0	0	20
110-120	4	0	0	0	11	2	0	0	17
120-130	3	0	0	0	1	0	0	0	4
130-140	1	0	0	1	3	2	1	0	8
140-150	0	0	0	0	1	0	0	0	1
150-160	0	0	0	0	0	0	0	0	0
160-170	0	0	0	0	0	1	0	0	1
<u>170-180</u>	<u>0</u>	<u>0</u>	<u>0</u>	<u>0</u>	<u>0</u>	<u>0</u>	<u>0</u>	<u>0</u>	<u>0</u>
Total	19	7	51	103	66	22	4	1	273

Table 10. Percent of C & GS-located events detected by each system, as a function of epicentral distance from UBSO

Epicentral distance (degrees)	SYSTEM						
	Primary	MAP I	MAP II	Primary or MAP I	Primary or MAP II	MAP I or MAP II	Primary or MAP I or MAP II
20-30	89.5	89.5	78.9	89.5	89.5	89.5	89.5
30-40	66.7	60.0	53.3	73.4	73.4	60.0	73.4
40-50	89.2	70.3	75.7	91.9	91.9	78.4	91.9
50-60	94.2	64.7	70.6	100.0	100.0	70.6	100.0
60-70	85.7	92.9	85.7	92.9	85.7	92.9	92.9
70-80	94.7	78.9	73.6	100.0	100.0	78.9	100.0
80-90	97.8	86.9	82.6	97.8	97.8	86.9	97.8
90-100	50.9	32.7	30.9	50.9	50.9	32.7	50.9
100-110	10.0	5.0	5.0	10.0	10.0	5.0	10.0
110-120	70.6	29.4	35.3	70.6	70.6	41.2	70.6
120-130	100.0	100.0	100.0	100.0	100.0	100.0	100.0
130-140	100.0	75.0	50.0	100.0	100.0	75.0	100.0
140-150	100.0	100.0	100.0	100.0	100.0	100.0	100.0
150-160	--	--	--	--	--	--	--
160-170	0.0	100.0	100.0	100.0	100.0	100.0	100.0
170-180	--	--	--	--	--	--	--
20-180	75.5	61.1	59.0	77.6	77.4	63.4	77.7

Table 11. Percent of C&GS-located events detected by each system, as a function of C&GS magnitude

C&GS magnitude	SYSTEM						
	Primary	MAP I	MAP II	Primary or MAP I	Primary or MAP II	MAP I or MAP II	Primary or MAP I or Map II
no mag	31.6	21.0	21.0	31.6	31.6	21.0	31.6
3.5	100.0	85.7	71.5	100.0	100.0	85.7	100.0
4.0	86.3	62.7	56.8	88.2	86.3	64.7	88.2
4.5	78.6	63.1	62.1	80.6	80.6	65.1	80.6
5.0	66.7	53.0	51.5	66.7	66.7	57.6	66.7
5.5	90.9	95.5	95.5	100.0	100.0	95.5	100.0
6.0	75.0	75.0	75.0	100.0	100.0	75.0	100.0
6.5	100.0	100.0	100.0	100.0	100.0	100.0	100.0
<u>all events</u>	<u>75.5</u>	<u>61.1</u>	<u>59.0</u>	<u>77.6</u>	<u>77.4</u>	<u>63.4</u>	<u>77.7</u>

between 0 and 10. The average grade values for the subsystems of MAP I and MAP II are given in tables 12 and 13, respectively.

Table 12. Average detection grades for subsystems, MAP I

<u>System</u>	<u>Average detection grade</u>
Z	1.86
MCF4	6.22
MCF1	6.74
MCF3	6.48
$\Sigma$ SBS	8.56

Table 13. Average detection grades for subsystems, MAP II

<u>System</u>	<u>Average detection grade</u>
MCF13	5.49
MCF14	7.21
MCF16	7.49
BSSV1	8.83
DH	2.33
$\Sigma$ D	2.49
$\Sigma$ DF	6.17

For the MAP I subsystems, the seismograms were so similar that the assignment of grades was almost arbitrary for most signal occurrences. The seismograms of the deghost filters and the beam-steered summations of MAP II were also very similar, except for differences in operating magnifications, for most signal occurrences. In addition, for moderately strong to strong signals, overlining of the traces makes evaluation of the relative worth of the subsystems difficult, especially on MAP II. For these reasons, the S/N comparison (section 9) is considered to be a more reliable method of ranking the subsystems than is the subjective assignment of grades. However, the results of this subjective grading are in general agreement with the results of the S/N comparison.

## 10. DISCUSSION AND CONCLUSIONS

### 10.1 GENERAL

None of the MAP systems are superior to the simple filtered summation of the 10 elements of the shallow-buried array ( $\Sigma$ SSF) for detecting weak tele-seismic signals. Therefore, none of the MAP systems should be considered as a possible replacement for  $\Sigma$ SSF. Considered as an addition to the standard UBSO instrumentation, certain of the MAP systems can increase the detection capability of the observatory slightly. The slight improvement in detection capability achievable by using one or more MAP systems in conjunction with the standard instrumentation must be weighed against the time and effort required to maintain the MAP systems.

### 10.2 MAP I

Of the MAP I systems, MCF4 helped slightly in the detection of weak signals when road noise was strong; at other times, MCF4 did not increase the capability of the observatory. MCF3 helped in identifying near-regional signals; however, the beam-steered summations performed this function more effectively, since they yielded an estimate of direction to the signal source. MCF1 did not add to the capability of the standard UBSO instrumentation.

If any of the MAP I systems are retained as part of the UBSO instrumentation, they should be redesigned to operate on the elements of the shallow-buried array rather than on the elements of the surface array.

### 10.3 MAP II

Of the MAP II systems, the beam-steered summations designed to enhance up-going and down-going vertically incident P-waves (BSSV1 and BSSV2) are the only ones of the existing systems that could be retained profitably. However, deghost filters (up-going and down-going), operating on all 6 elements of the vertical array or on the deep-hole elements plus one element of the shallow-buried array (SZ1), should be quite valuable. The outputs of the deghost filters should be recorded on the same Develocorder as are the outputs of the individual array elements (DH's and SZ1), together with the outputs of two beam-steered summations and a simple summation of the array elements. The frequency response of the DH elements should be shaped to match that of the shallow-buried array elements. The MAP band-pass frequency filter could be applied to each element of the array (DH's and SZ1) to attenuate the low-frequency microseisms and high frequency noise, thus making it possible to operate the individual array elements at a high gain. The optimum filter settings would need to be determined empirically, but would probably turn out to be close to the settings of the current MAP band-pass filter or the settings used for  $\Sigma$ SSF (section 2.2). If this band-pass filtering is not applied

to the individual array elements, it should be incorporated into the deghost filters, beam-steered summations, and the simple summation.

#### 10.4 POSSIBLE OTHER USES OF THE MAP SYSTEMS

The time-delay and sum capability of either of the MAP systems could be used to beam-steer an array of short-period seismometers larger than the present UBSO array. The maximum diameter of a proposed beam-steered array depends upon the maximum time delay available from the processor to be used and on the minimum velocity to which it is desired to steer the array. The delay lines of both MAP I and MAP II have a maximum delay time of 2.000 seconds. For a minimum steered velocity of interest of 8 kilometers/second, the maximum diameter of an array that could be beam-steered using these units is 16 kilometers. However, MAP I can accommodate inputs from only 10 seismometers which is too few for an array of this size. On the other hand, the 19-channel capacity of MAP II could be used effectively for this type of application. A 19-element hexagonal array with a uniform detector spacing of 4 kilometers and a diameter of 16 kilometers could be beam-steered by MAP II to a minimum velocity of 8 kilometers/second. The coherence properties of neither signals nor noise over the distances involved are known for the UBSO area. The coherence of both signals and noise as a function of distance would need to be determined before an array was implemented.

### 11. RECOMMENDATIONS

We recommend that operation of the current MAP systems at UBSO be discontinued.

We recommend that a 7-element vertical array, composed of the 6 deep-hole elements and SZ1, be implemented as soon as the deep-hole seismometers have been reinstalled in the deep hole. Optimum locations of the seismometers in the deep hole will be determined from the vertical array evaluation, currently in progress. We recommend that two deghost filters (one to enhance up-traveling vertically incident P-waves, the other to enhance the down-traveling reflected waves of vertically incident P-waves) and two beam-steered summations to enhance vertically incident P-waves (up-going and down-going) be designed to operate on the 7 elements of the recommended vertical array, after the locations of the 6 deep-hole seismometers in the deep hole have been established. A simple summation of the 7 elements of the recommended vertical array should also be provided. Band-pass frequency filtering, in addition to that imposed by the seismometer-galvanometer combination, should be applied to each output.

We recommend that the MAP I hardware be used to implement the deghost filters, beam-steered summations, and simple summation operating on the recommended 7-element vertical array.

The MAP II hardware will then be available for other uses; e.g., to beam-steer a 19-element short-period array, either at UBSO or at some other location, if required. We recommend that a study be undertaken to determine short-period signal coherence and noise coherence as a function of distance in the UBSO area, over the distance range of 1 kilometer to 30 kilometers. Knowledge of signal and noise coherence as a function of detector separation will provide a rational basis for the design of a medium sized array in the UBSO area.

## 12. REFERENCES

Edwards, J. P., III, 1965a, Texas Instruments Incorporated, Noise analysis for Uinta Basin Seismological Observatory: Technical report - UBSO

\_\_\_\_\_ 1965b, Texas Instruments Incorporated, Multiple array processor: Final report

Burrell, George C., and Lintz, Paul R., 1967, Texas Instruments Incorporated, Array research, array processing at UBO: Special report no. 22

Alsop, Stephen A., 1965, Geotech Division of Teledyne Industries, Preliminary evaluation of multiple array processing data at UBSO: Technical note no. 5/65

\_\_\_\_\_ 1966, Geotech Division of Teledyne Industries, Preliminary evaluation of the operation and maintenance of the multiple array processors at UBSO: Technical note no. 13/66

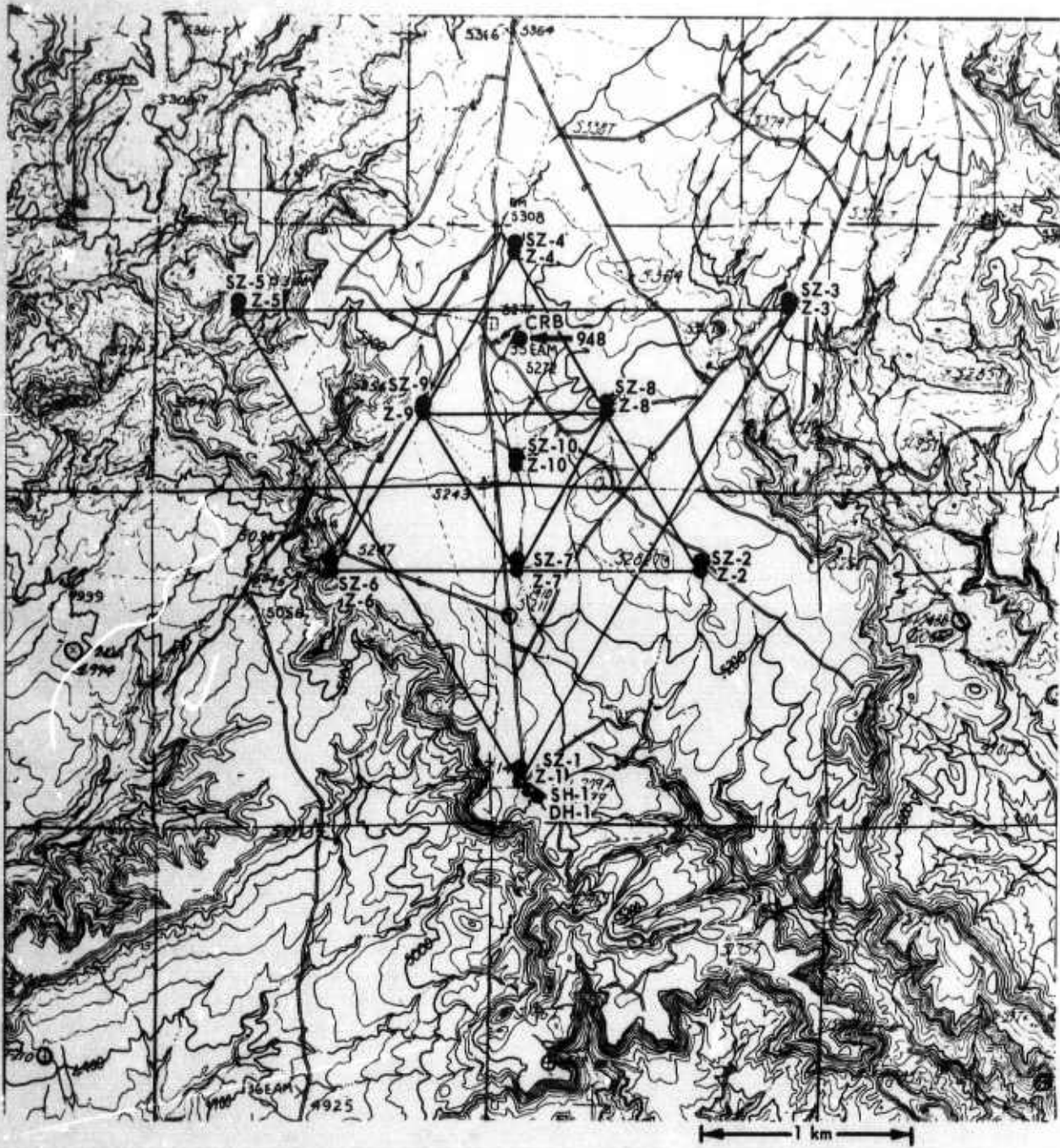


Figure 1. Orientation and configuration of UBSO arrays

G 901

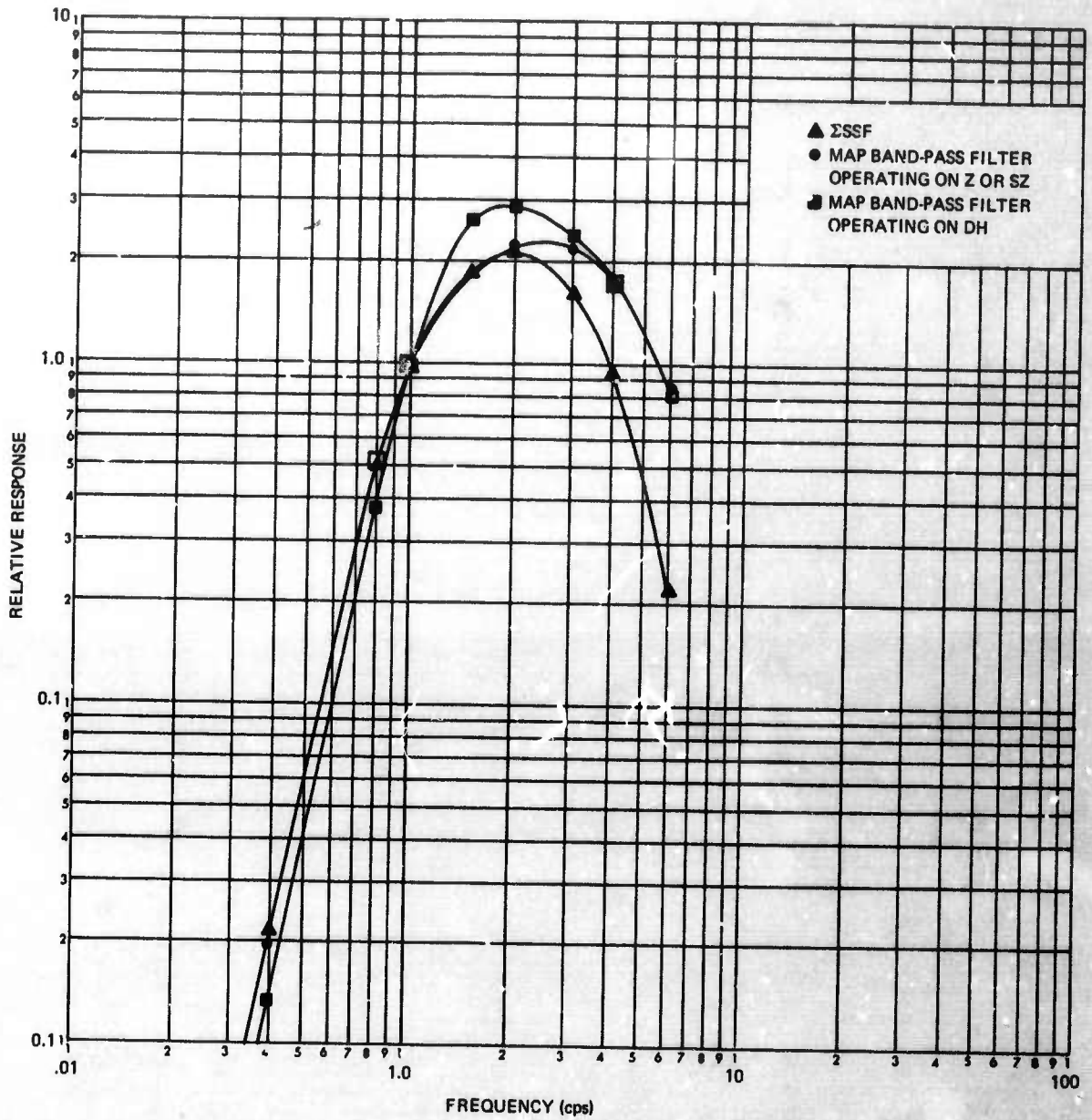


Figure 2. Relative frequency responses of the filtered summation of the shallow-buried array ( $\Sigma$ SSF) and of the MAP band-pass filter operating on elements of a surface array (Z or SZ) and on elements of the vertical array (DH)

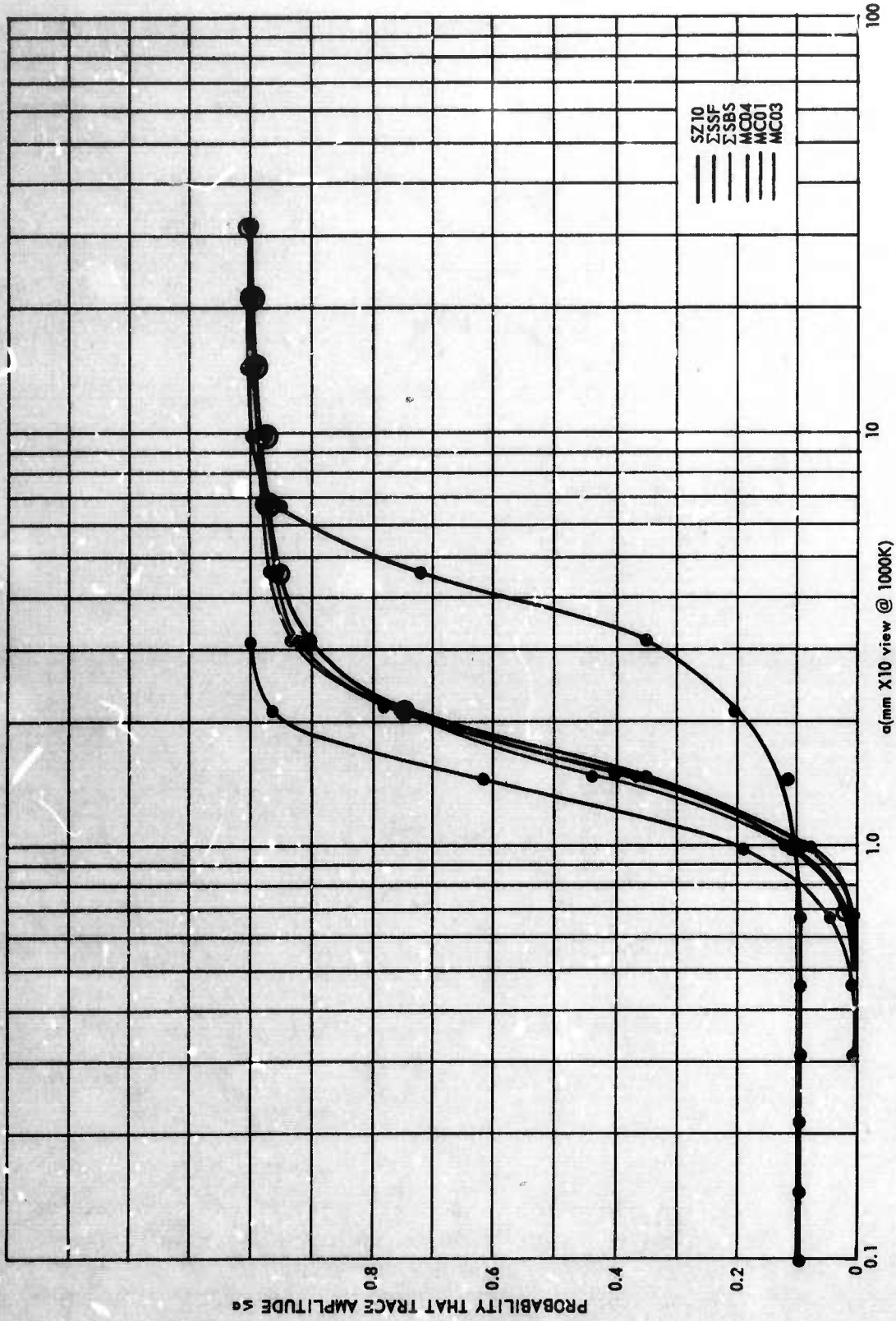


Figure 3. Cumulative frequency distributions of noise amplitudes in the period band 0.4-1.4 seconds recorded by MAP I and Primary systems, 1 January through 12 March 1967

G 2995

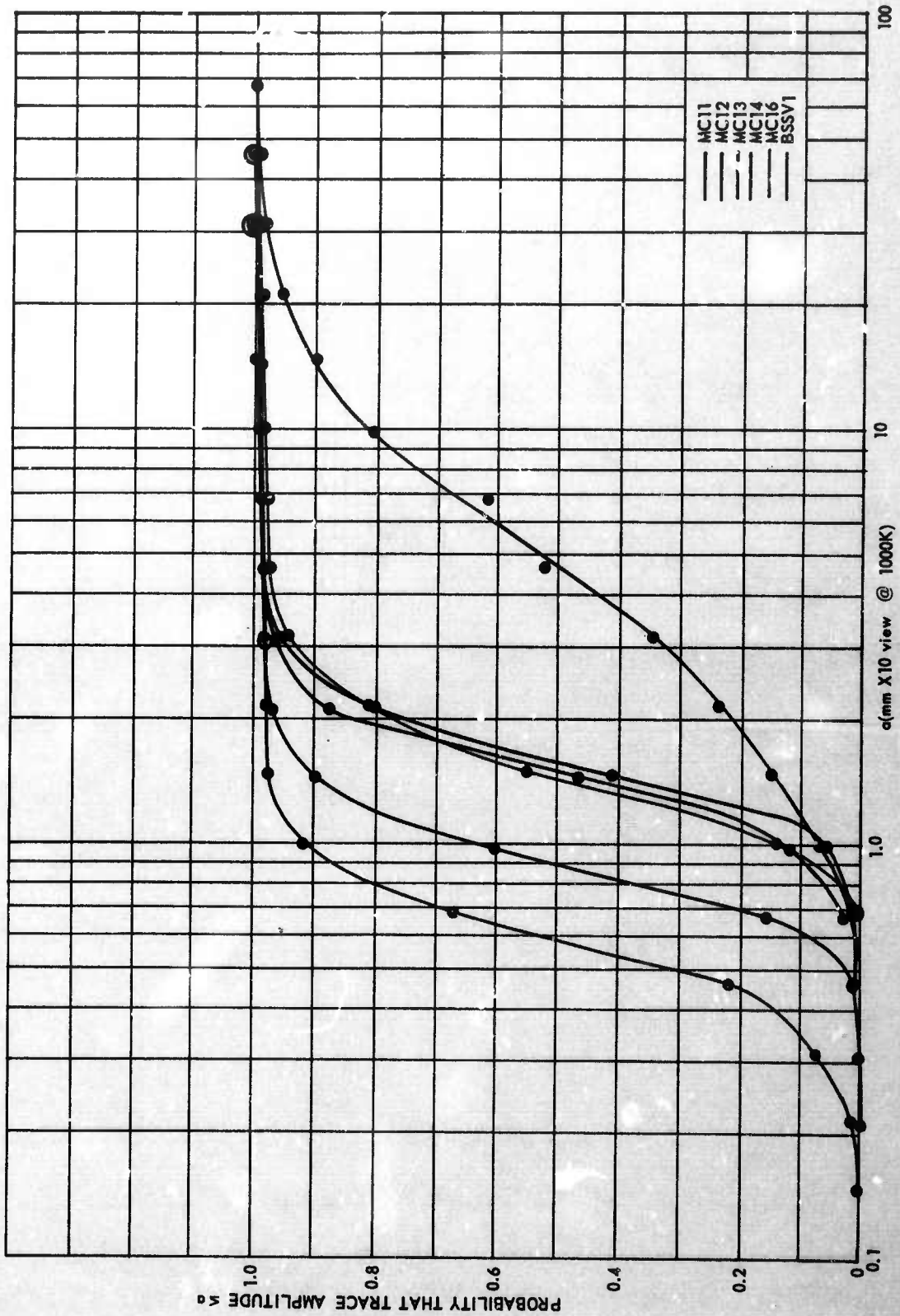


Figure 4. Cumulative frequency distributions of noise amplitudes in the period band 0.4-1.4 seconds recorded by MAP II systems, 1 January through 12 March 1967

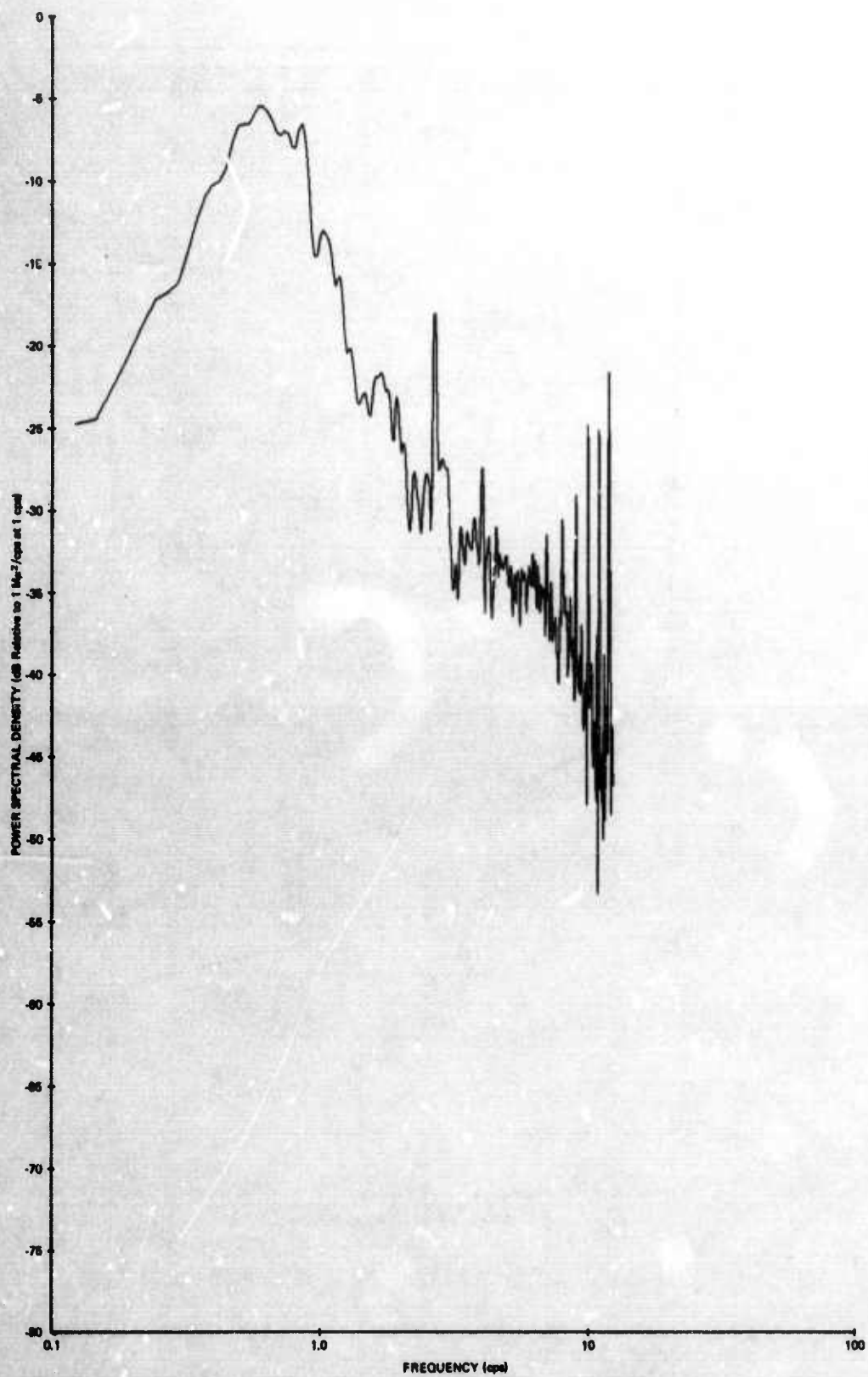


Figure 5. Power spectral density estimate of a sample of low-level microseismic noise, recorded by  $\Sigma$ SSF

G 3551

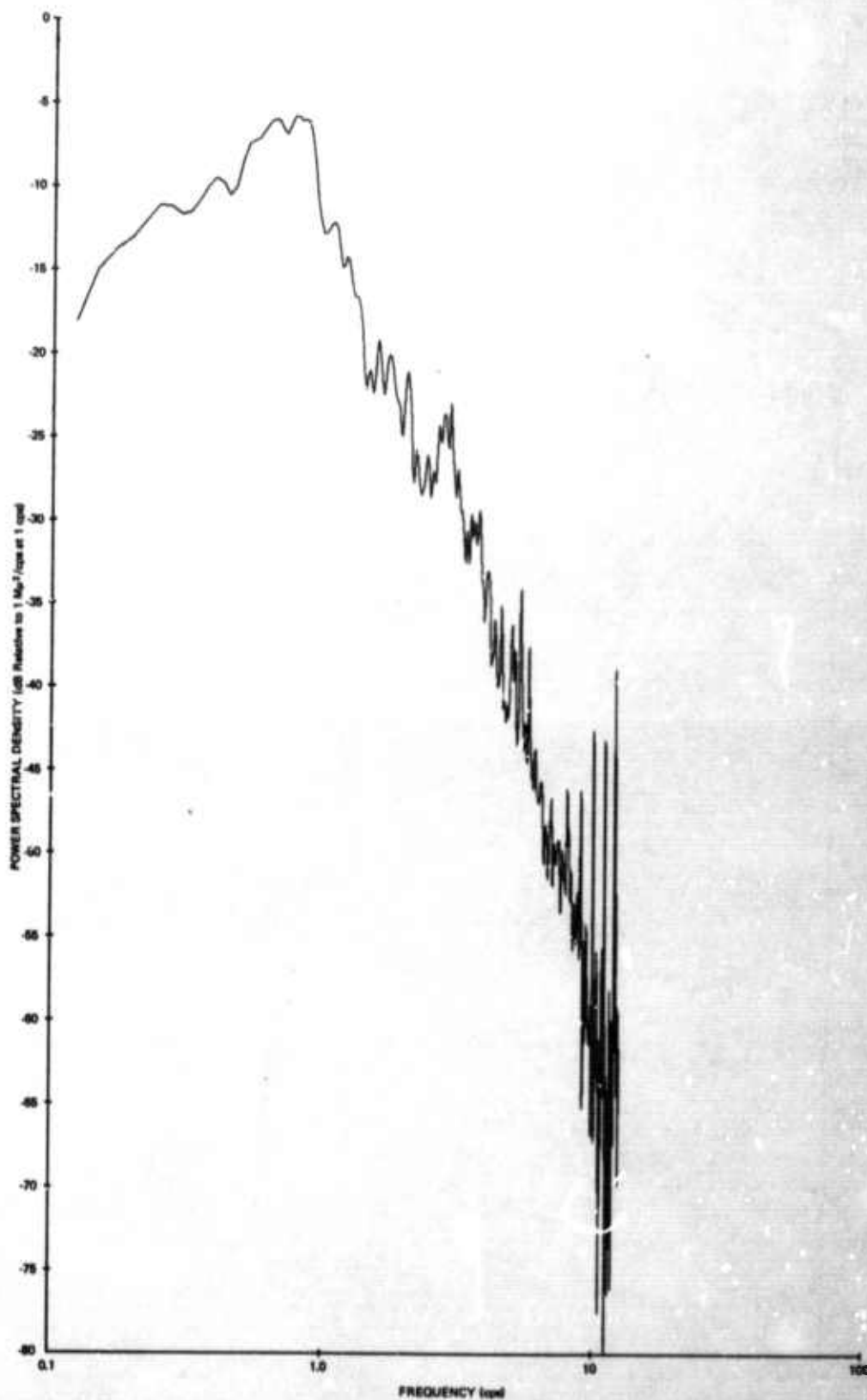


Figure 6. Power spectral density estimate of a sample of low-level microseismic noise, recorded by MCF4

G 3682

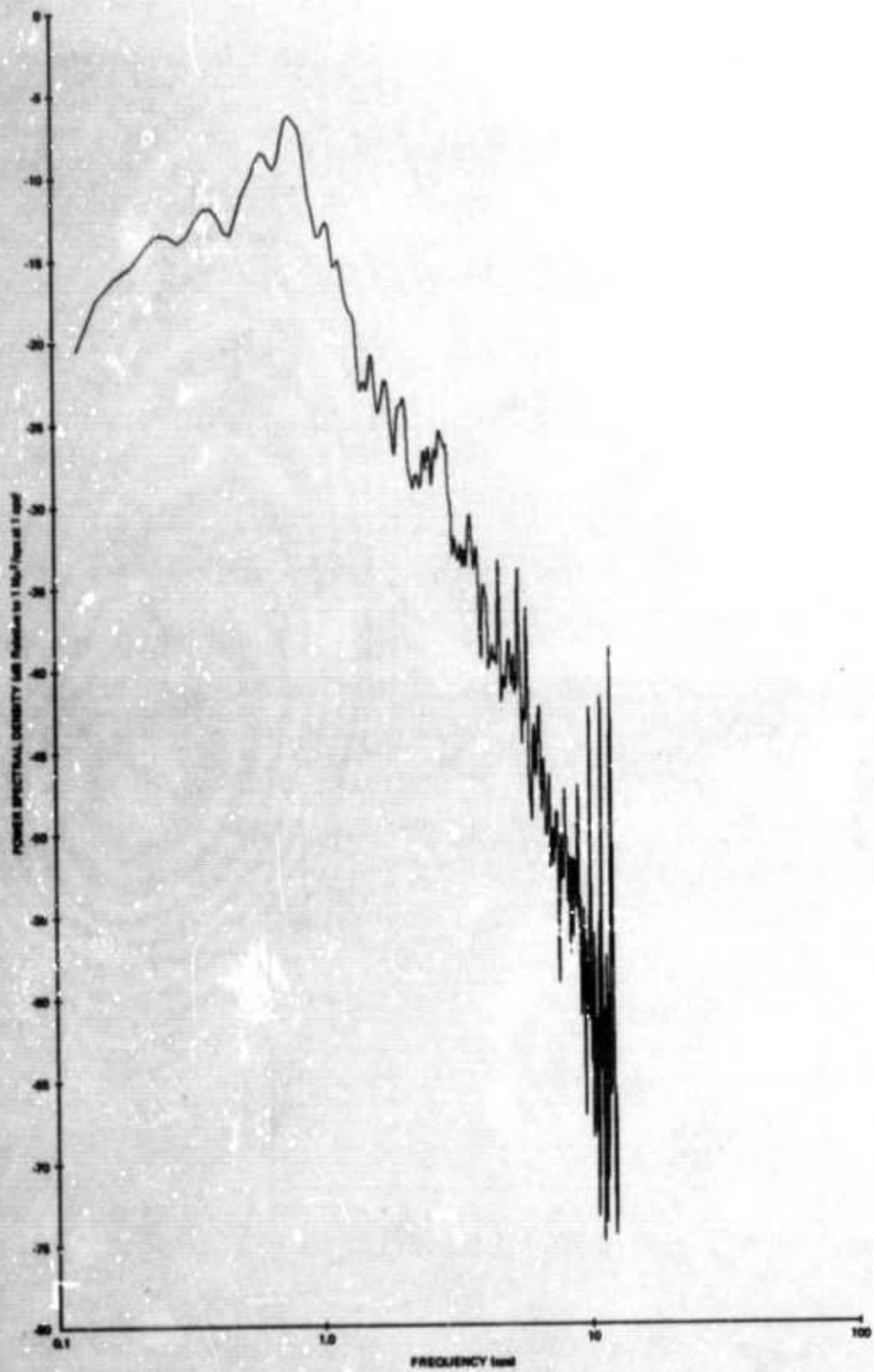


Figure 7. Power spectral density estimate of a sample of low-level microseismic noise, recorded by MCF1

G 3353

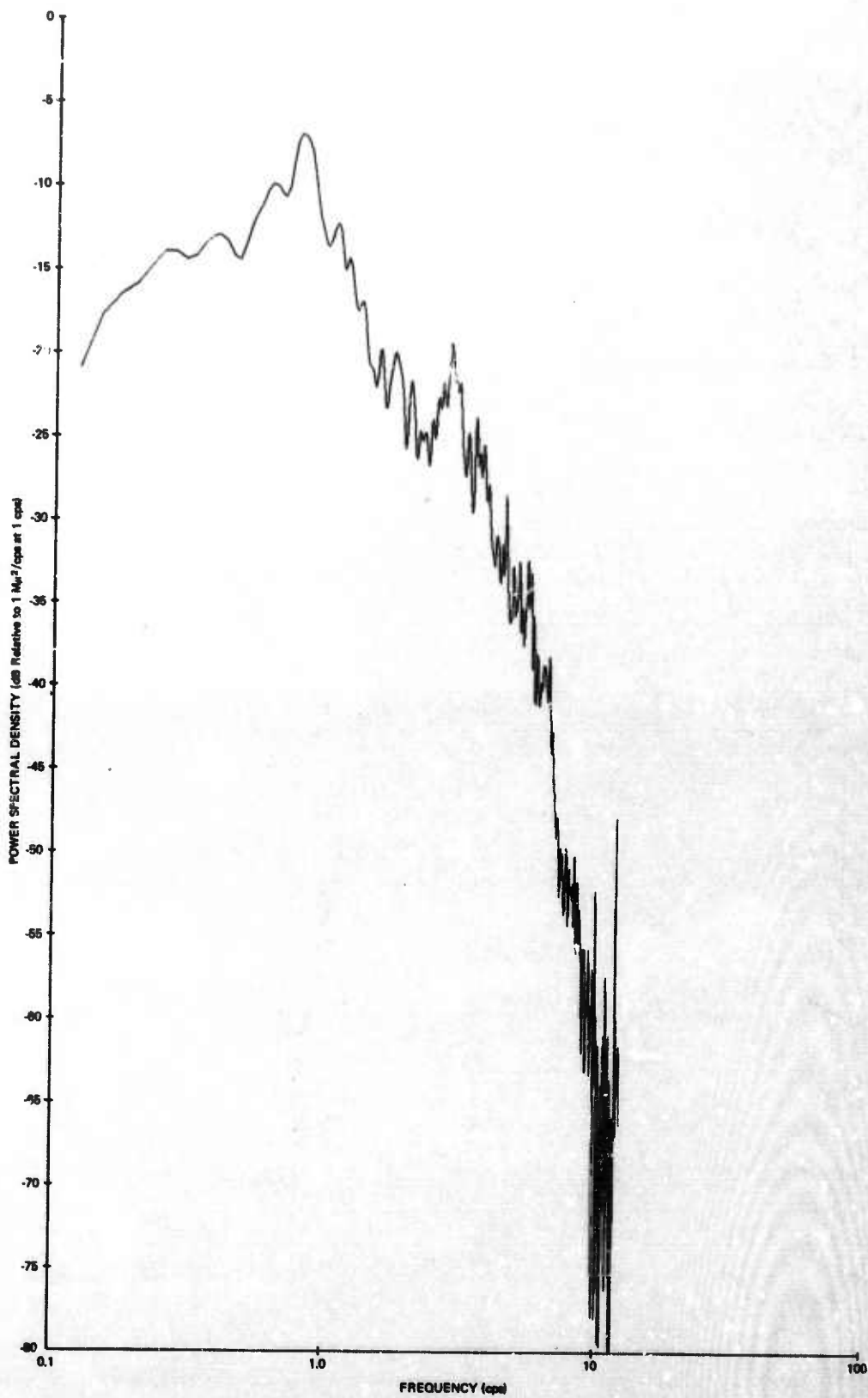


Figure 8. Power spectral density estimate of a sample of low-level microseismic noise, recorded by MCF3

G 3654

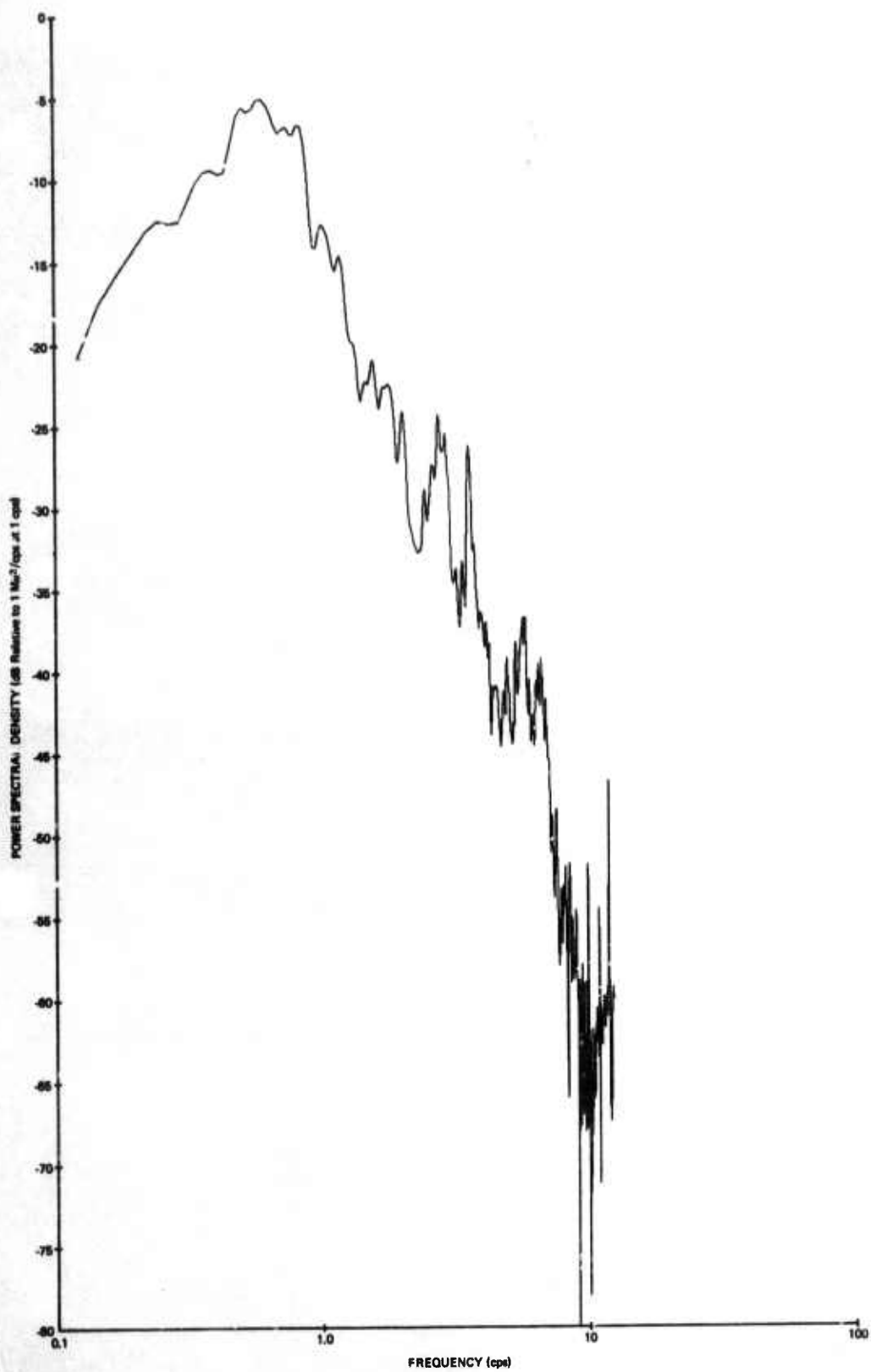


Figure 9. Power spectral density estimate of a sample of low-level microseismic noise, recorded by MCF11

G 3655

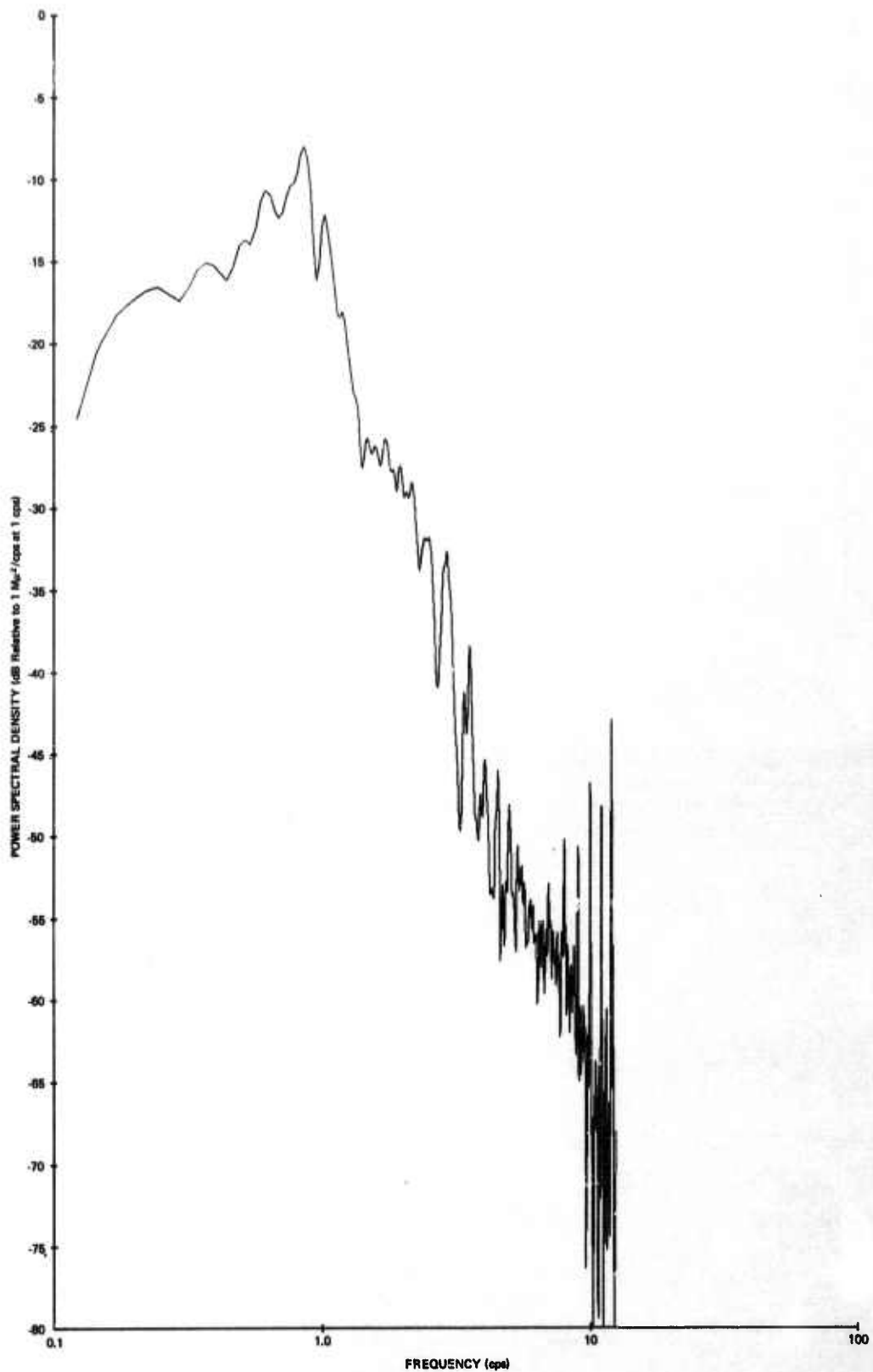


Figure 10. Power spectral density estimate of a sample of low-level microseismic noise recorded by MCF12

G 3656

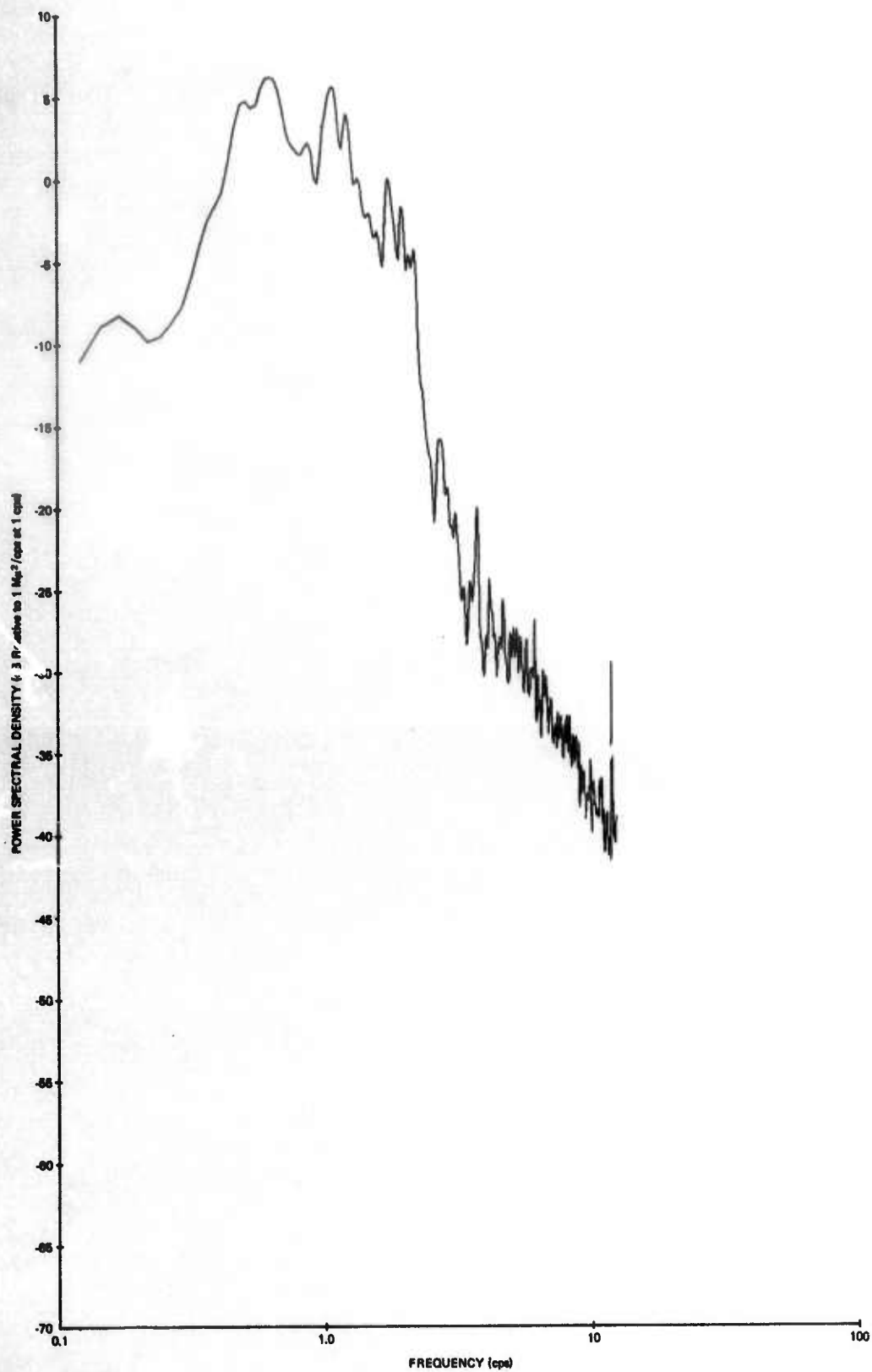


Figure 11. Power spectral density estimate of a sample of low-level microseismic noise recorded by MCF13

© 3657

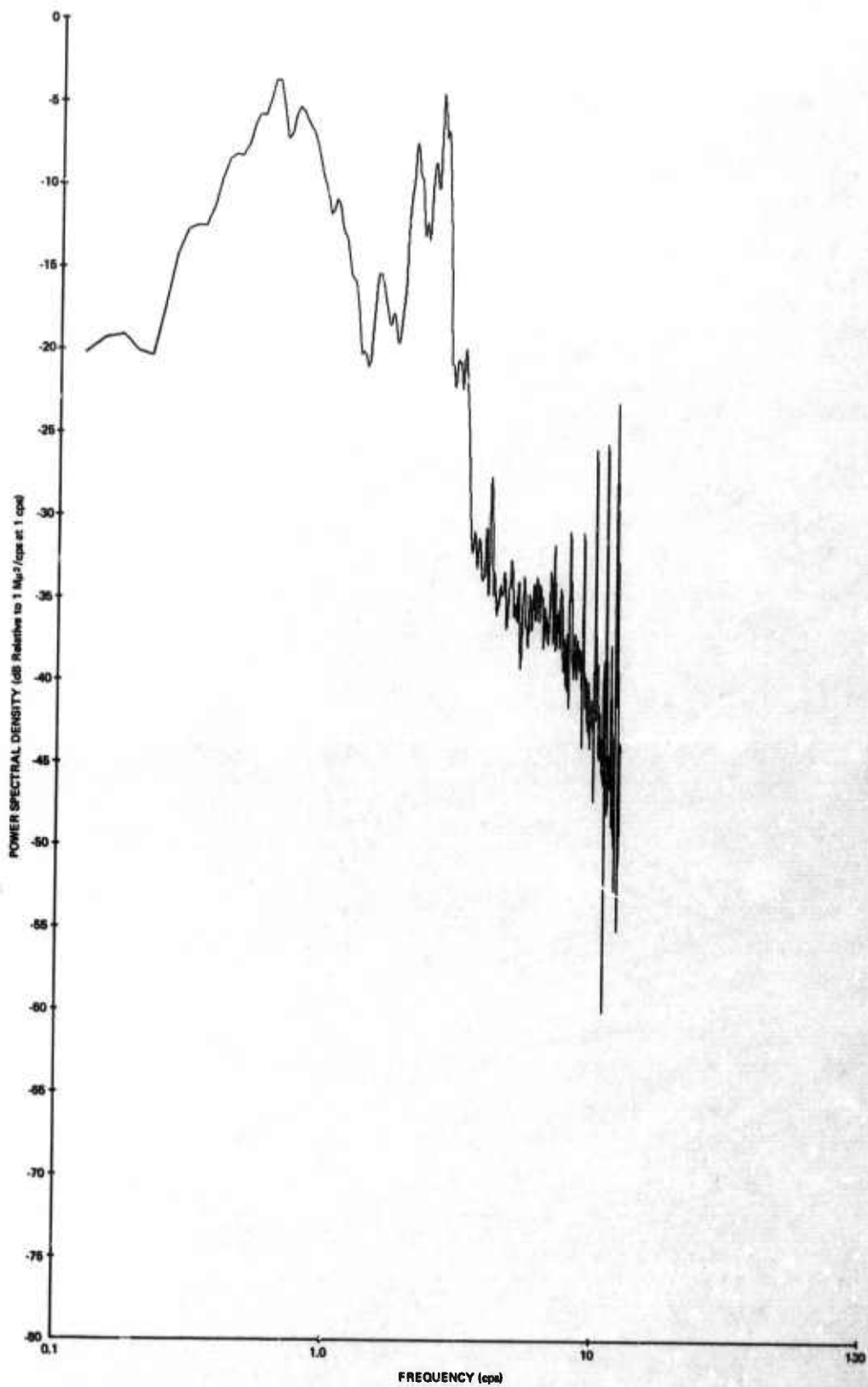


Figure 12. Power spectral density estimate of a sample of low-level microseismic noise, with road noise, recorded by  $\Sigma$ SSF

G 3658

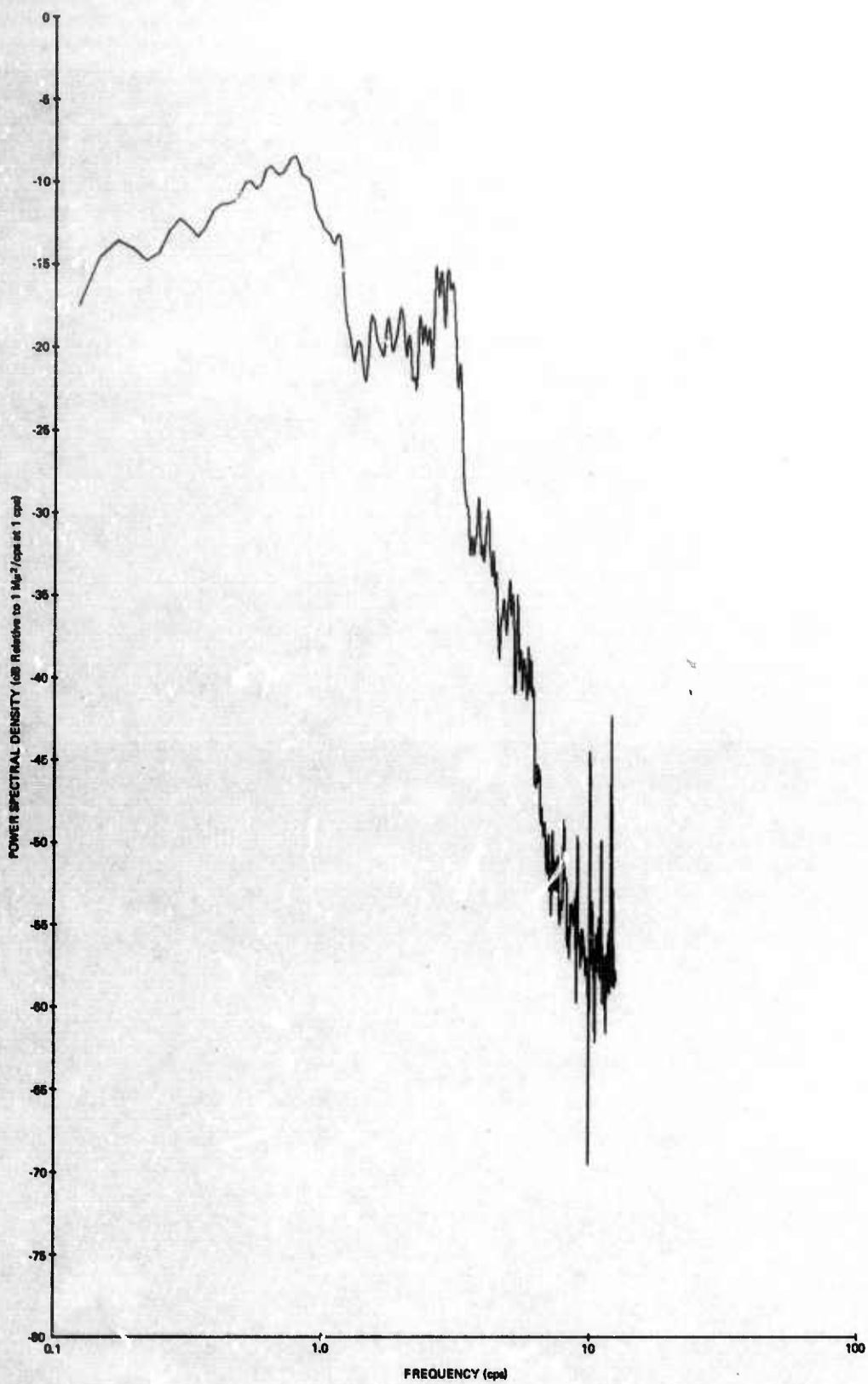


Figure 13. Power spectral density estimate of a sample of low-level microseismic noise, with road noise, recorded by MCF4

G 3659

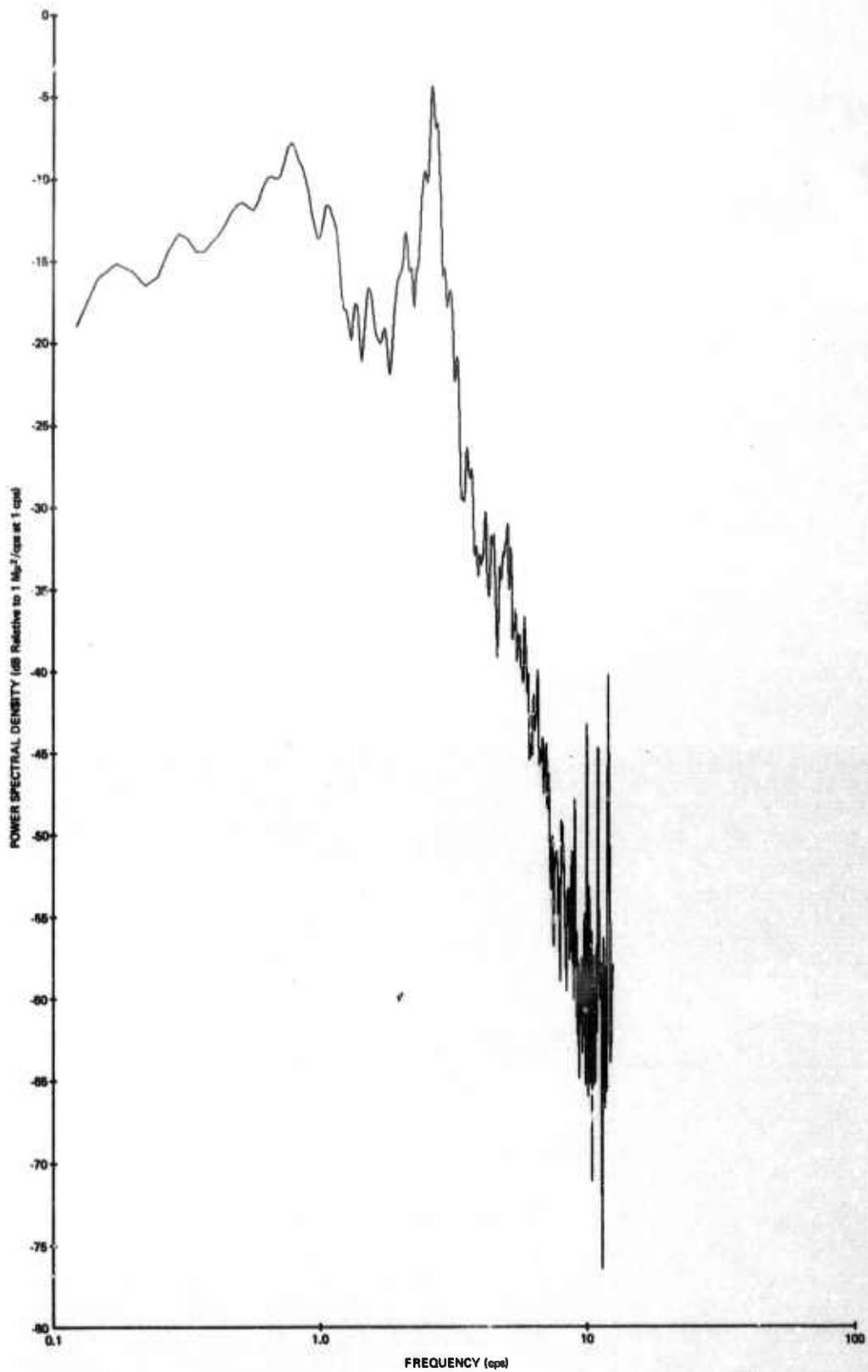


Figure 14. Power spectral density estimate of a sample of low-level microseismic noise, with road noise, recorded by MCF1

G 3660

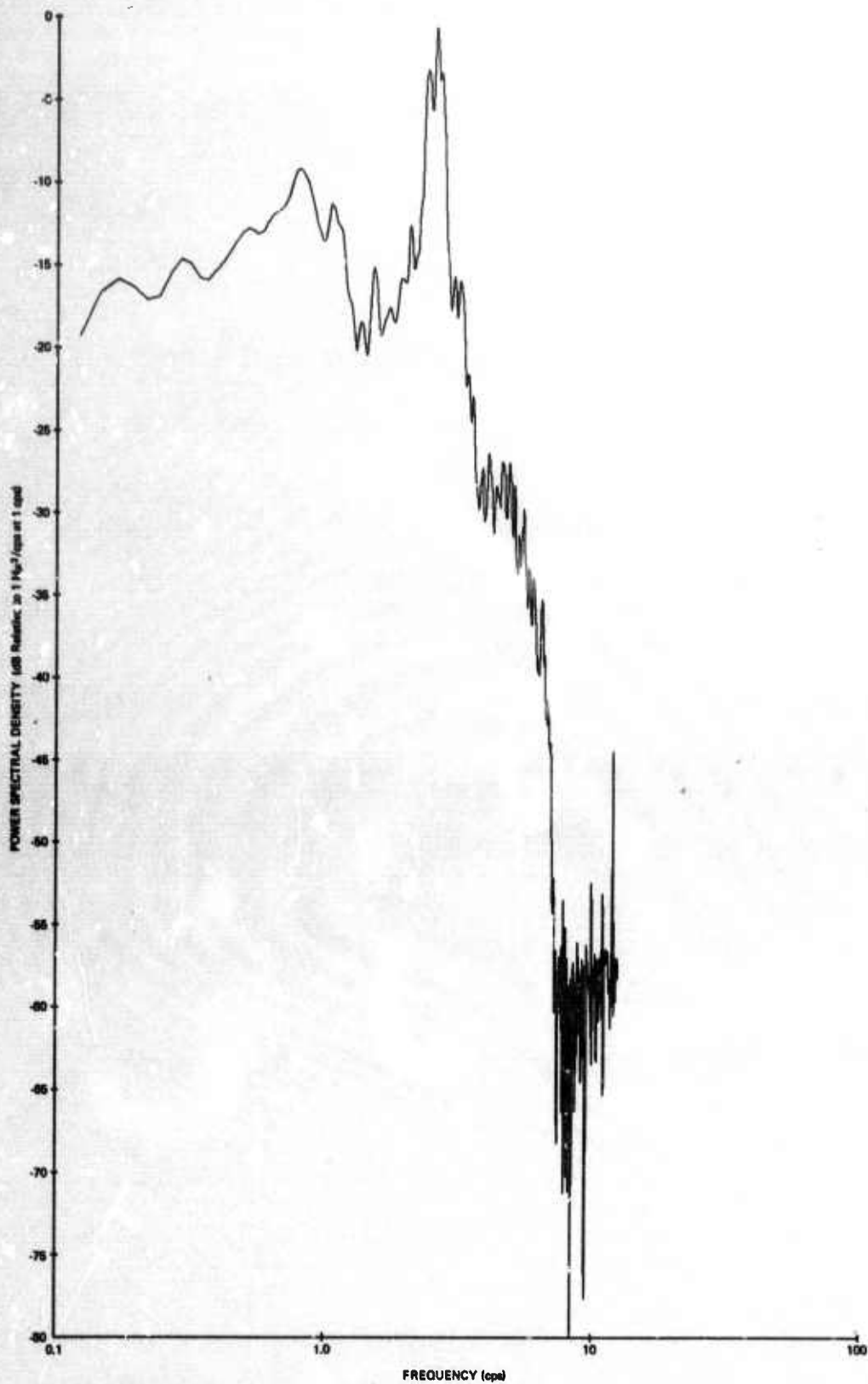


Figure 15. Power spectral density estimate of a sample of low-level microseismic noise, with road noise, recorded by MCF3

G 3661

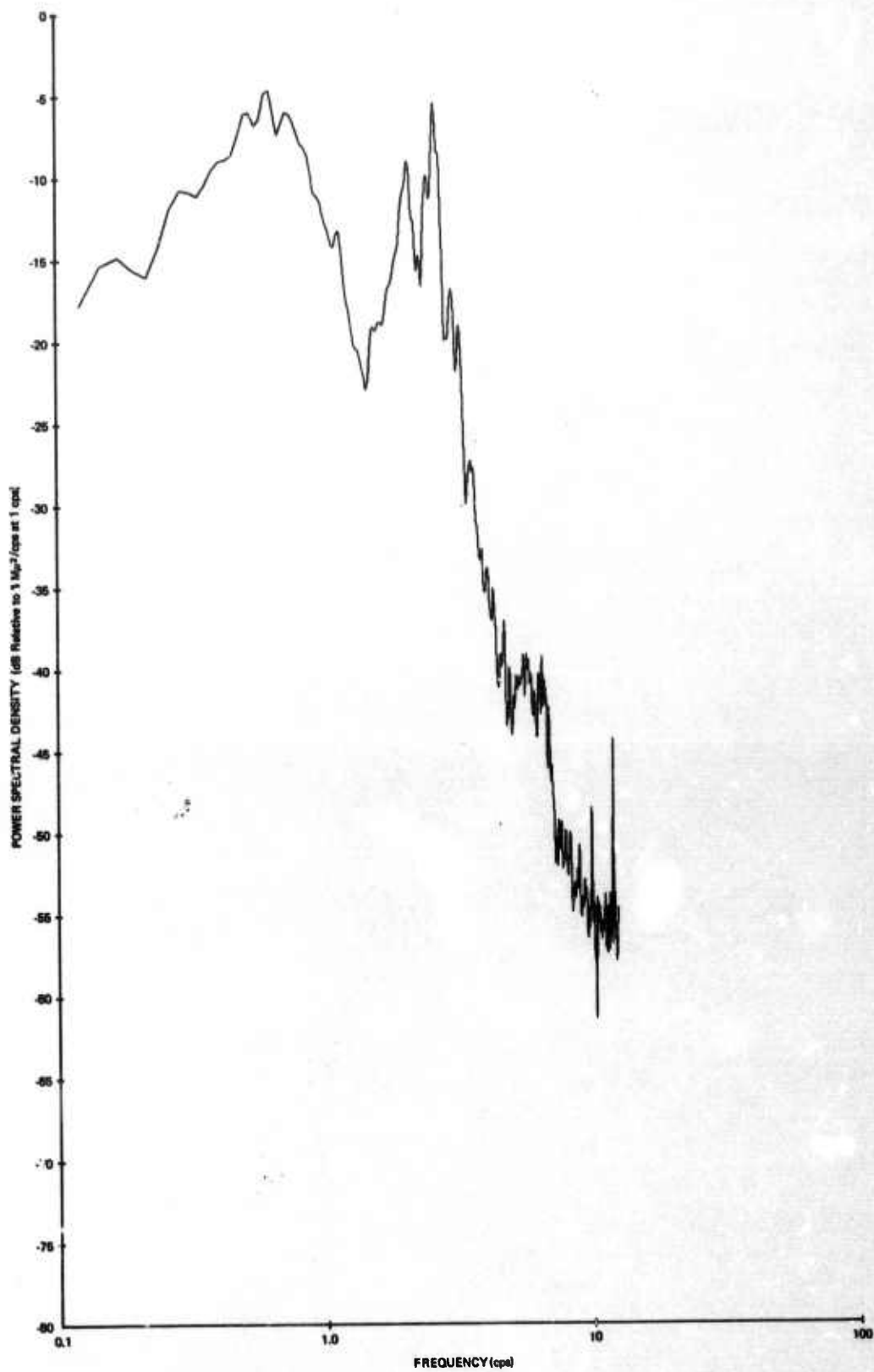


Figure 16. Power spectral density estimate of a sample of low-level microseismic noise, with road noise, recorded by MCF11

G 3662

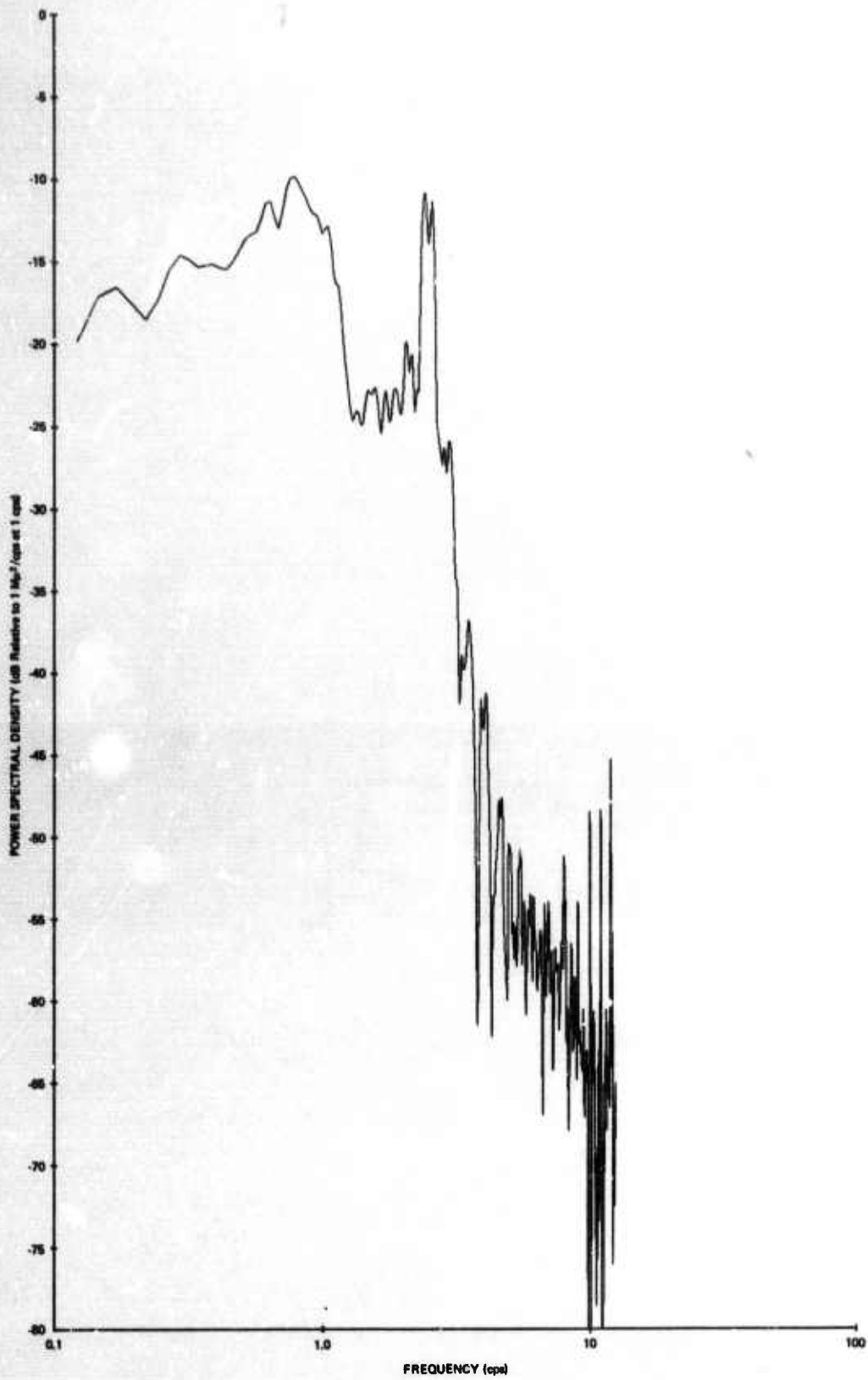


Figure 17. Power spectral density estimate of a sample of low-level microseismic noise, with road noise, recorded by MCF12

G 3663

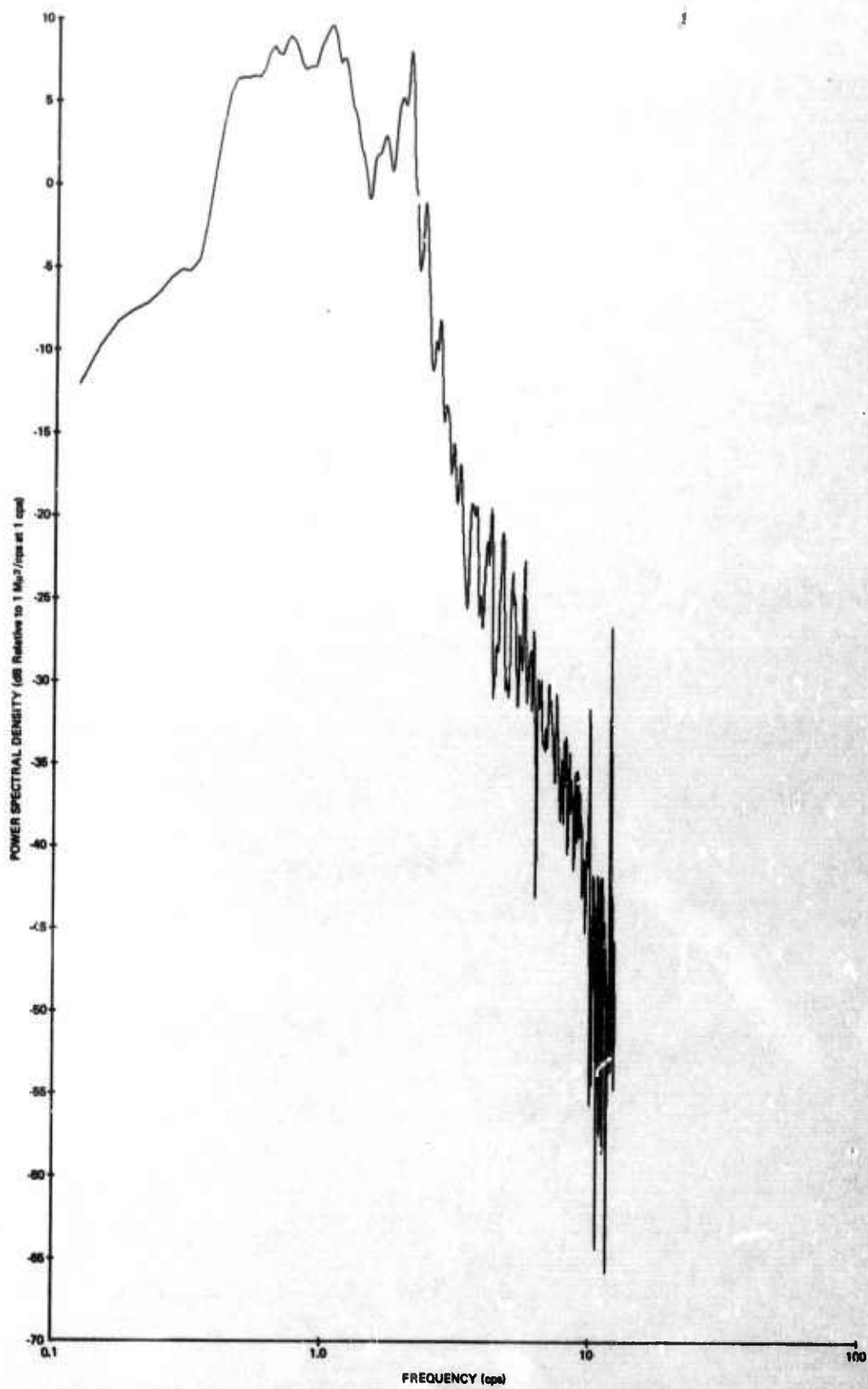


Figure 18. Power spectral density estimate of a sample of low-level microseismic noise, with road noise, recorded by MCF13

G 3664

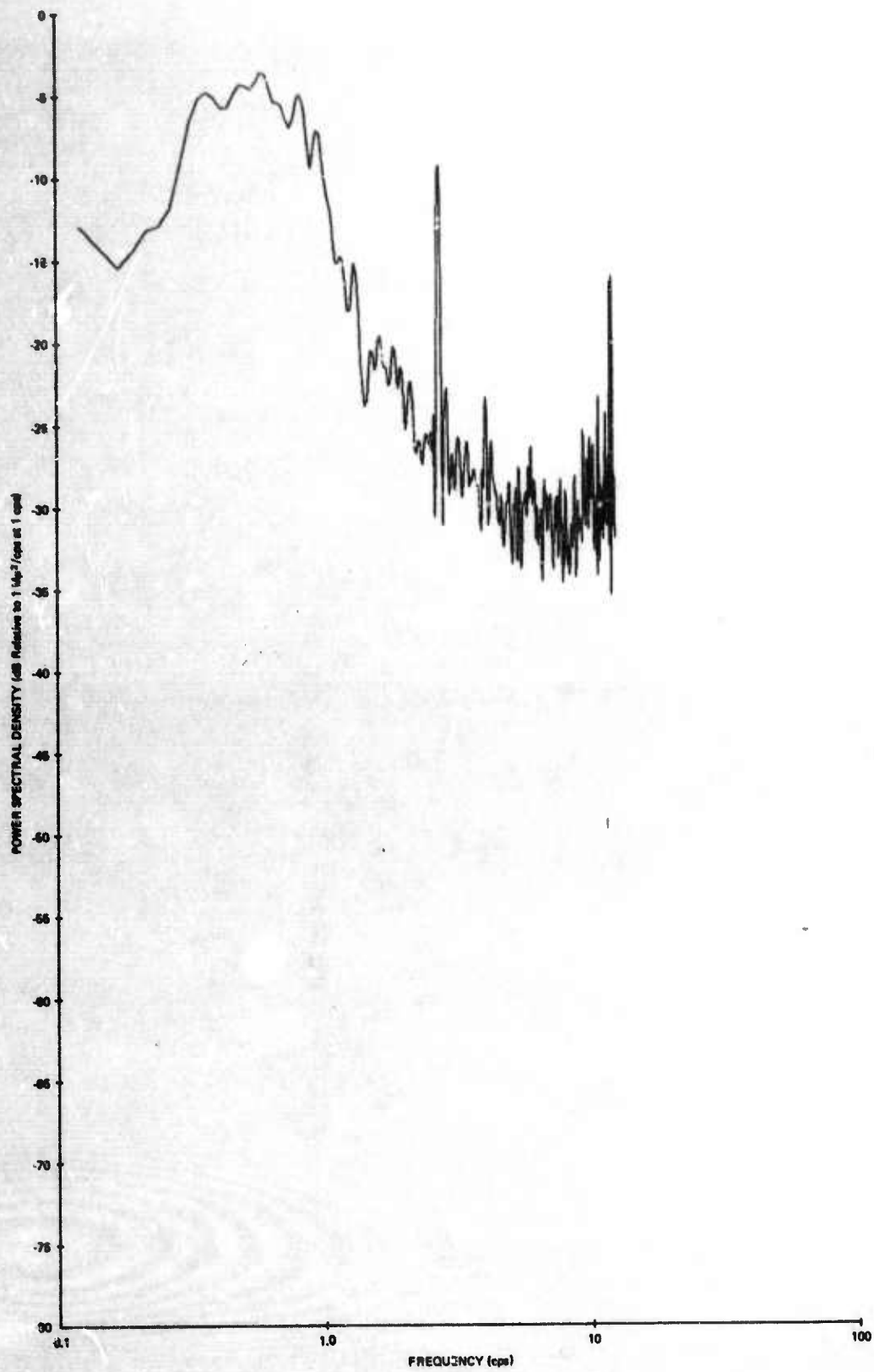


Figure 19. Power spectral density estimate of a sample of intermediate-level microseismic noise, recorded by ESSF

G 3665

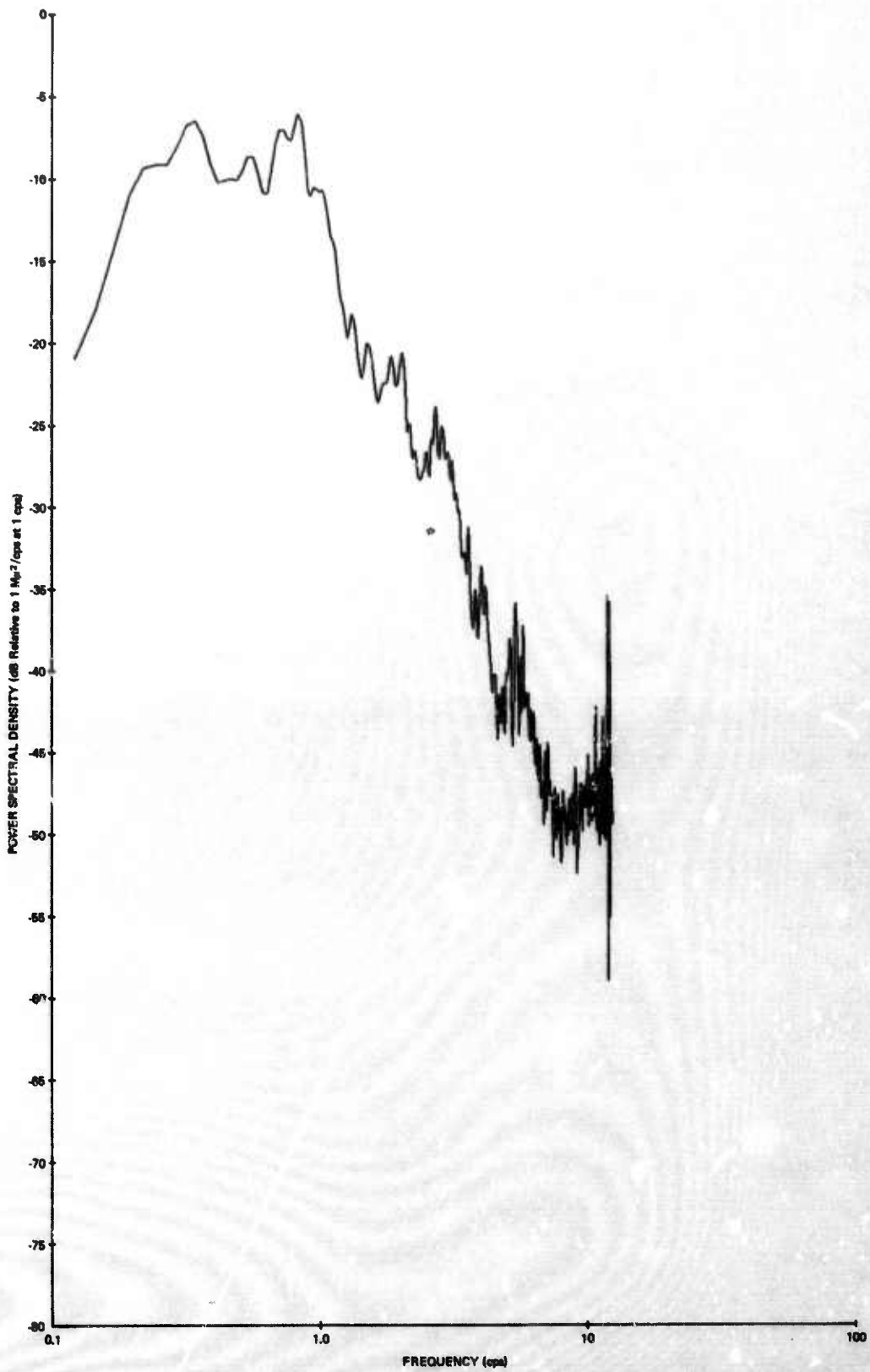


Figure 20. Power spectral density estimate of a sample of intermediate-level microseismic noise, recorded by MCF4

G 3886

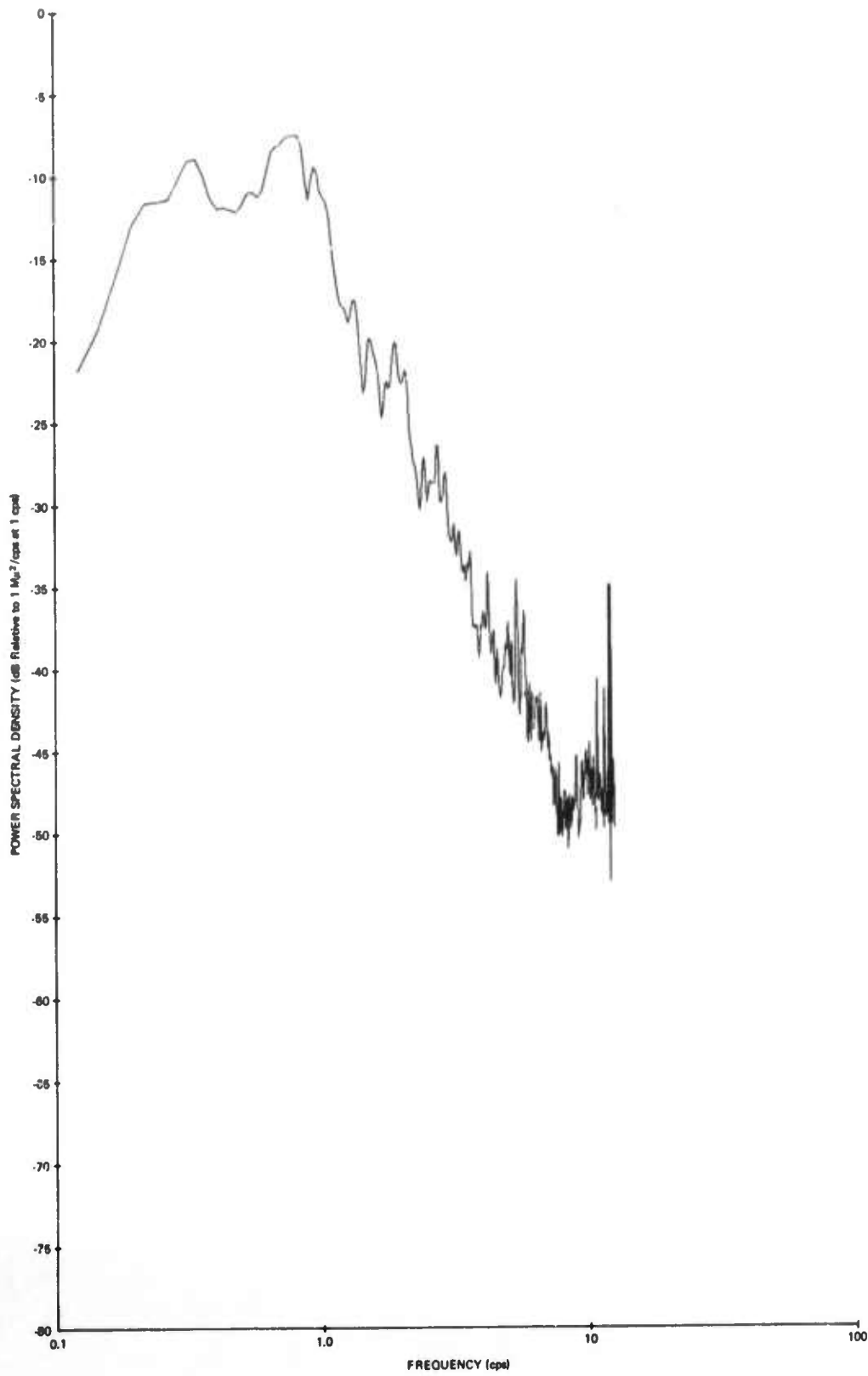


Figure 21. Power spectral density estimate of a sample of intermediate-level microseismic noise, recorded by MCF1

G 3667

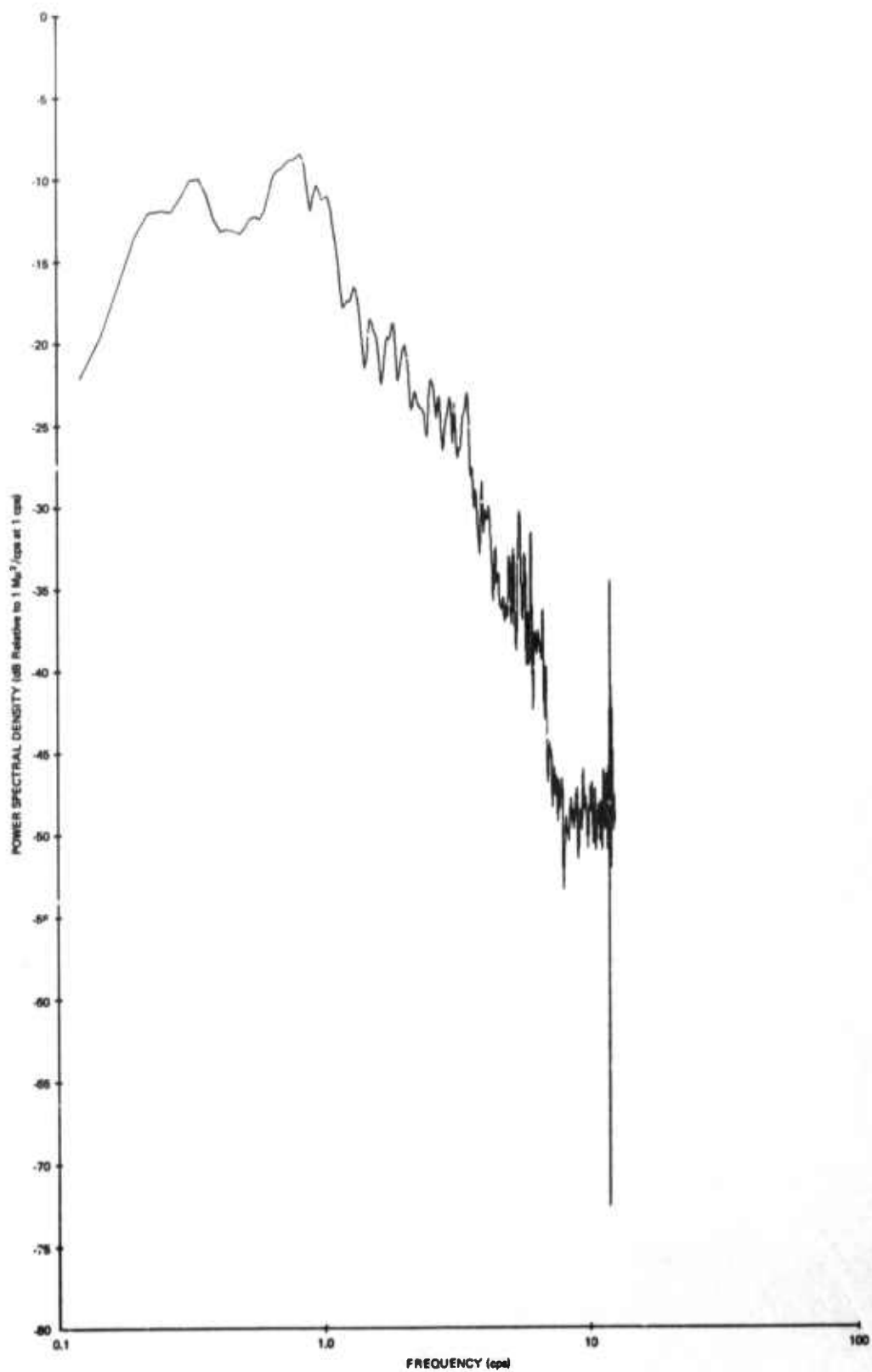


Figure 22. Power spectral density estimate of a sample of intermediate-level microseismic noise, recorded by MCF3

G 3668

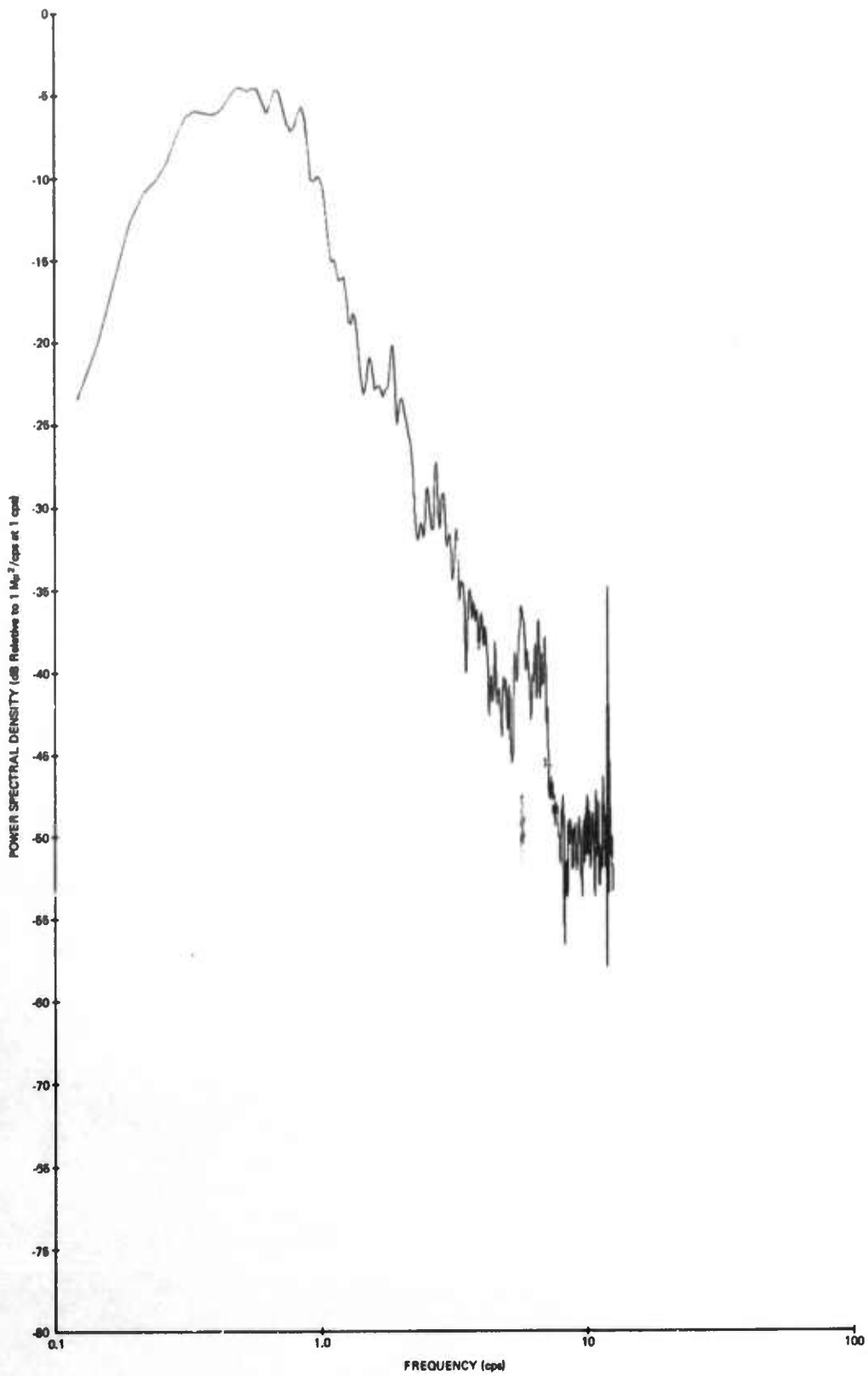


Figure 23. Power spectral density estimate of a sample of intermediate-level microseismic noise, recorded by MCF11

G 3669

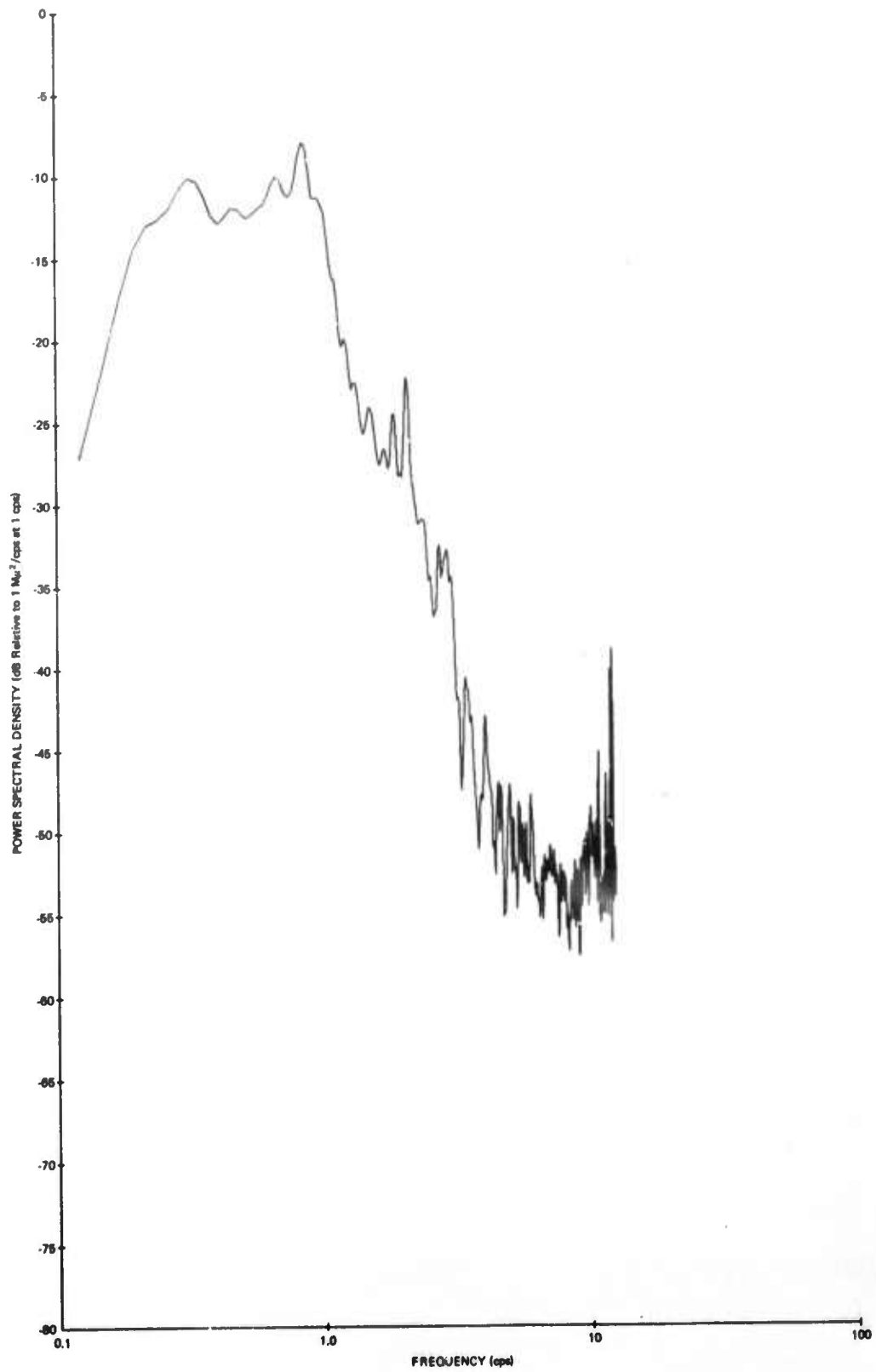


Figure 24. Power spectral density estimate of a sample of intermediate-level microseismic noise, recorded by MCF12

G 3670

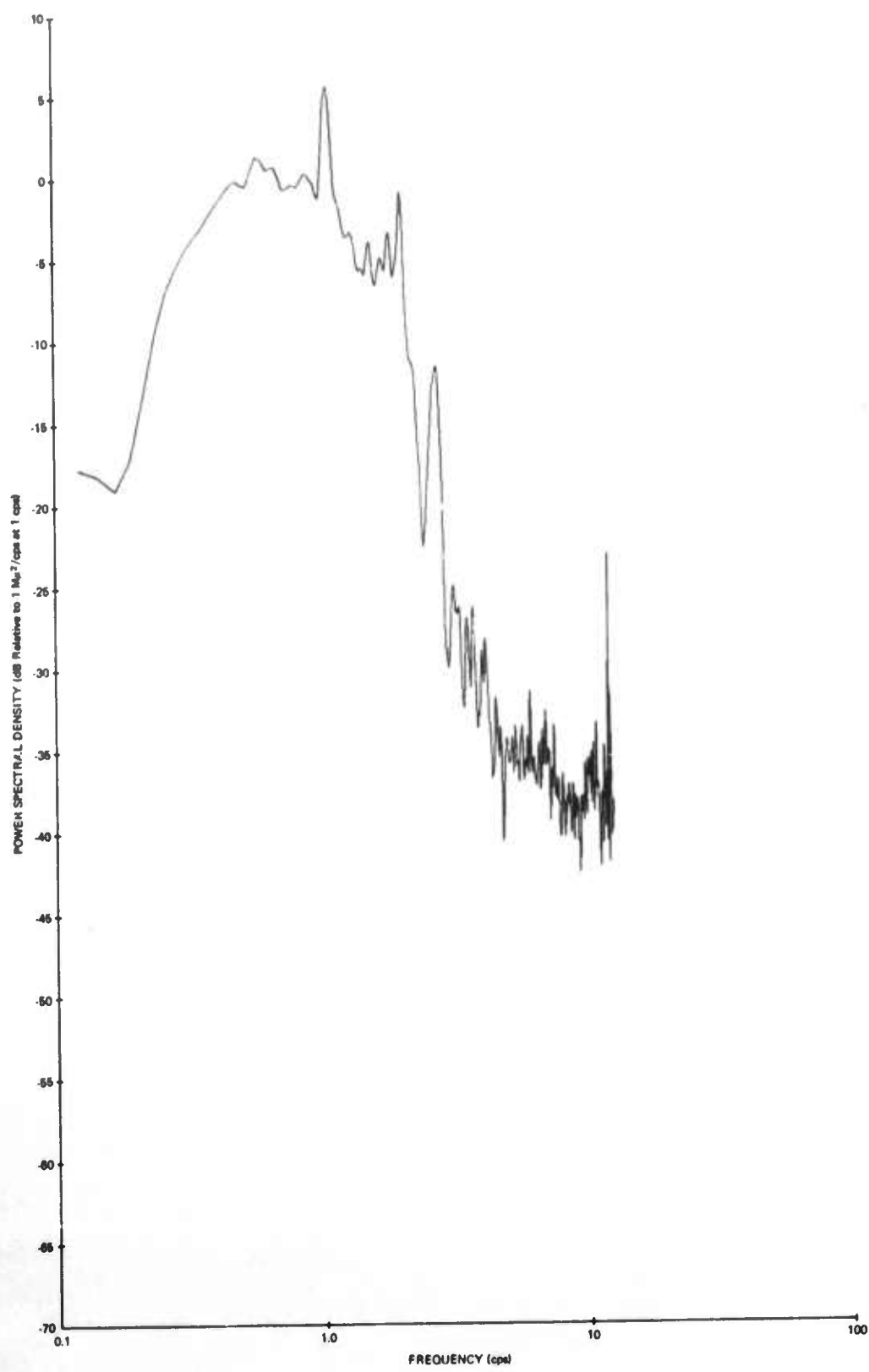


Figure 25. Power spectral density estimate of a sample of intermediate-level microseismic noise, recorded by MCF13

G 3671

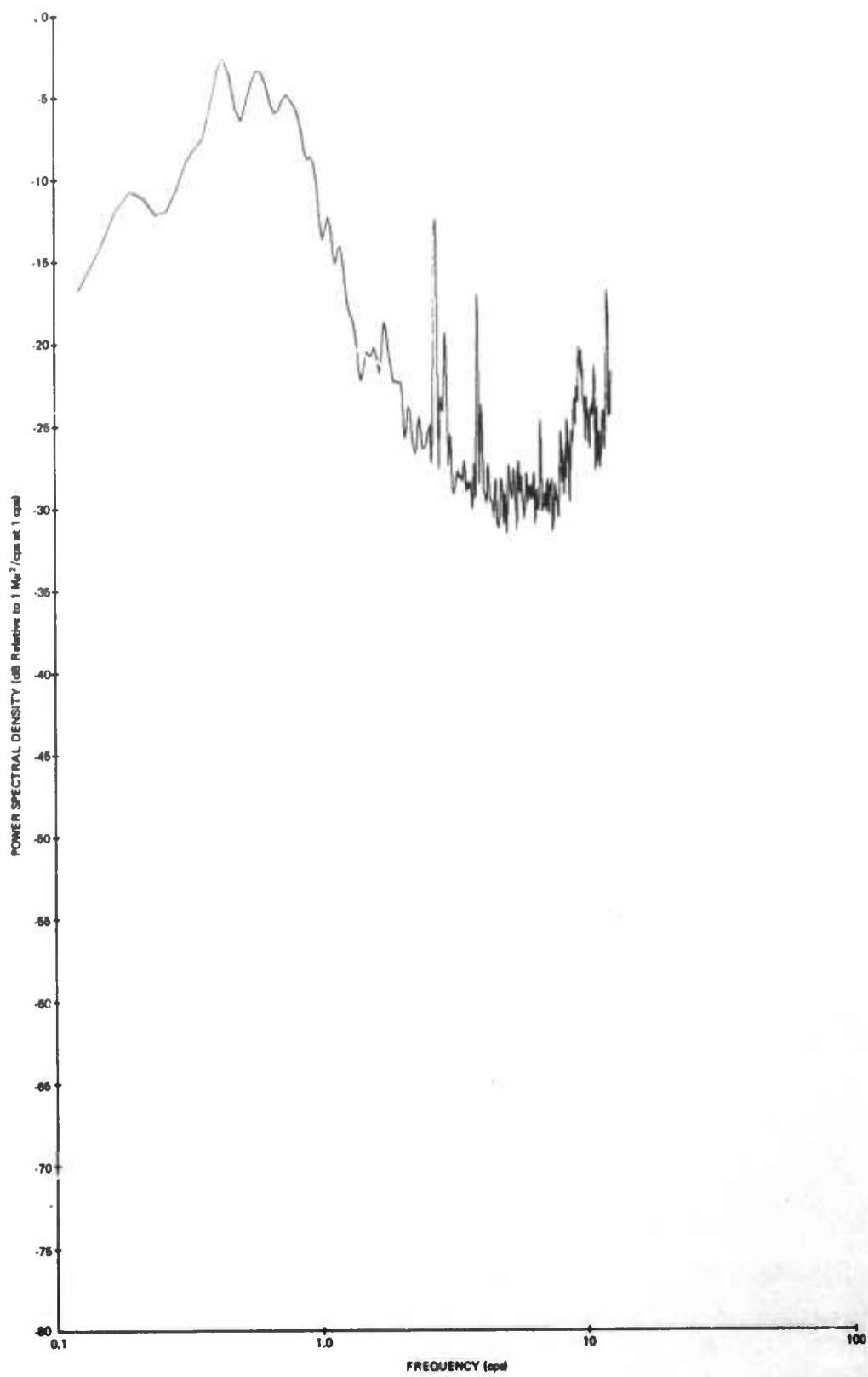


Figure 26. Power spectral density estimate of a sample of high-level microseismic noise, recorded by  $\Sigma$ SSF

G 3672

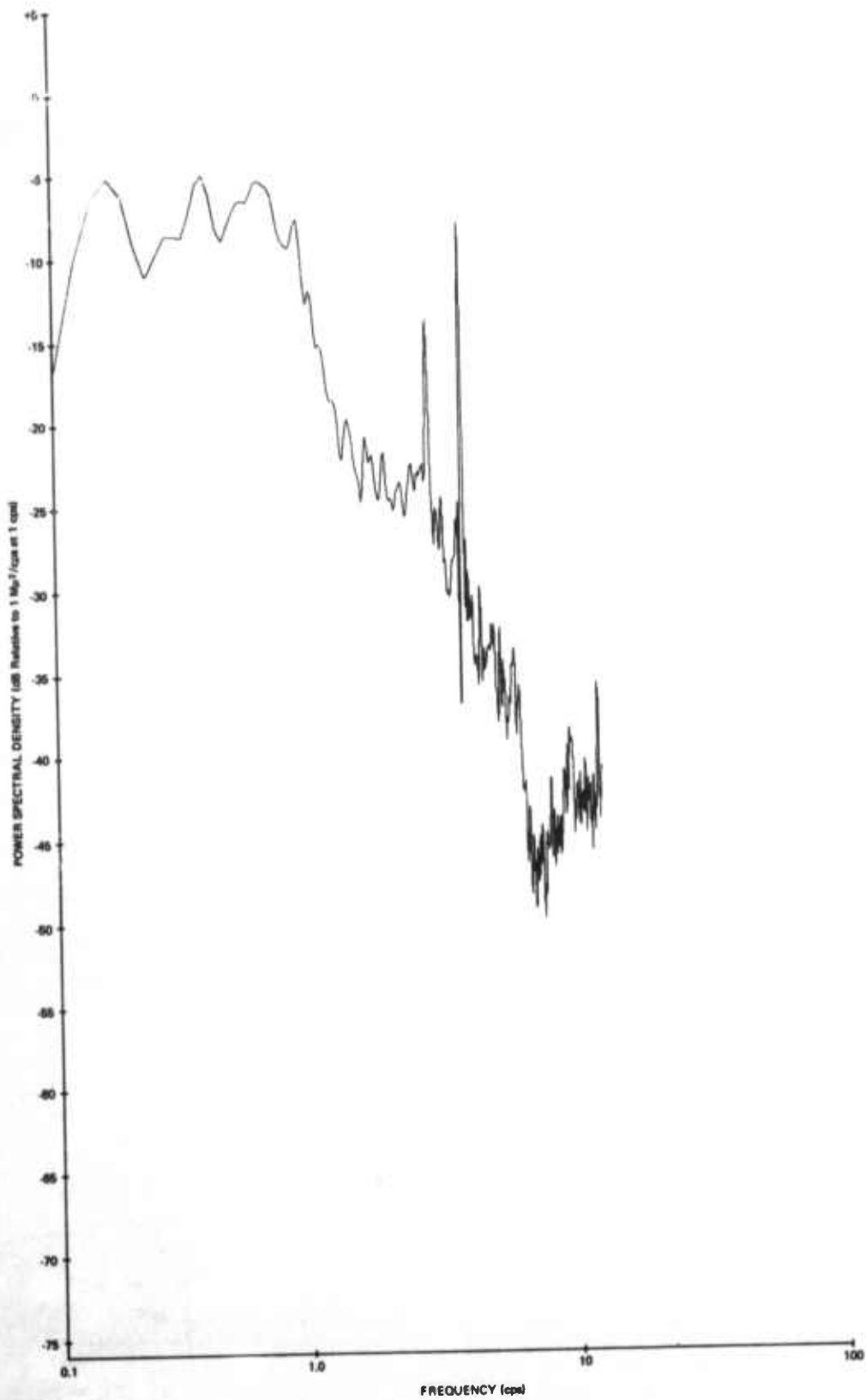


Figure 27. Power spectral density estimate of a sample of high-level microseismic noise, recorded by MCF4

G 3673

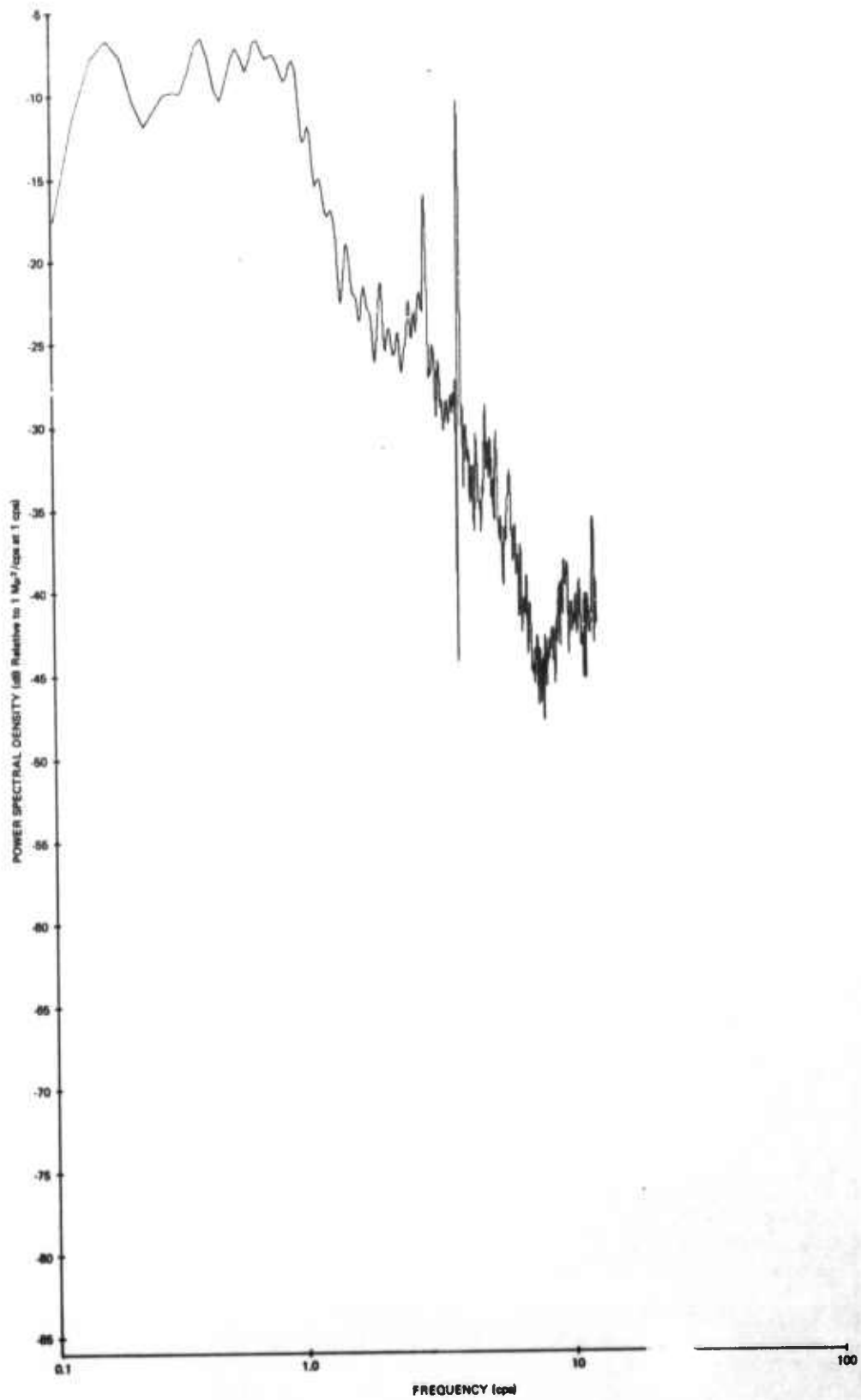


Figure 28. Power spectral density estimate of a sample of high-level microseismic noise, recorded by MCF1

G 3674

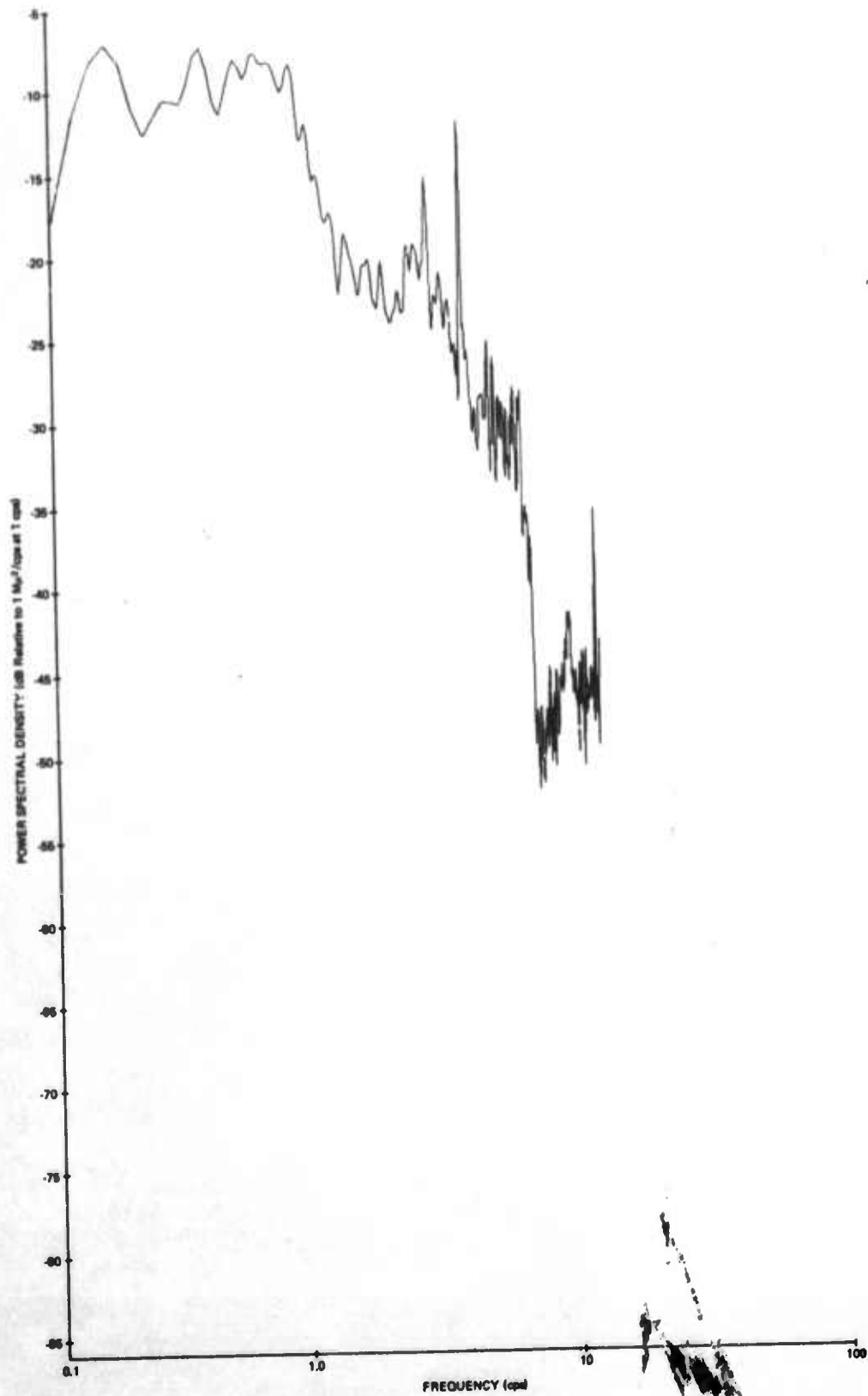


Figure 29. Power spectral density estimate of a sample of high-level microseismic noise, recorded by MCF3

G 3675

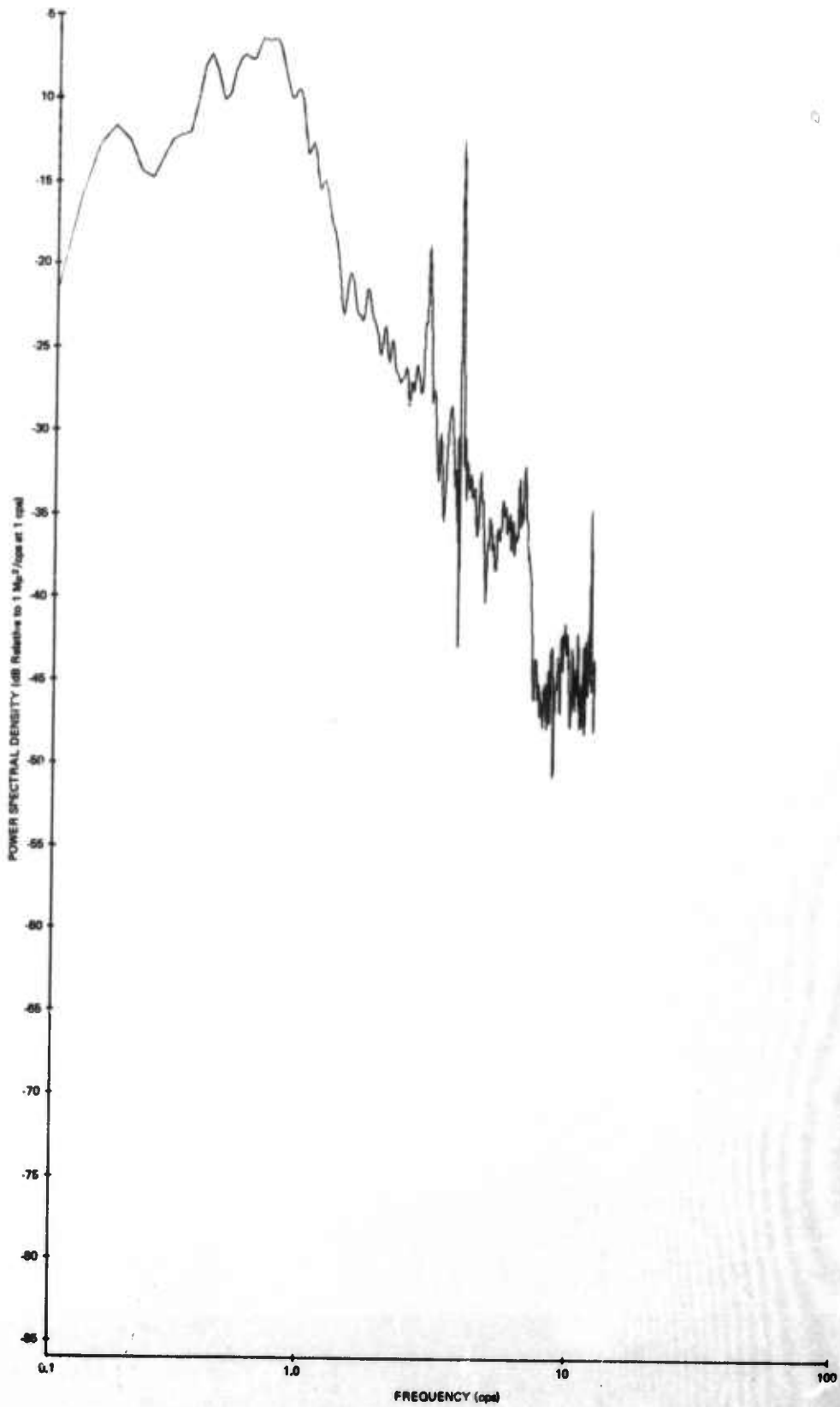


Figure 30. Power spectral density estimate of a sample of high-level microseismic noise, recorded by MCF11

G 3676

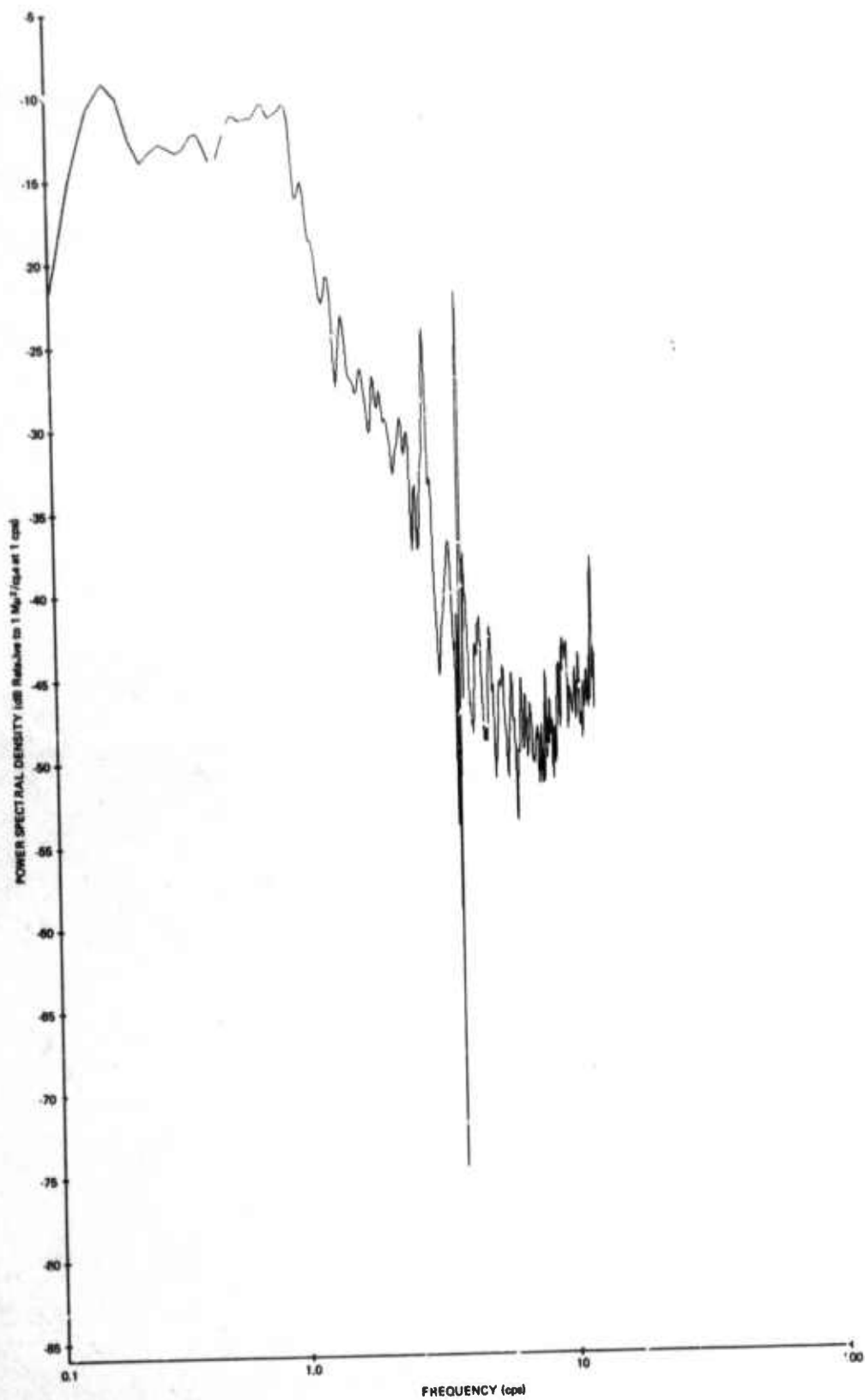


Figure 31. Power spectral density estimate of a sample of high-level microseismic noise, recorded by MCF12

G 3677

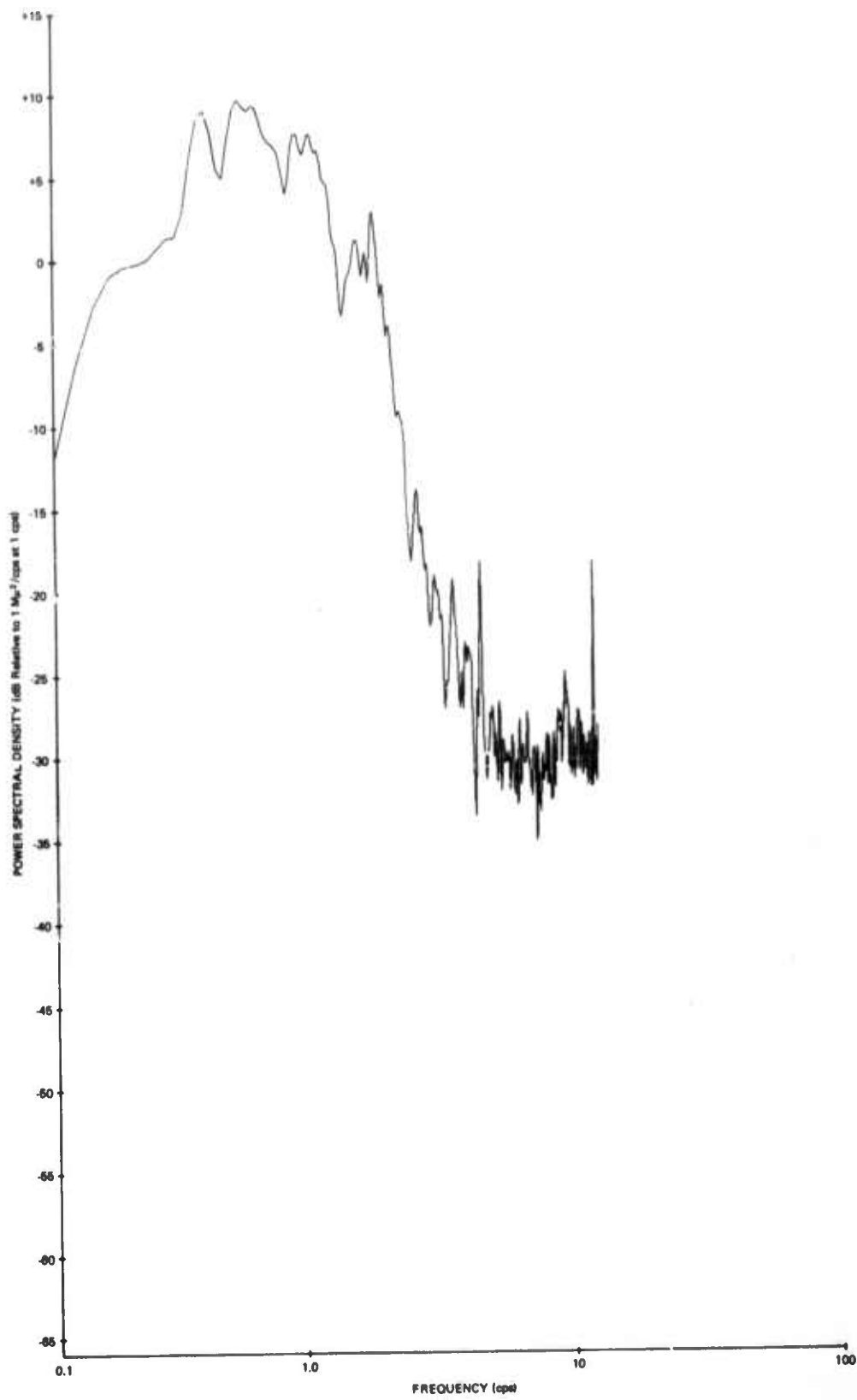


Figure 32. Power spectral density estimate of a sample of high-level microseismic noise, recorded by MCF13

G 3678

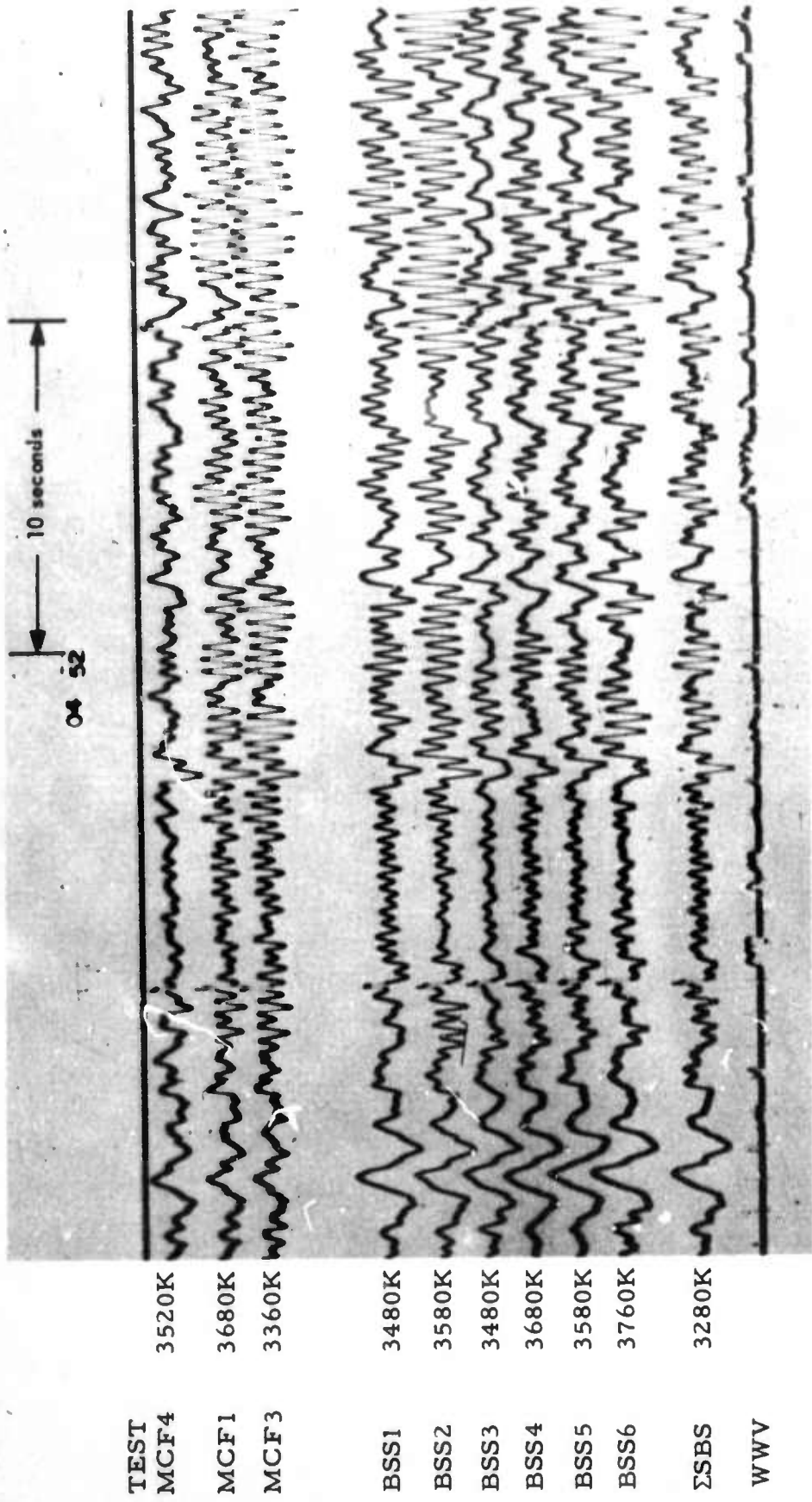


Figure 33. MAP I seismogram illustrating response of MAP I system to strong road noise. (X10 enlargement of 16-millimeter film)

UBSO  
 11 Mar 67  
 RPN 070  
 DG 5070

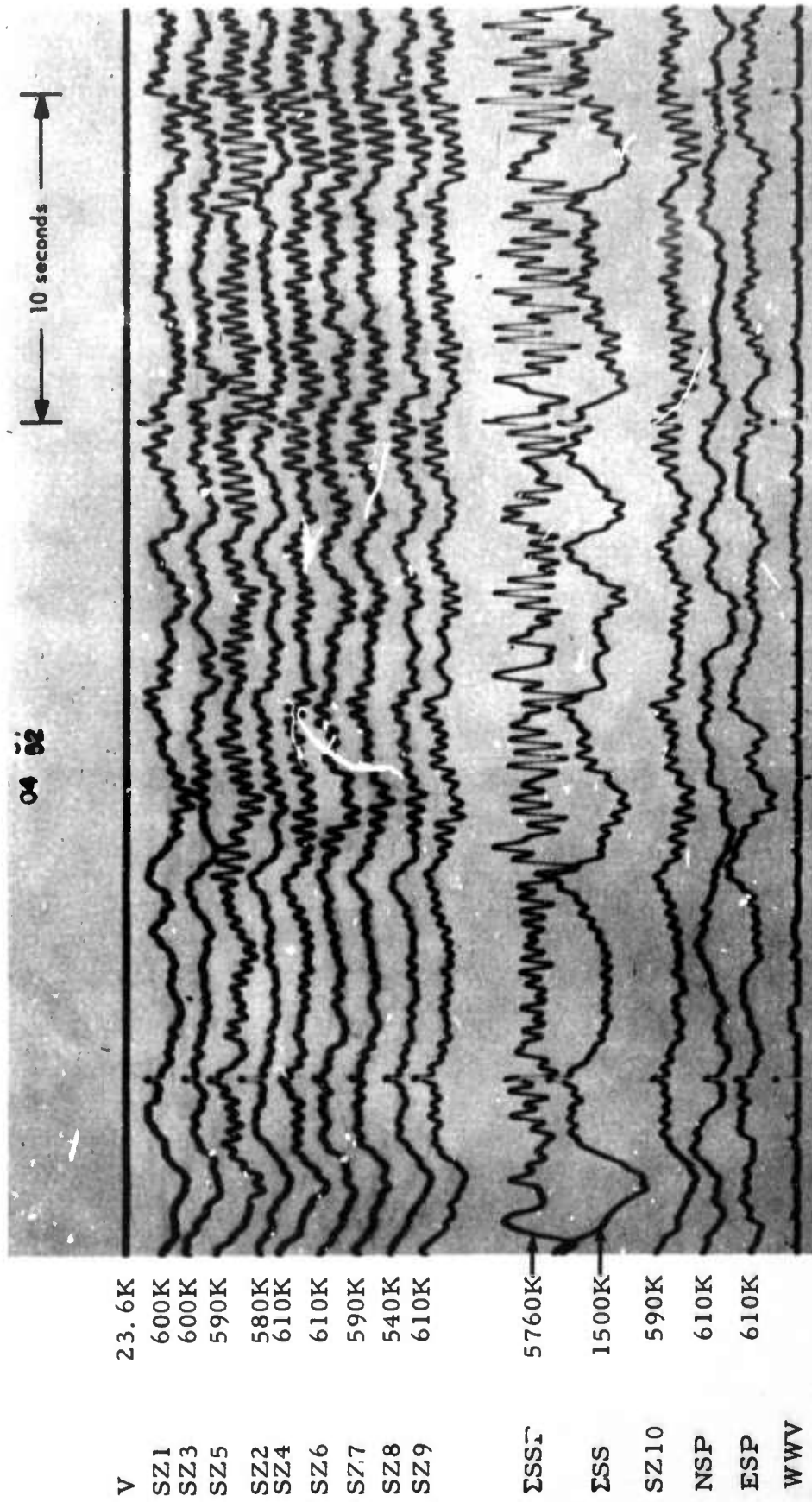


Figure 34. Primary system seismogram illustrating response of primary systems to strong road noise. (X10 enlargement of 16-millimeter film)

UBSO  
11 Mar 67  
RPN 070  
DG 5044

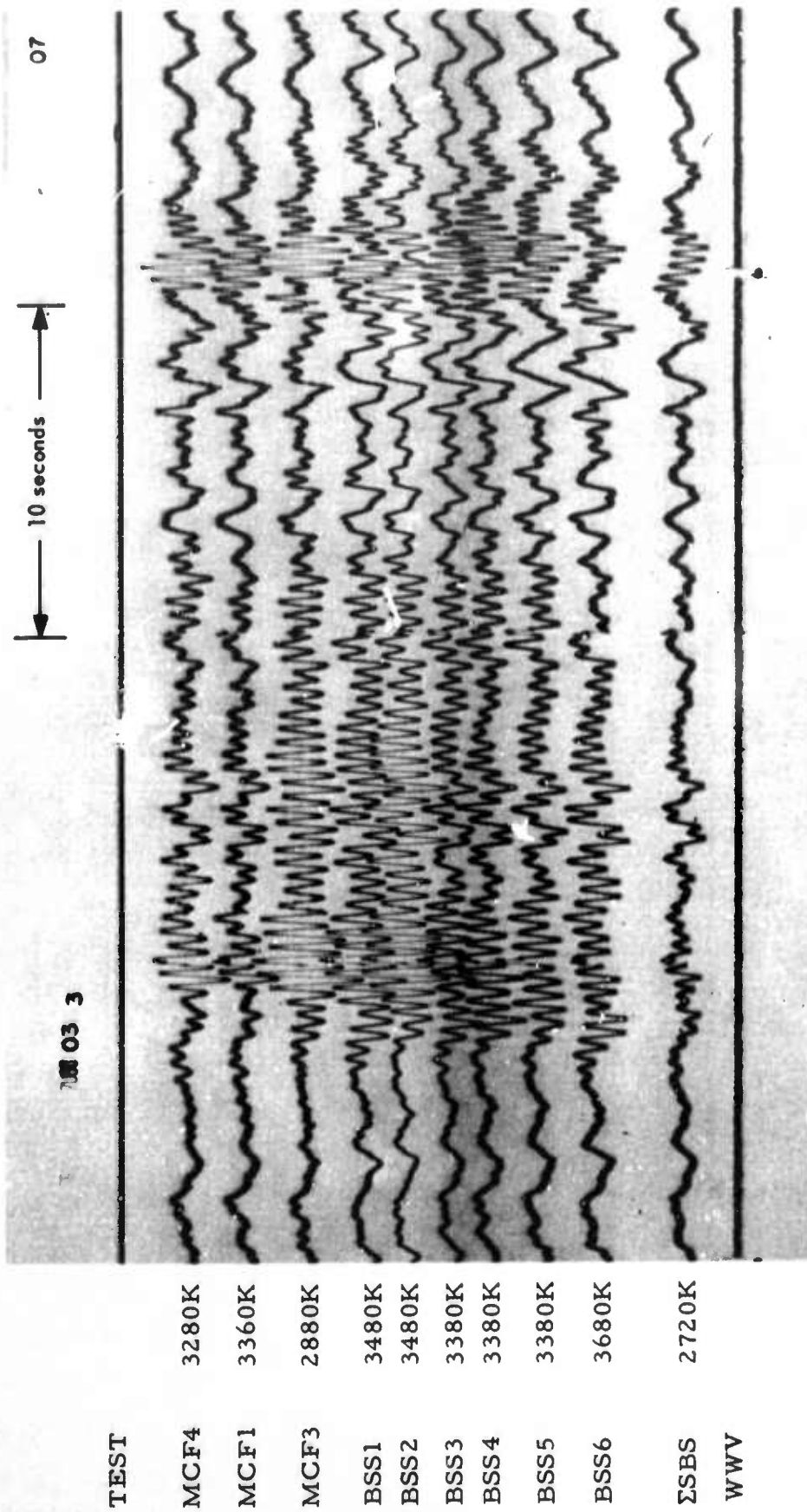
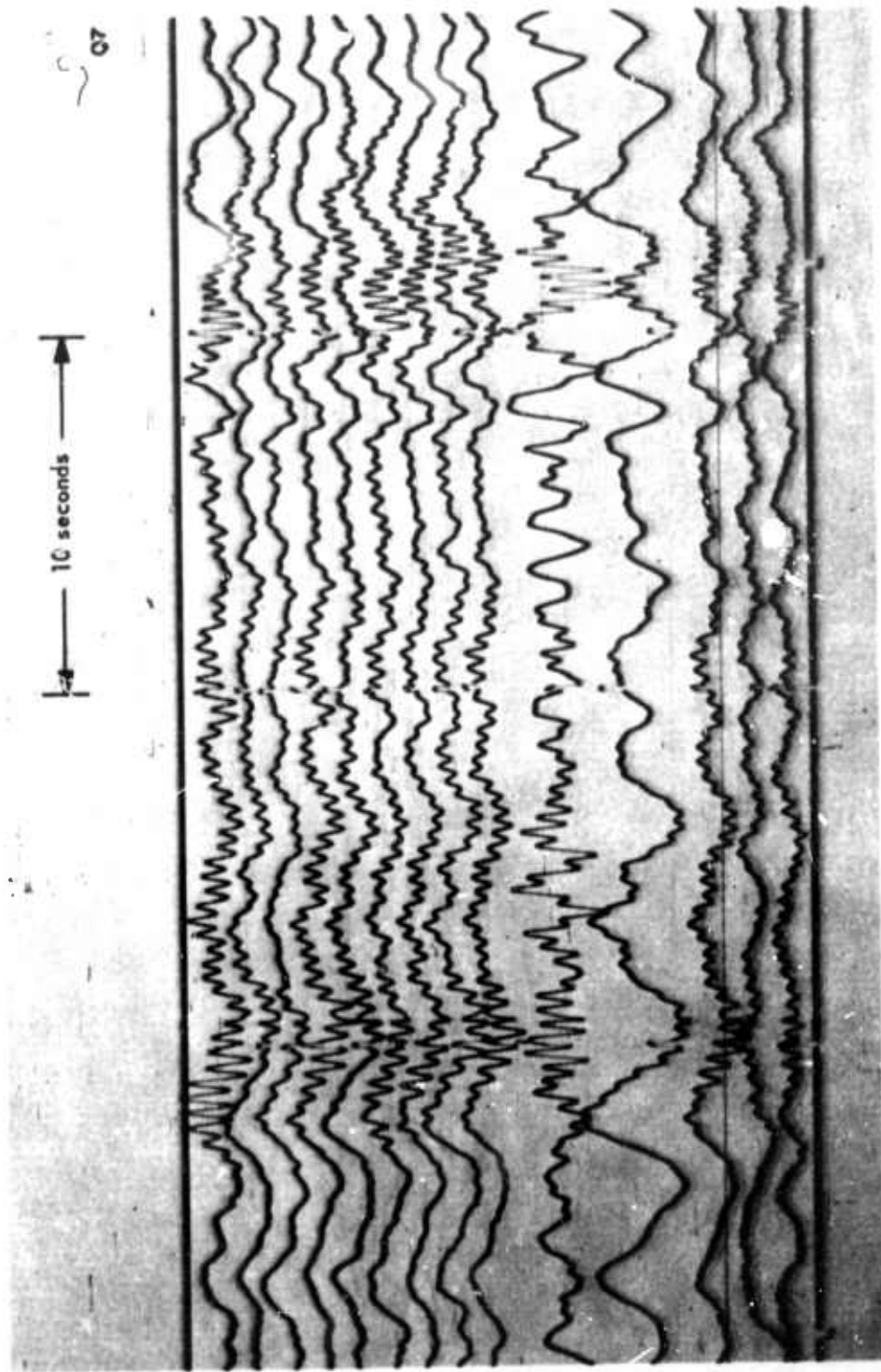


Figure 35. MAP I seismogram illustrating response of MAP I systems to high frequency cultural noise, not road noise. (X10 enlargement of 16-millimeter film)

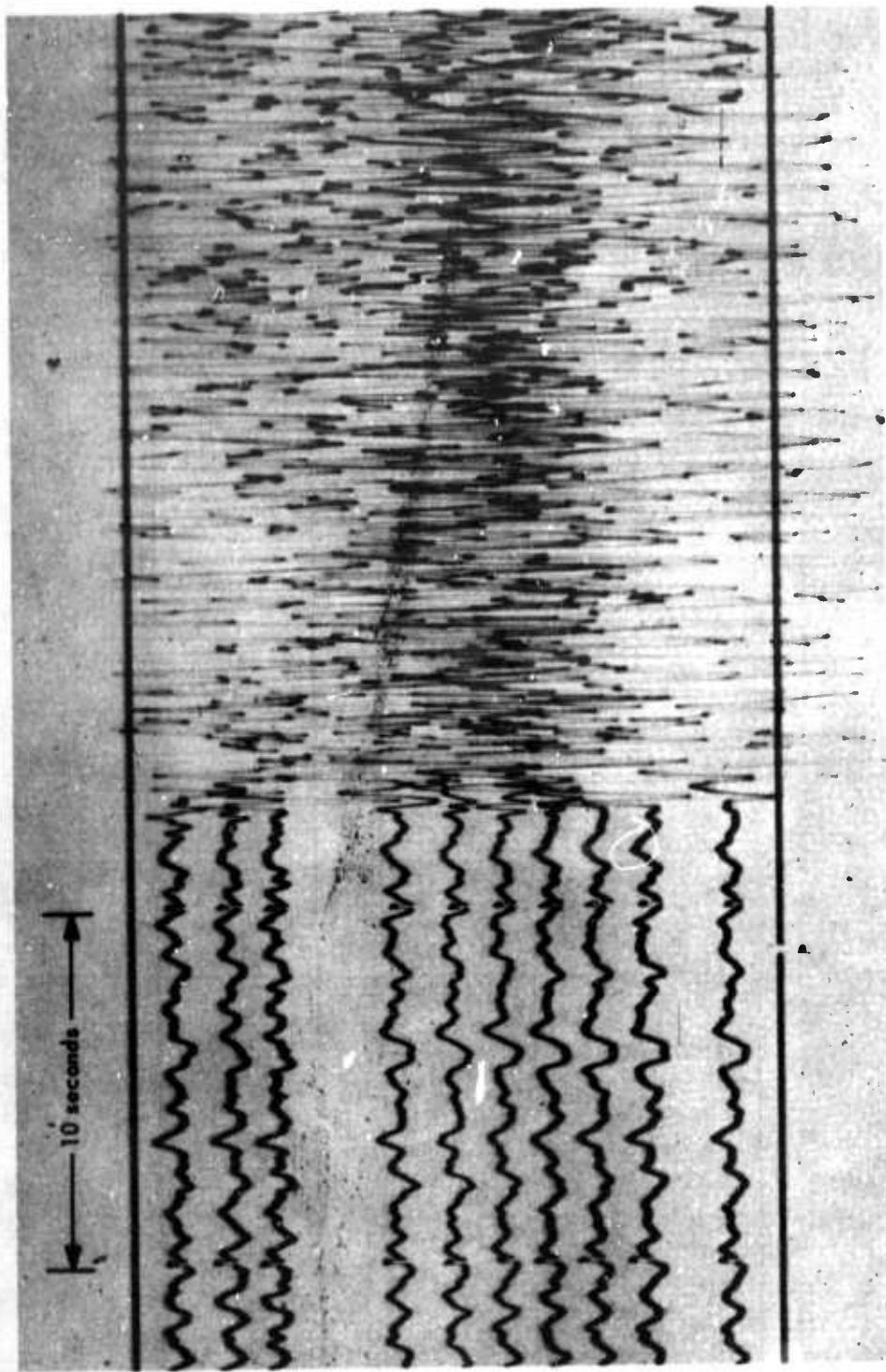
UBSO  
 2 Feb 67  
 RPN 033  
 DG 5070



V	2.4K
SZ1	620K
SZ3	630K
SZ5	600K
SZ2	610K
SZ4	640K
SZ6	600K
SZ7	560K
SZ8	710K
SZ9	600K
ΣSSF	600K
ΣSS	1460K
SZ10	580K
NSP	590K
ESP	600K
WWV	

Figure 36. Primary system seismogram illustrating response of primary system to high-frequency cultural noise, not road noise. (X10 enlargement of 16-millimeter film)

UBSO  
2 Feb 67  
RPN 033  
DG 5044



TEST	
MCF4	3520K
MCF1	3680K
MCF3	3360K
BSS1	3760K
BSS2	3580K
BSS3	3580K
BSS4	3580K
BSS5	3580K
BSS6	3860K
ESBS	3280K
WWV	

UBSO  
 10 Mar 67  
 RPN 069  
 DG 5070

Figure 37. MAP I seismogram illustrating response of MAP I systems to near regional signal. Epicentral data:  $O = 05:34:58.5$ ,  $\Delta = 1.9^\circ$ , azimuth =  $285^\circ$ ,  $h = 5$  km.  
 (X10 enlargement of 16-millimeter film)

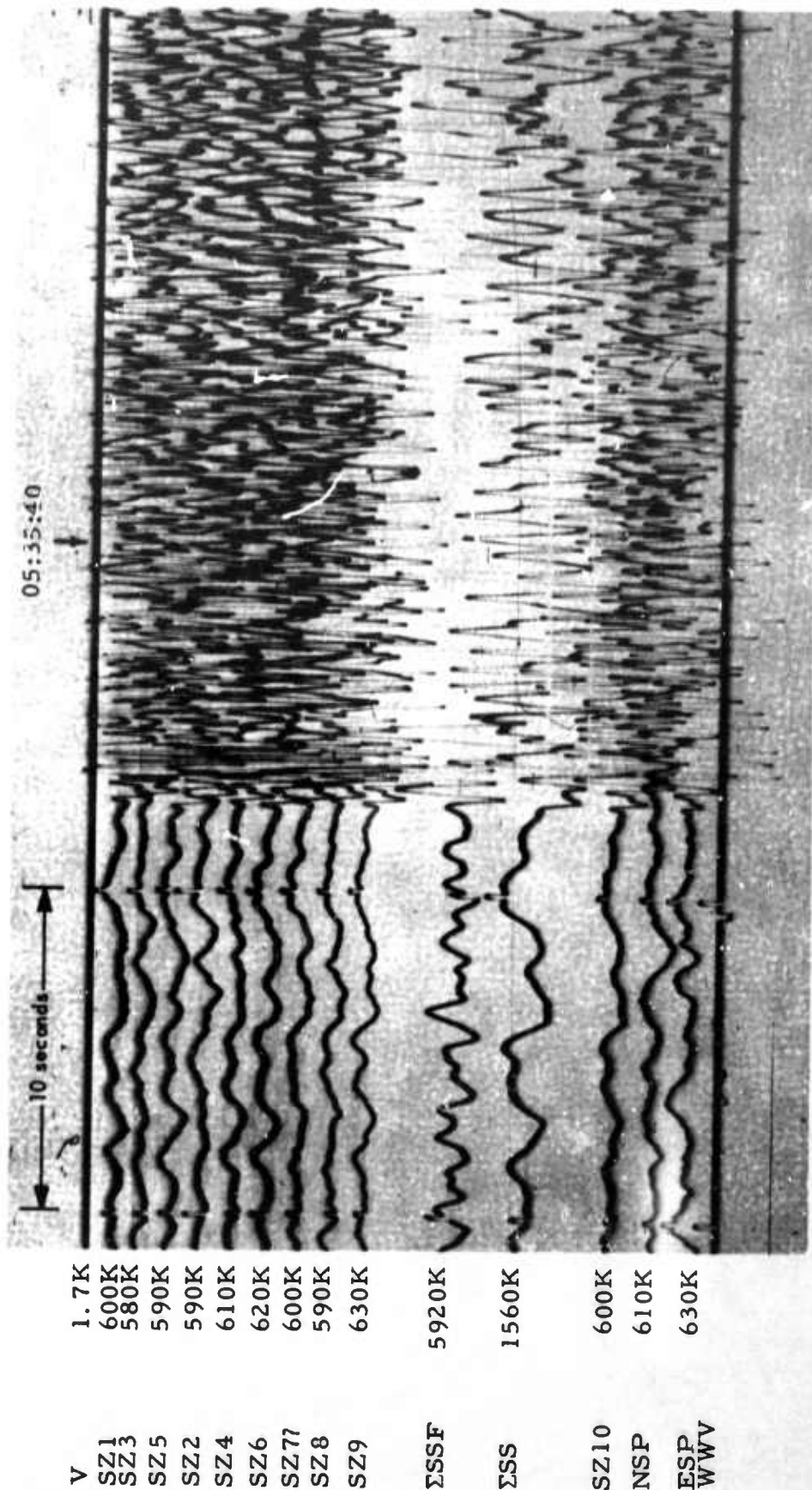


Figure 38. Primary system seismogram, illustrating response of primary system to near-regional signal. Epicentral dist.: O = 05:34:58.5,  $\Delta = 1.9^\circ$ , azimuth = 285 $^\circ$ , h = 5 km. (X10 enlargement of 16-millimeter film)

UBSO  
10 Mar 67  
RPN 069  
DG 5044

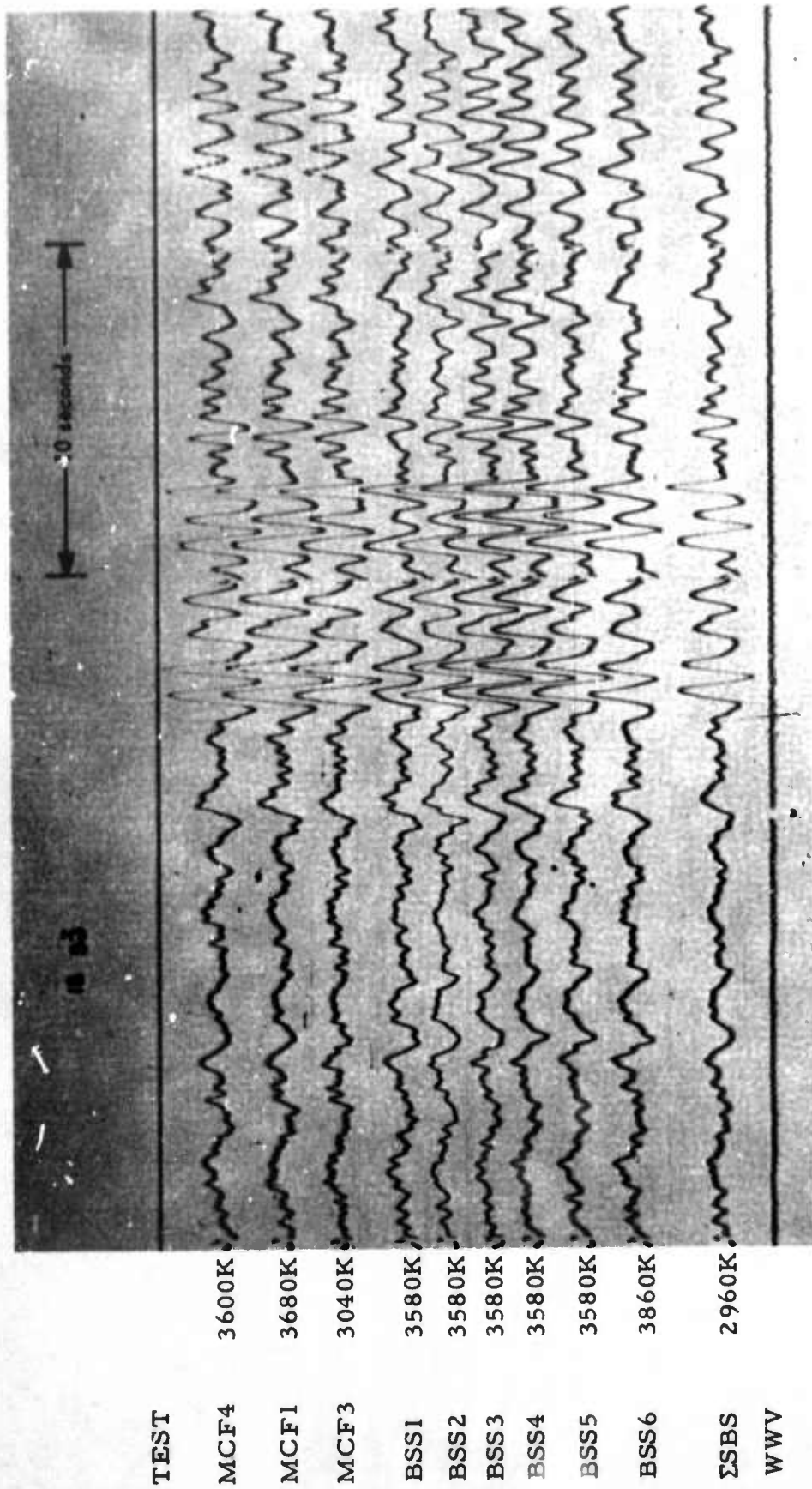


Figure 39. MAP I seismogram, illustrating response of MAP I systems to close teleseism. Epicentral data:  $O = 15:47:32.0$ ,  $\Delta = 26.1^\circ$ , azimuth =  $155^\circ$ ,  $h = 33$  km, USC&GS magnitude = 3.7.  
(X10 enlargement of 16-millimeter film)

TEST  
MCF4 3600K  
MCF1 3680K  
MCF3 3040K  
BSS1 3580K  
BSS2 3580K  
BSS3 3580K  
BSS4 3580K  
BSS5 3580K  
BSS6 3860K  
ΣSBS 2960K  
WWV

UBSO  
5 Feb 67  
RPN 036  
DG 5070

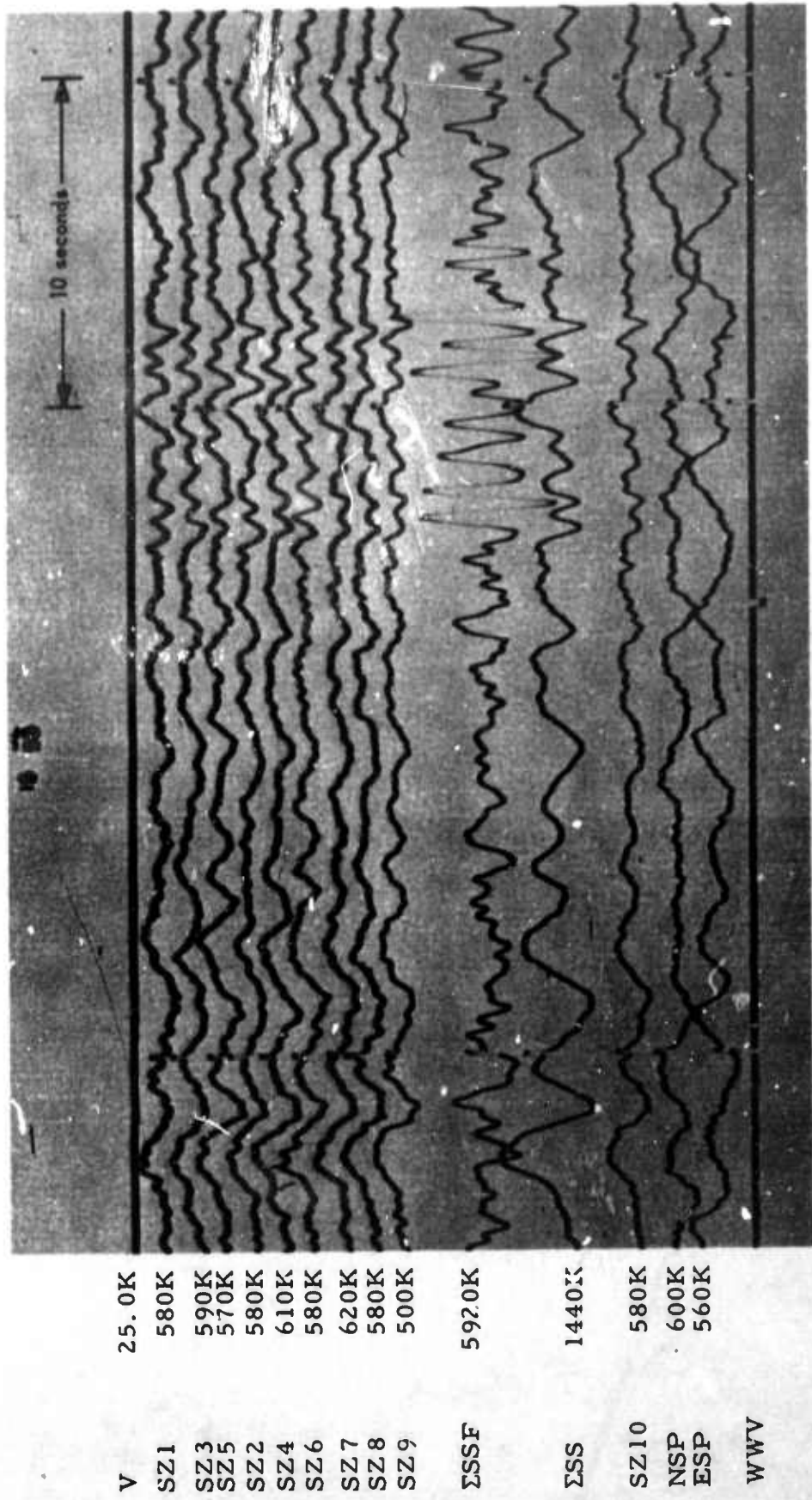
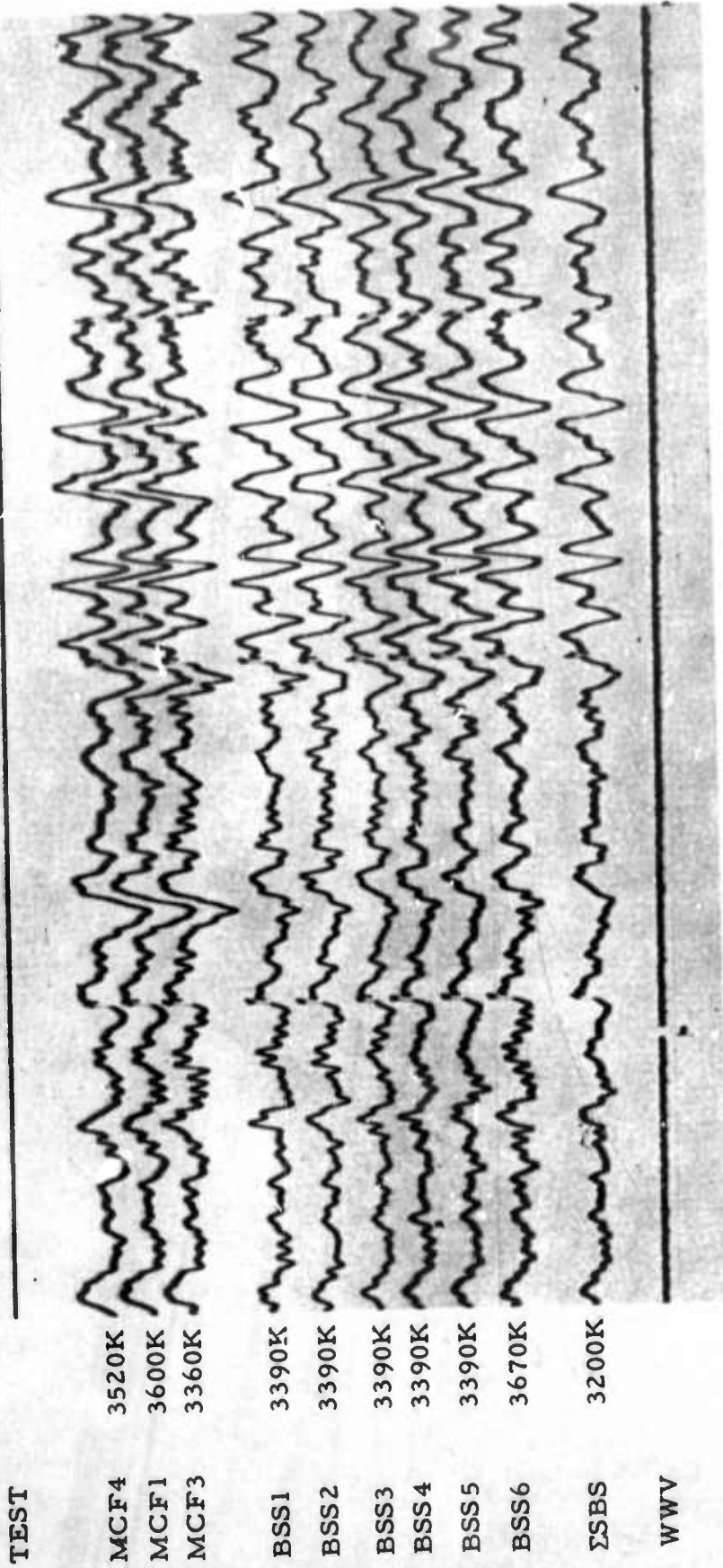


Figure 40. Primary system seismogram illustrating response of primary system to near teleseism. Epicentral data:  $O = 15:47:32.0$ ,  $\Delta = 20.1^\circ$ , azimuth =  $155^\circ$ ,  $h = 33$  km, USC&GS magnitude = 3.7.  
 (X10 enlargement of 16-millimeter film)

UBSO  
 5 Feb 67  
 RPN 036  
 DG 5044

10 seconds



UBSO  
 20 Feb 67  
 RPN 051  
 DG 5070

Figure 41. MAP I seismogram, illustrating response of MAP I systems to weak teleseism in road noise. Epicenter unknown.  
 (X10 enlargement of 16-millimeter film)

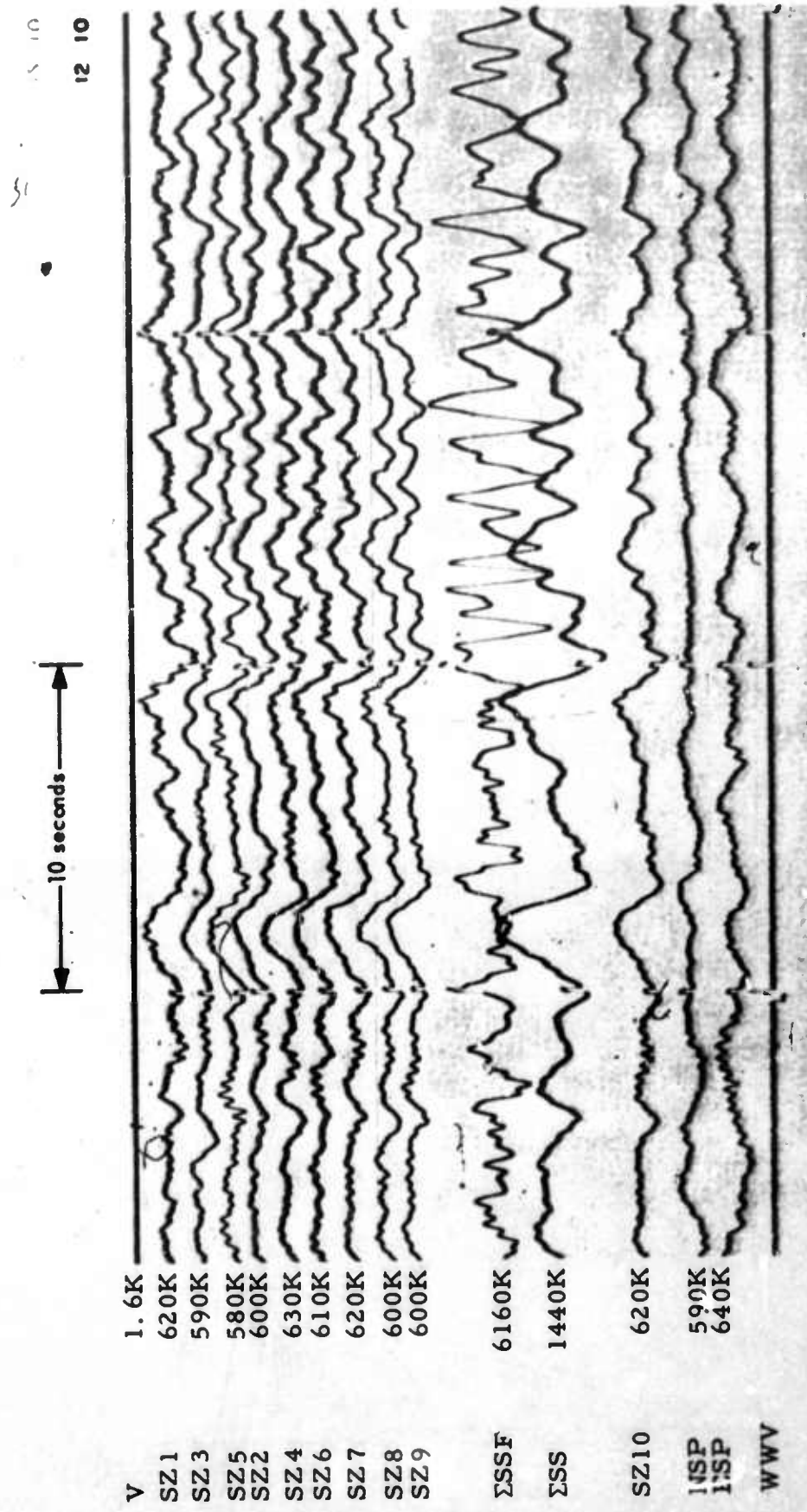


Figure 42. Primary system seismogram, illustrating response of primary system to weak teleseism in road noise. Epicenter unknown.  
 (X10 enlargement of 16-millimeter film)

UBSO  
 2 Feb 67  
 RPN 051  
 DG 5044

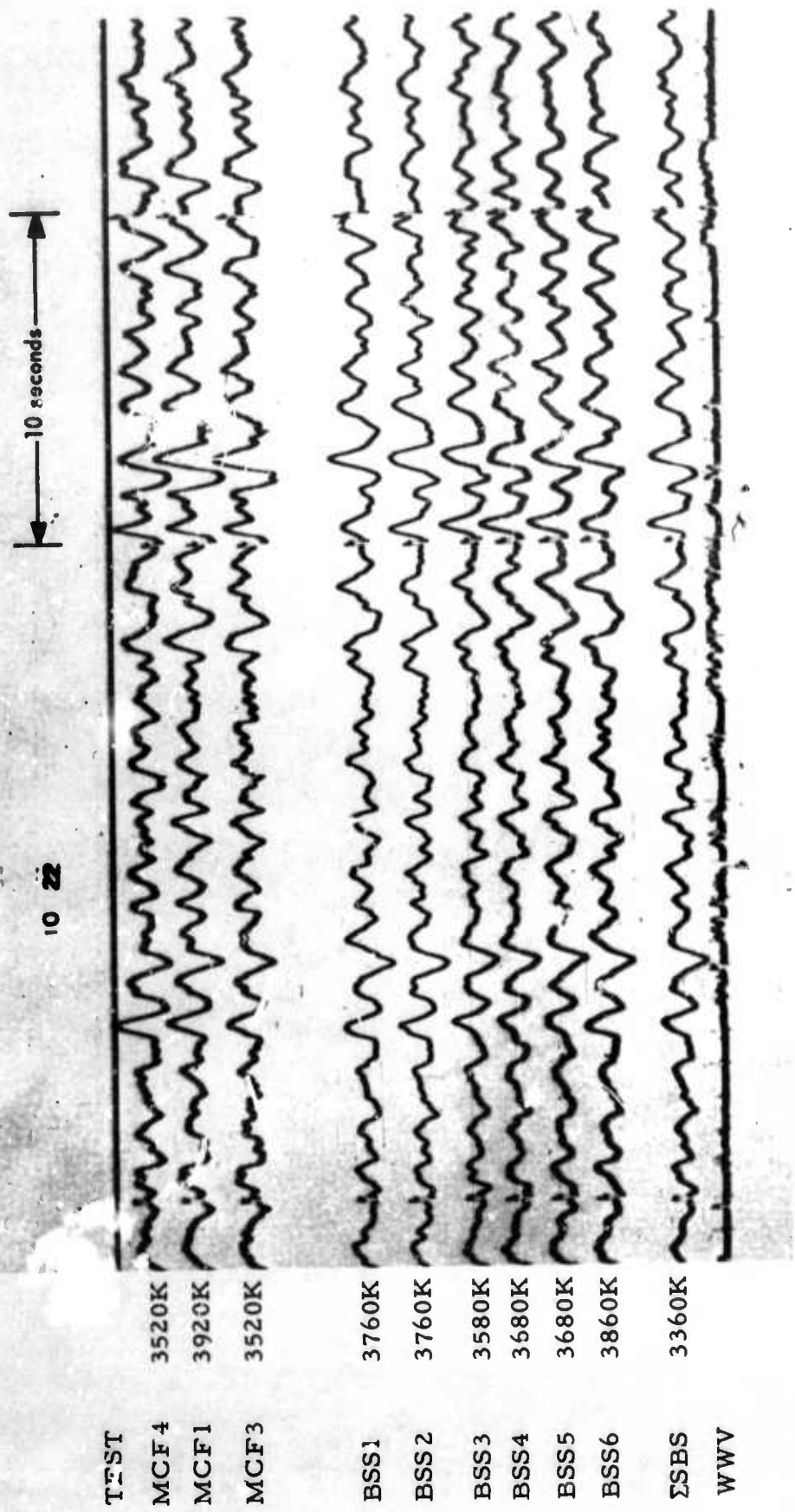


Figure 43. MAP I seismogram, illustrating response of MAP I systems to weak teleseism, background free of road noise. Epicentral data:  $O = 10:13:30.2$ ,  $\Delta = 50.6^\circ$ , azimuth =  $137^\circ$ ,  $h = 214$  km, USC&GS magnitude = 3.7.  
(X10 enlargement of 16-millimeter film)

UBSO  
5 Mar 67  
RPN 064  
DG 5070

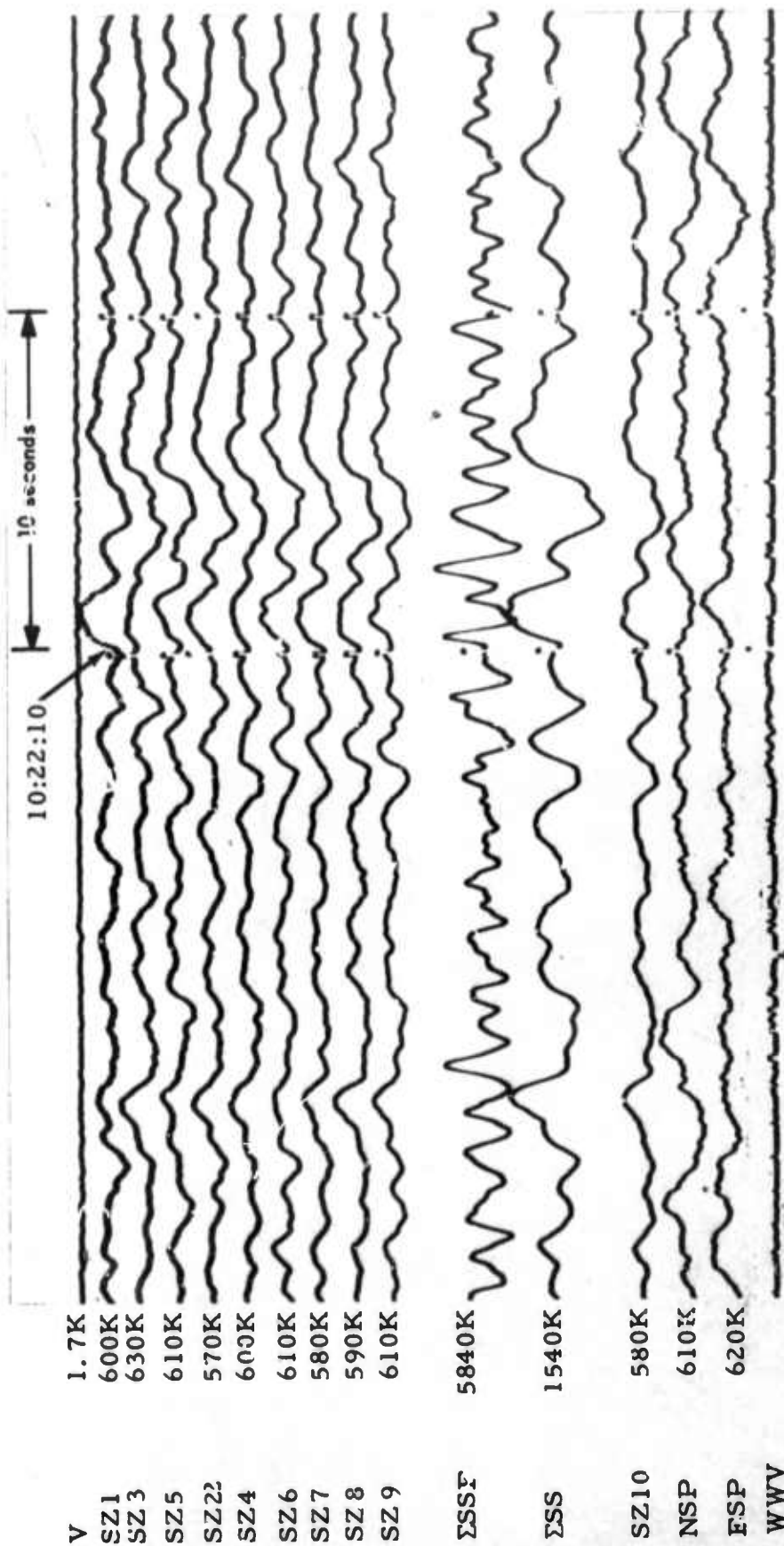


Figure 44. Primary system seismogram, illustrating response of primary system to weak teleseism, background free of road noise. Epicentral data:  
 $O = 10:13:30.2$ ,  $\Delta = 50.6^\circ$ , azimuth =  $137^\circ$ ,  $h = 214$  km,  
 USC&GS magnitude = 3.7. (X10 enlargement of 16-millimeter film)

UBSO  
 5 Mar 67  
 RPN 064  
 DG 5044

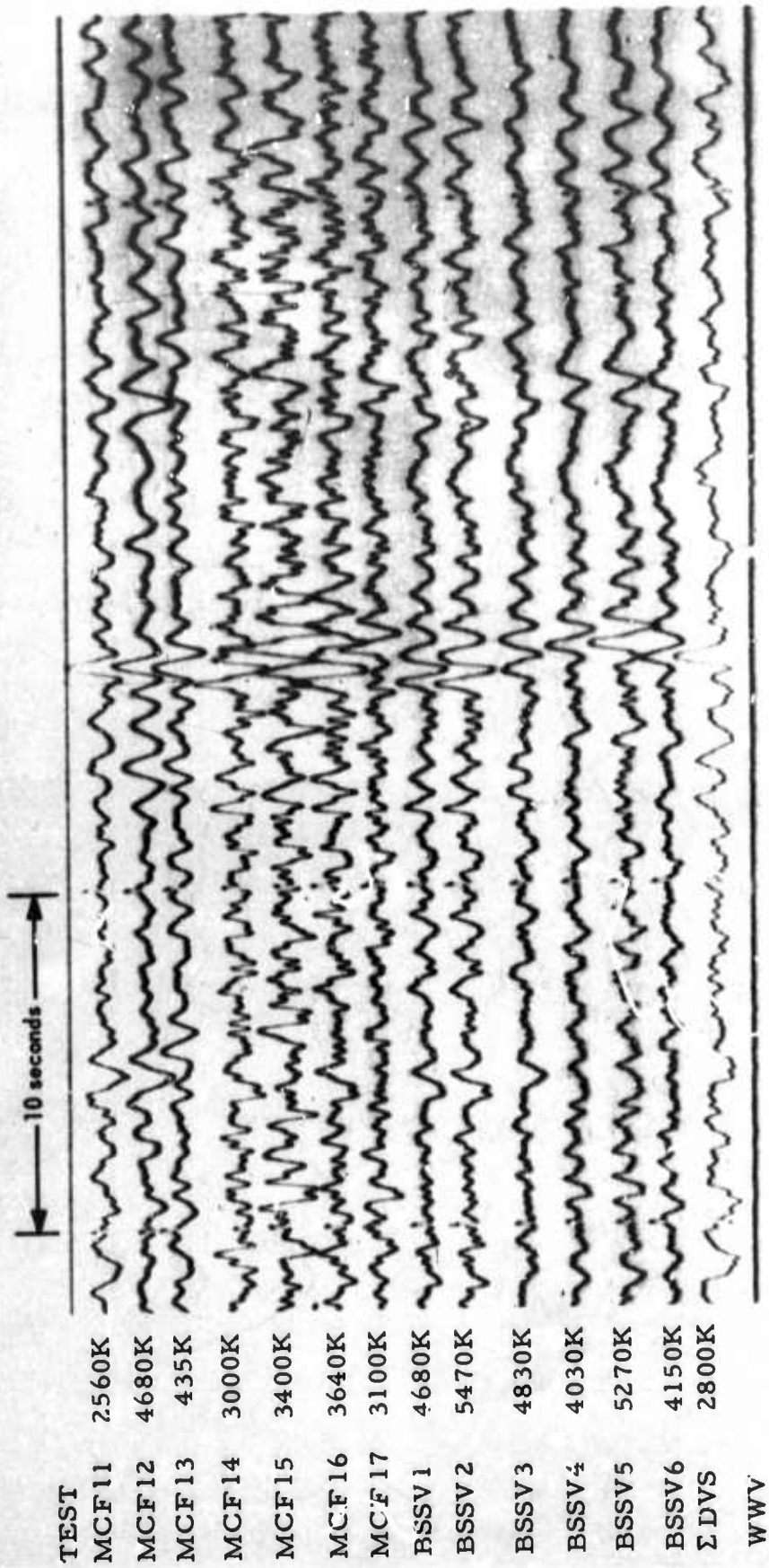


Figure 45. MAP 11 seismogram illustrating precursor effect on MCF15 epicenter unknown. (X10 enlargement of 16-millimeter film)

UBSO  
4 Feb 67  
RPN 035  
DG 5072

01 M

10 seconds

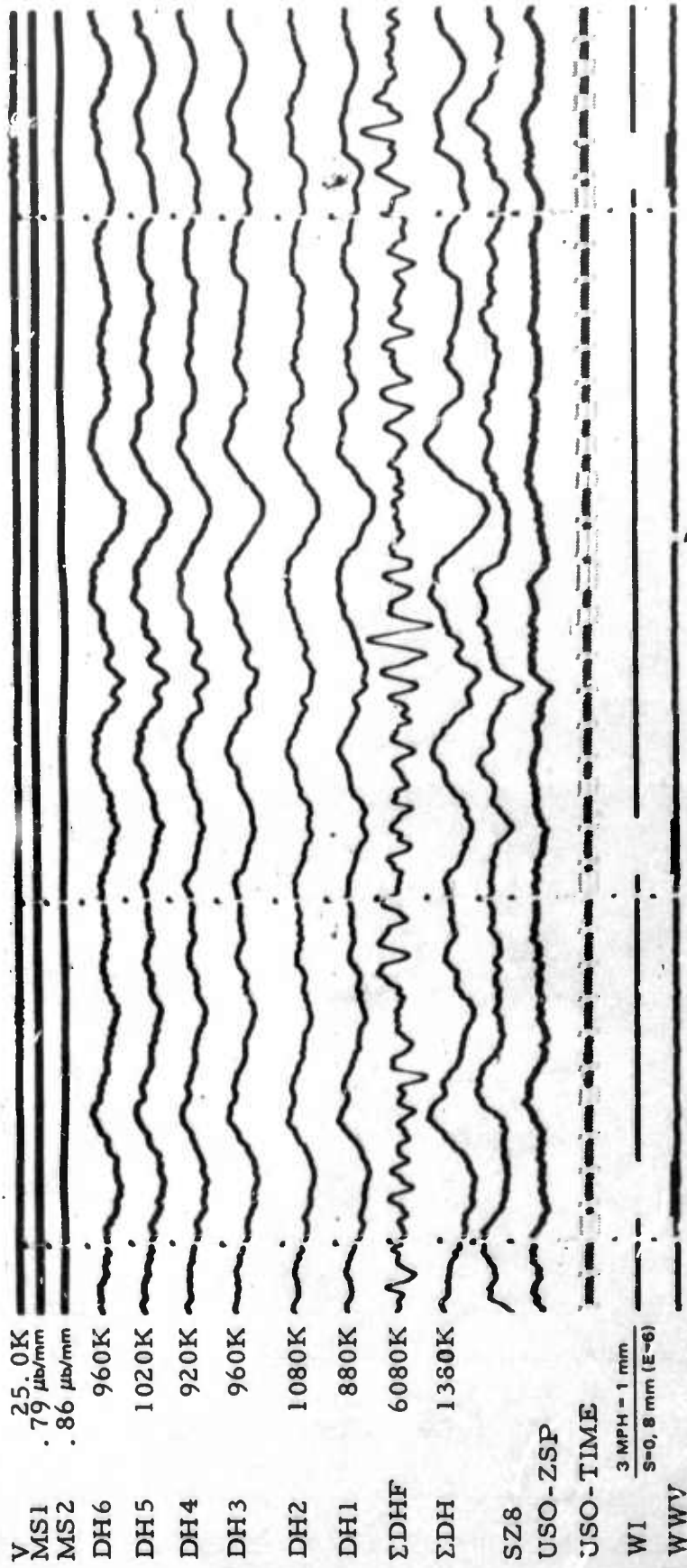


Figure 46. Vertical array seismogram of same event as is illustrated in figure 45. Epicenter unknown. (X10 enlargement of 16-millimeter film)

UBSO  
4 Feb 67  
RPN 035  
DG 5064

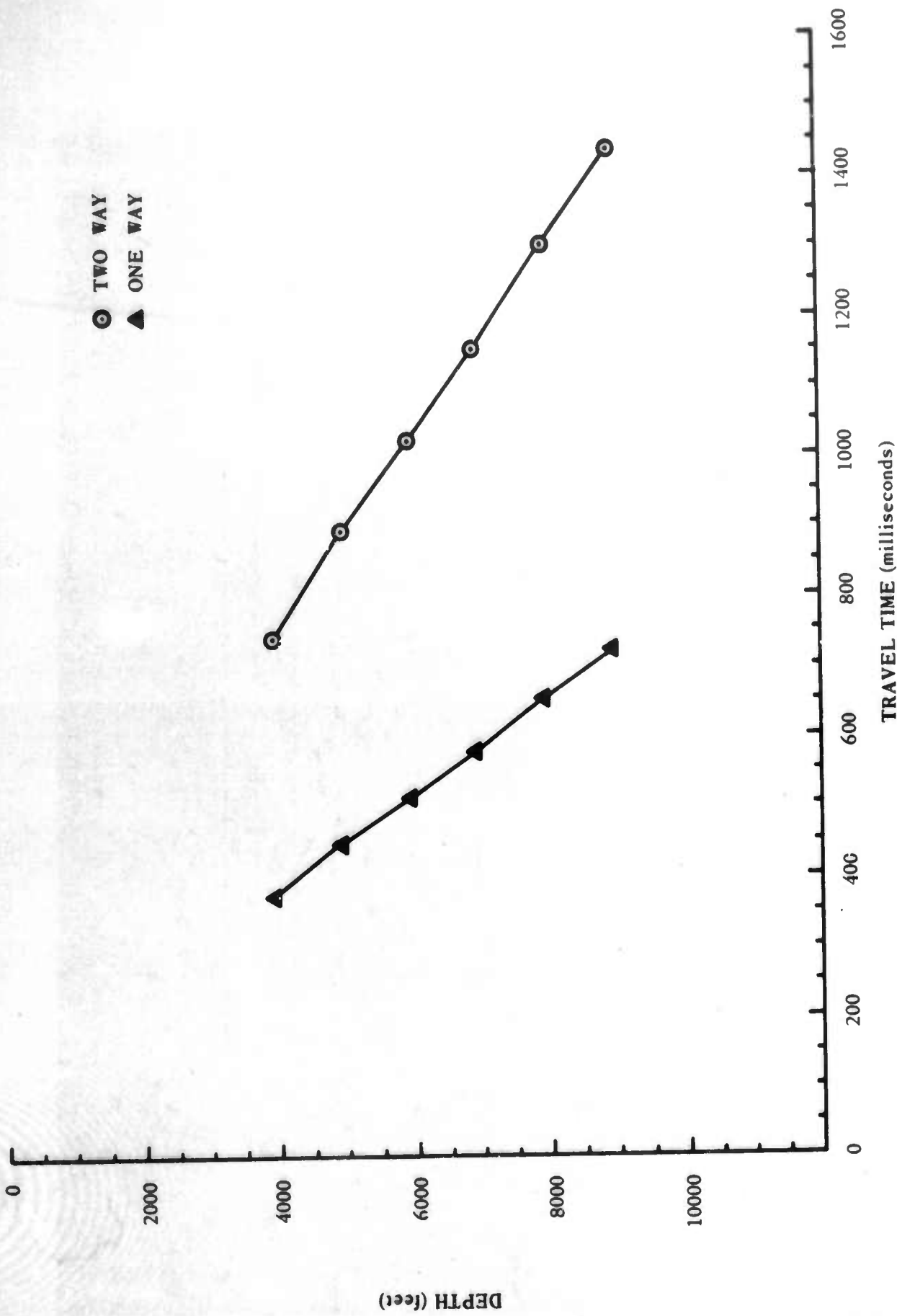


Figure 47. One-way and two-way travel times for the vertical array G 3679

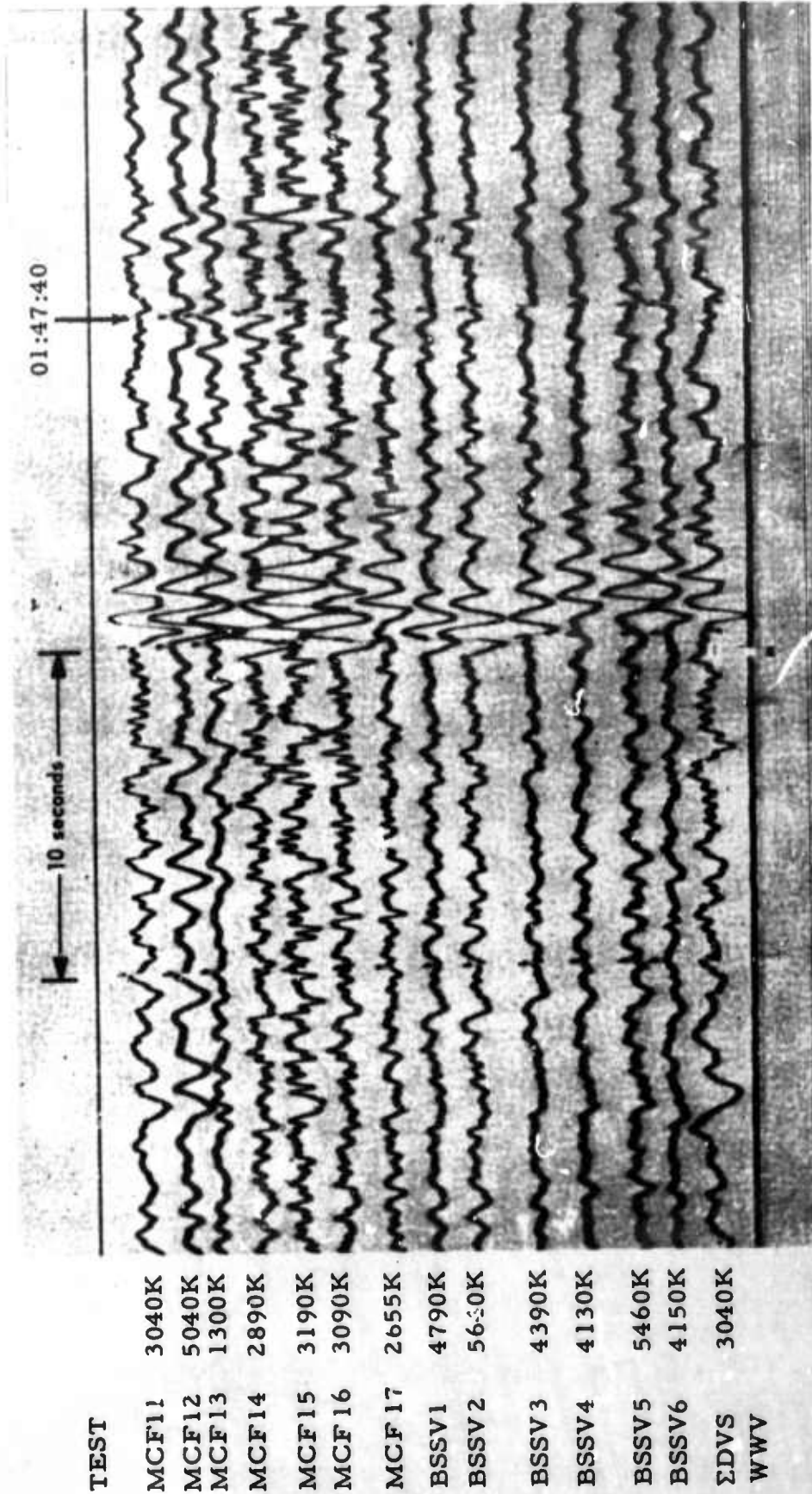
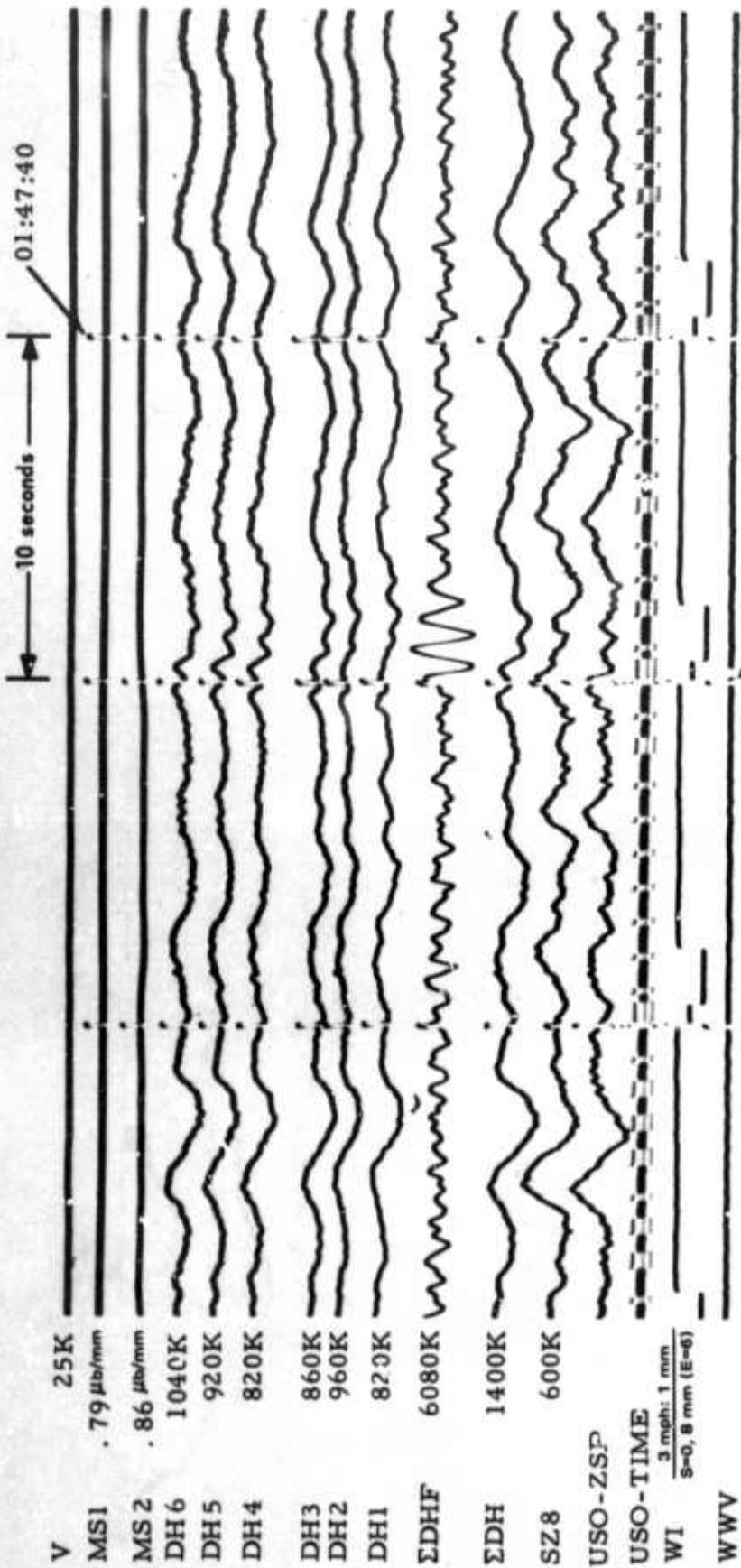


Figure 48. MAP II seismogram, illustrating response of the MAP II systems to a simple P wave. Epicentral data:  $O = 01:35:18.0$ ,  $\Delta = 86.4^\circ$ , azimuth =  $240^\circ$ ,  $h = 280$  km, USC&GS magnitude = 4.1.  
(X10 enlargement of 16-millimeter film)

UBSO  
6 Feb 67  
RPN 037  
DG 5072



UBSO  
 6 Feb 67  
 RPN 037  
 DG 5064

Figure 49. Vertical array seismogram, illustrating response of vertical array to a simple P wave. Epicentral data:  $O = 01:35:18.0$ ,  $\Delta = 86.4^\circ$ , azimuth =  $240^\circ$ ,  $h = 280$  km, USC&GS magnitude = 4.1.  
 (X10 enlargement of 16-millimeter film)

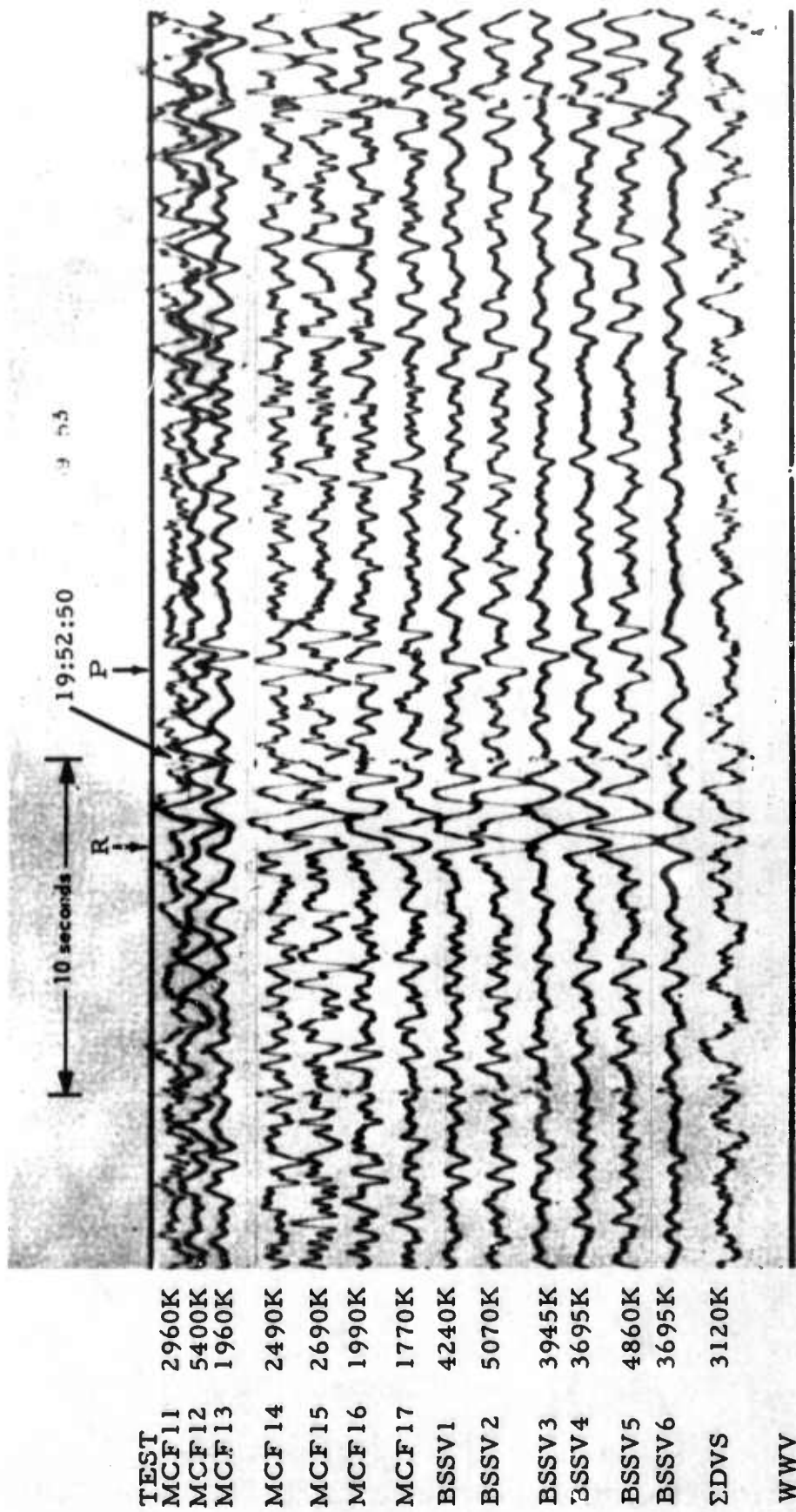
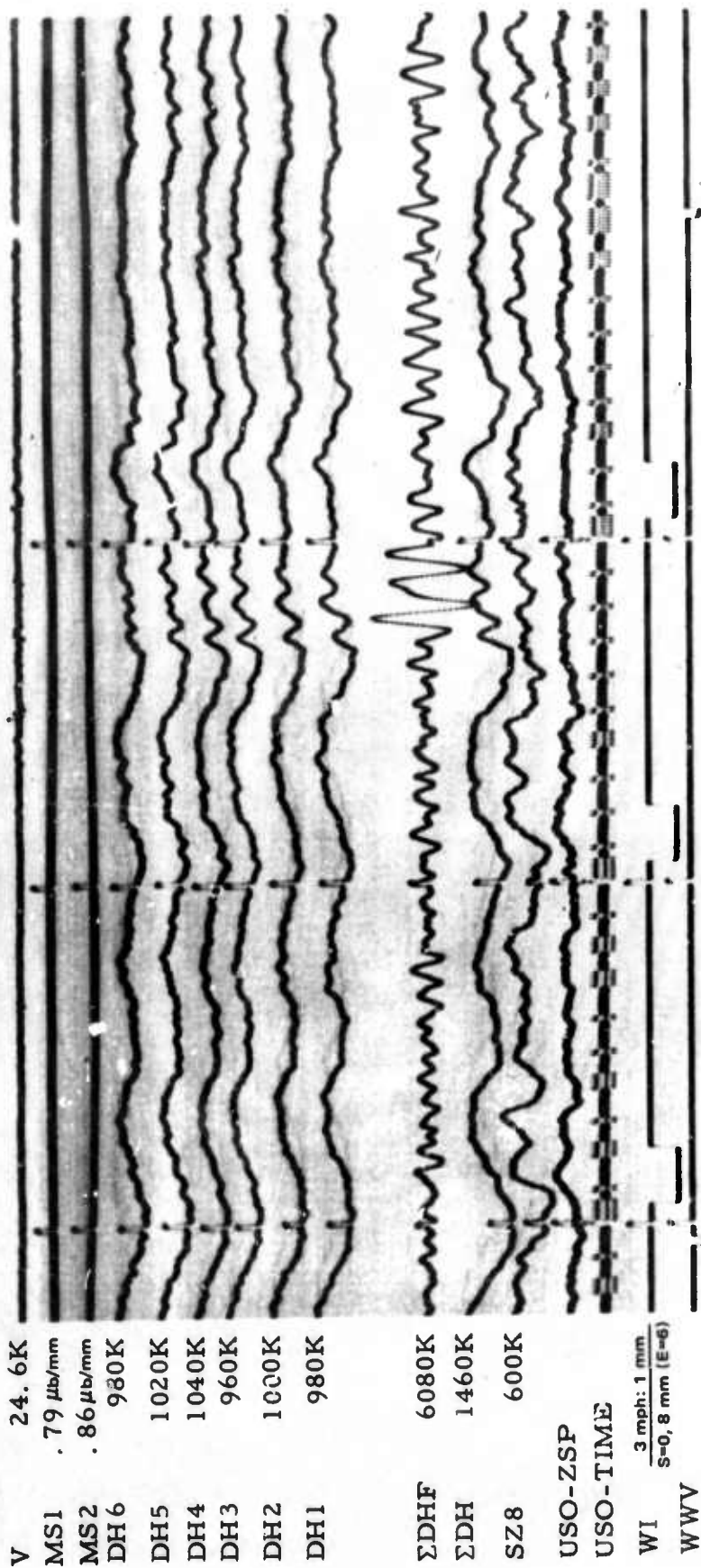


Figure 50. MAP II seismogram, illustrating response of MAP II systems to a short-duration Rayleigh wave. (X10 enlargement of 16-millimeter film)

UBSO  
14 Feb 67  
RPN 045  
DG 5072

10 55

10 seconds



UBSO

14 Feb 67

RPN 045

DG 5064

Figure 51. Vertical array seismogram, illustrating response of vertical array to a short-duration Rayleigh wave. (X10 enlargement of 16-millimeter film)

01:55:10

55

10 seconds

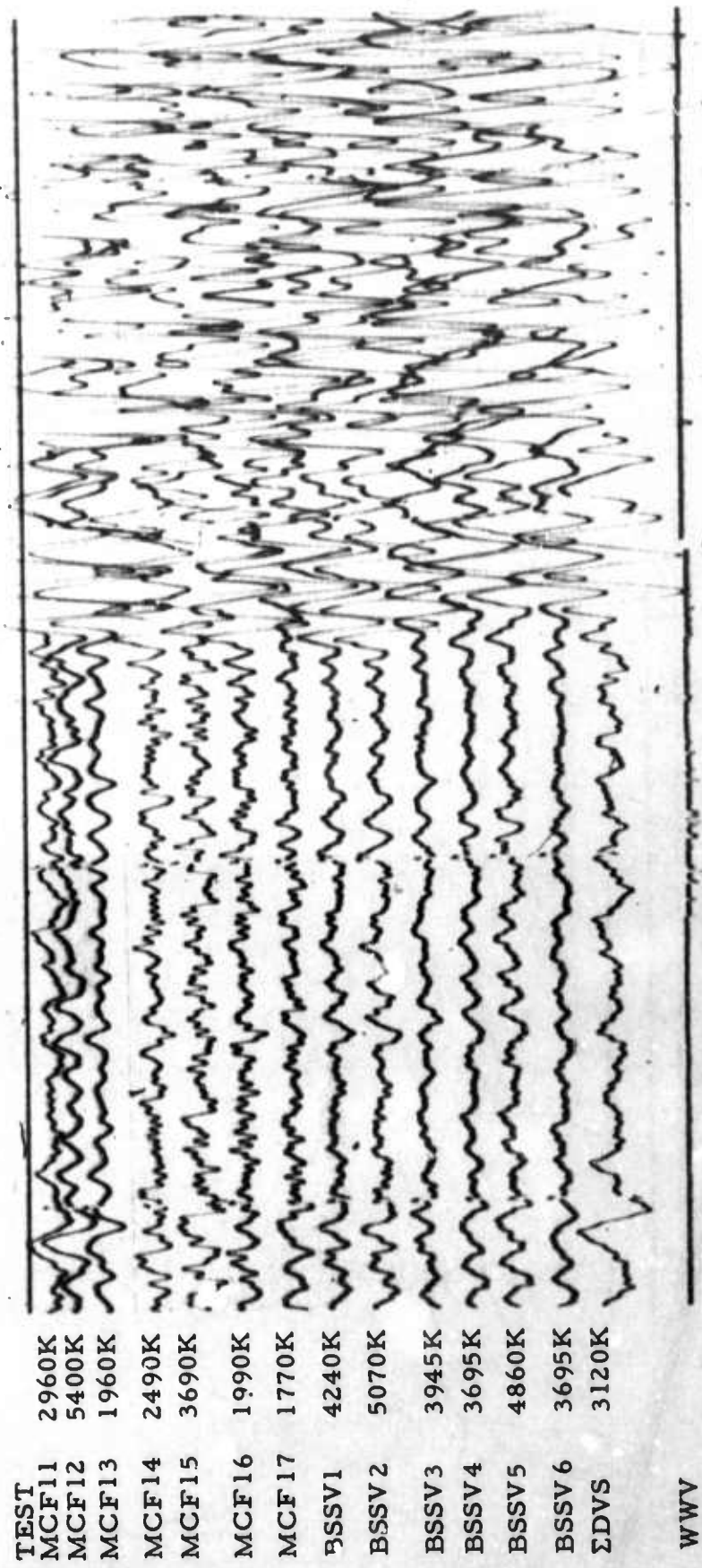


Figure 52. MAP II seismogram, illustrating response of MAP II systems to a complex signal (PKP). Epicentral data:  $O = 01:36:04.7$ ,  $\Delta = 121.1^\circ$ , azimuth =  $330^\circ$ ,  $h = 27$  km, no USC&GS magnitude. (X10 enlargement of 16-millimeter film)

UBSO  
14 Feb 67  
RPN 045  
DG 5072

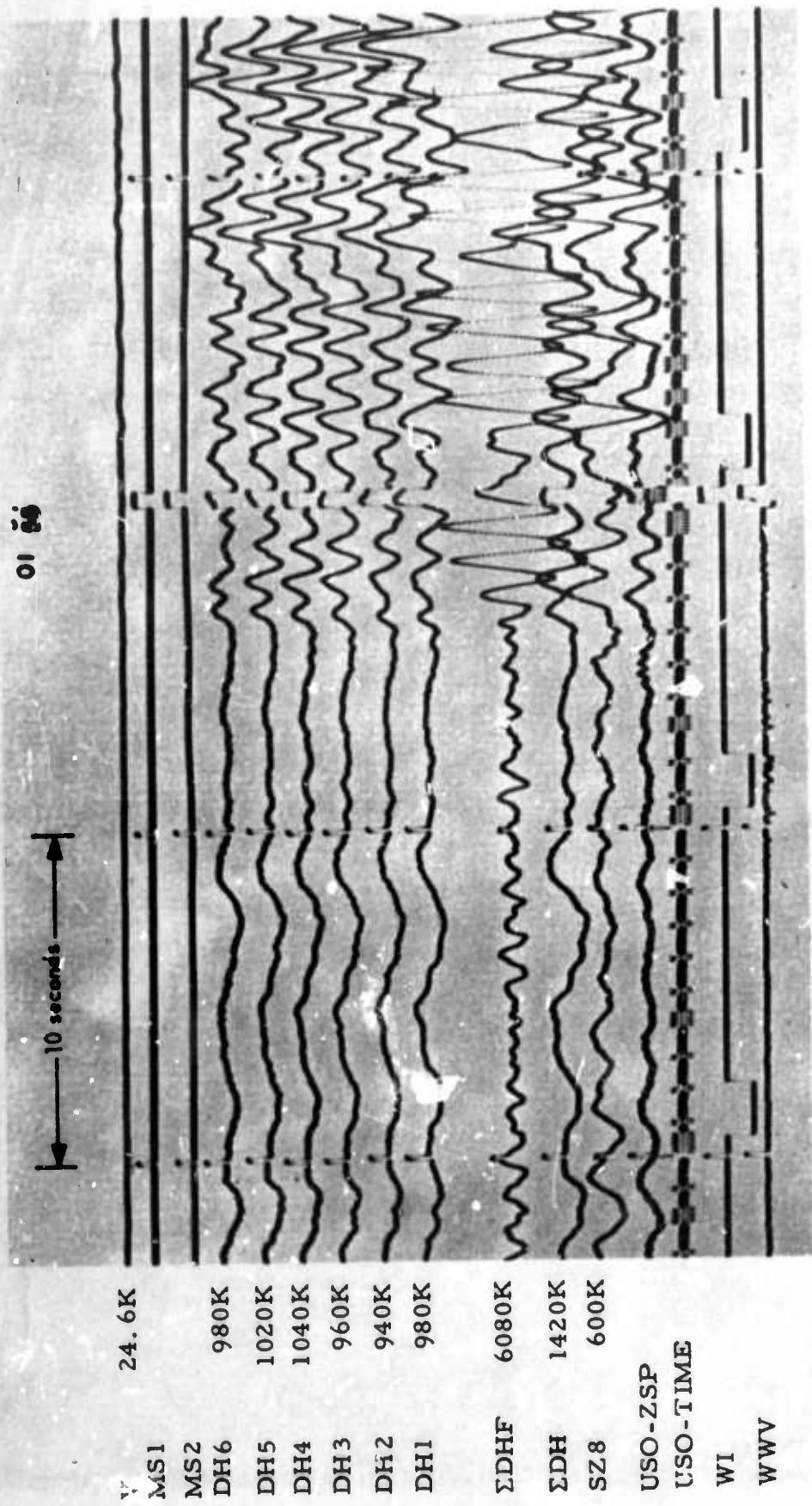


Figure 53. Vertical array seismogram, illustrating response of vertical array to a complex signal (PKP). Epicentral data:  $O = 01:36:04.7$ ,  $\Delta = 121.1^\circ$ , azimuth =  $330^\circ$ ,  $h = 27$  km, no USC&GS magnitudes.  
(X10 enlargement of 16-millimeter film)

UBSO  
14 Feb 67  
RPN 045  
DG 5064

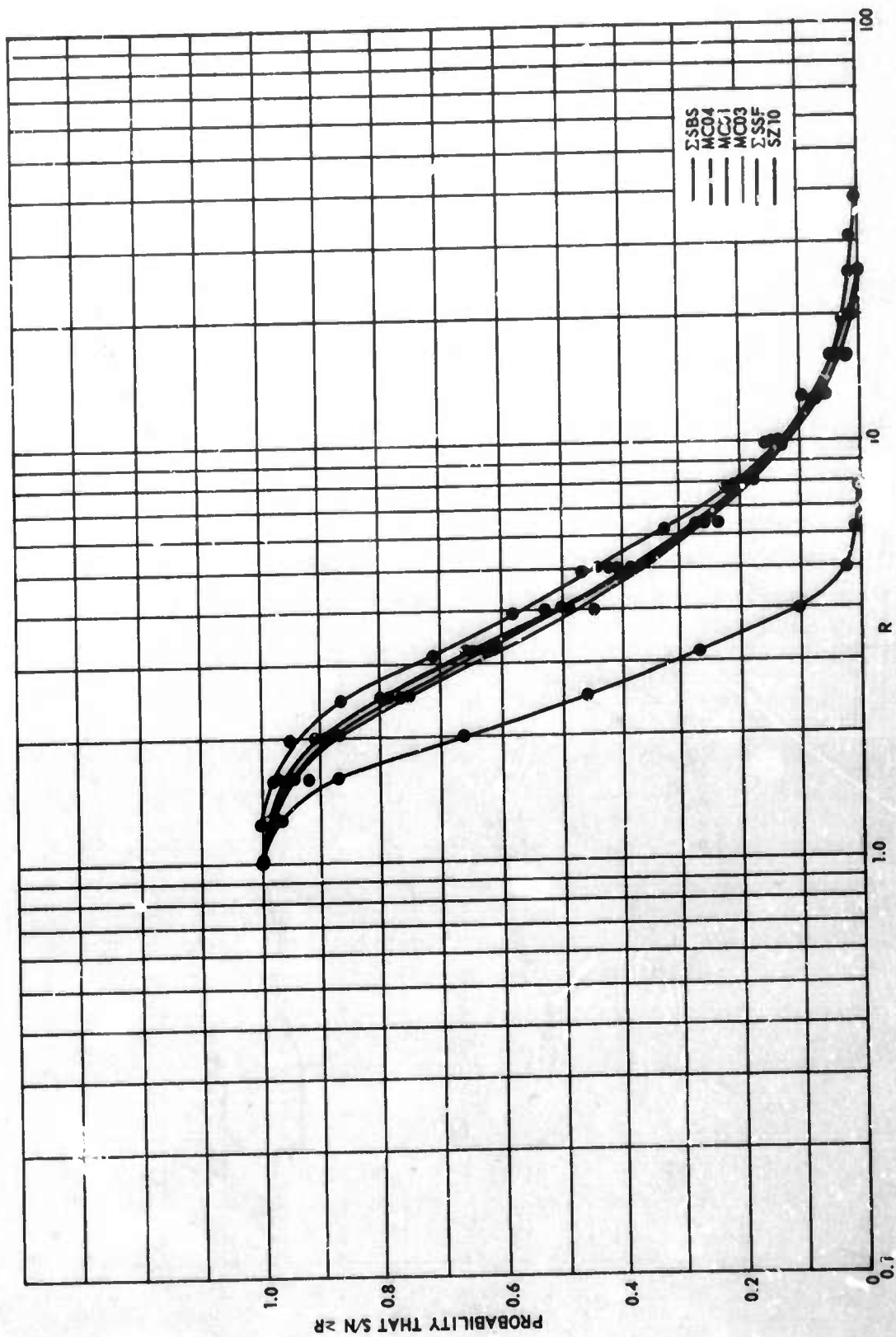


Figure 54. Cumulative frequency distributions of S/N for MAP I and Primary systems

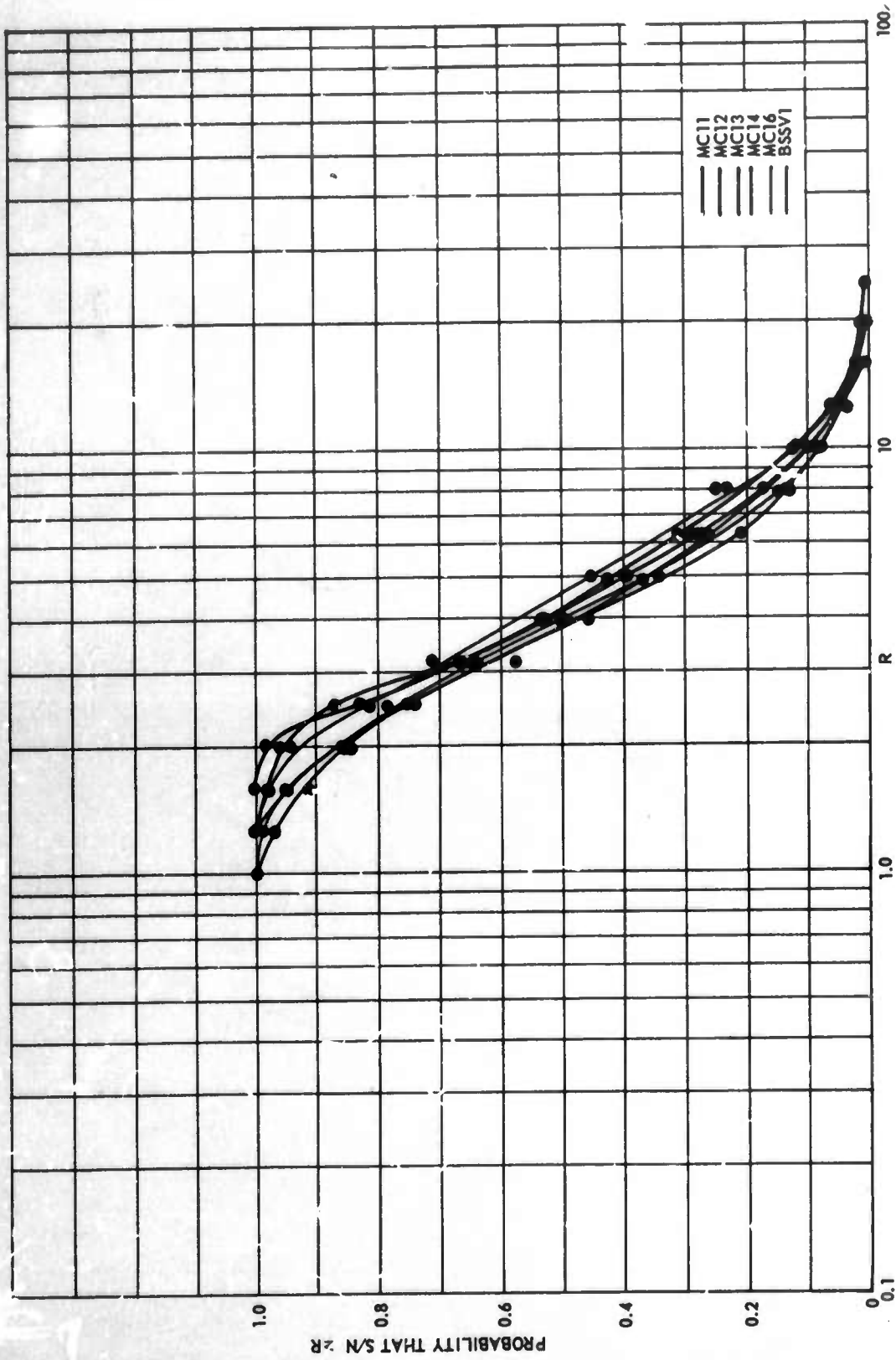


Figure 55. Cumulative frequency distributions of S/N for MAP II systems

G 2994